

**ISOTOPIC INVESTIGATION OF SUBSURFACE ROCK AND FLUID
INTERACTIONS: CASE STUDIES OF CO₂ SEQUESTRATION AND GAS-BEARING
SHALES FORMATIONS**

by

James B. Gardiner

B.S. Environmental Geology, University of Pittsburgh, 2008

Submitted to the Graduate Faculty of
the Kenneth P. Dietrich School of
Arts & Sciences in partial fulfillment
of the requirements for the degree of
Doctor of Philosophy

University of Pittsburgh

2013

UNIVERSITY OF PITTSBURGH
FACULTY OF THE KENNETH P. DIETRICH SCHOOL OF
ARTS AND SCIENCES

This dissertation was presented

by

James B. Gardiner

It was defended on

November 15, 2013

and approved by

Daniel Bain, Assistant Professor, University of Pittsburgh

Alexandra Hakala, Geochemist, National Energy Technology Laboratories

William Harbert, Professor, University of Pittsburgh

Brian Stewart, Associate Professor, University of Pittsburgh

Dissertation Advisor: Rosemary Capo, Associate Professor, University of Pittsburgh

Copyright © by James B. Gardiner

2013

**ISOTOPIC INVESTIGATION OF SUBSURFACE ROCK AND FLUID
INTERACTIONS: CASE STUDIES OF CO₂ SEQUESTRATION AND GAS-BEARING
SHALE FORMATIONS**

James B. Gardiner, PhD

University of Pittsburgh, 2013

Isotopic studies have been used for decades to gain insight into geochemical reactions and the mixing of subsurface fluids. The three studies presented here focus on the use of strontium (Sr) and neodymium (Nd) isotopes as geochemical tools that can complement geologic and geochemical knowledge and improve our understanding of how chemical reactions can alter subsurface fluids and surrounding geologic formations.

The first study investigates the groundwater in Chimayó, New Mexico, where upwelling CO₂ has affected the groundwater for over a century, making it a natural analog for an aquifer above a leaking CO₂ reservoir. Sr isotope data for Chimayó groundwaters span a wide range (0.7098-0.7176) over a limited spatial extent (6 km²) and indicate that different strontium sources are present in geochemically similar waters. When combined with geochemical data, Sr and C isotopes identify and quantify CO₂ transport processes predicted in previous work (Keating et al., 2010).

The second study is a geochemical and isotopic characterization of produced waters from an oil field prior to CO₂ enhanced oil recovery. Fluid samples were taken from the producing reservoir formation, which is currently flooded with water. Samples were also taken from the overlying groundwaters. Differences in Sr isotopic values between the produced waters and the groundwaters indicate that Sr isotopes could be used to monitor CO₂ storage permanence. When

compared with a conventional field that produces from the same reservoir formation, the water flooded field had distinct TDS and $^{87}\text{Sr}/^{86}\text{Sr}$ values. The geochemical isotopic differences between the waters suggest that each field may have a distinct brine migration history.

The third study uses Sr and Nd isotopes to investigate the sediment sources of the Middle Devonian aged Marcellus shale and the rock units surrounding it. For the shale samples, the Nd isotope data was used to constrain a model mantle age of ~1.4-1.6 Ga, indicating a Grenville aged sediment source. The age-corrected Sr isotope data indicate a depositional age of ~390Ma. Together, this isotopic data indicates that these rocks are composed of Grenville aged sediments that experienced minimal post-depositional alteration.

TABLE OF CONTENTS

1.0	INTRODUCTION.....	1
1.1	GEOLOGIC CO₂ SEQUESTRATION	2
1.1.1	Natural Analogs for CO₂ Sequestration	3
1.1.2	CO₂ Enhanced oil recovery.....	4
1.2	BLACK, ORGANIC-RICH SHALE DEPOSITION: SEDIMENT SOURCE AND POST-DEPOSITIONAL HISTORY.....	5
1.3	STRONTIUM ISOTOPE SYSTEM	6
1.3.1	Sr isotopes applied to water-rock interaction	6
1.3.2	Sr isotopes applied to lithologic depositional history	8
1.4	NEODYMIUM ISOTOPE SYSTEM.....	9
1.4.1	Nd isotopes applied to lithologic depositional history	9
1.5	RESEARCH OBJECTIVES AND APPROACH	11
1.6	ORGANIZATION OF THIS DISSERTATION.....	12
2.0	SR ISOTOPE TRACKING OF CO₂ SOURCE AND MIGRATION PATHWAYS AT A NATURAL ANALOG SITE FOR GEOLOGIC CARBON STORAGE: CHIMAYÓ, NEW MEXICO	14
2.1	INTRODUCTION	14
2.2	GEOLOGY AND HYDROGEOLOGY OF THE ESPAÑOLA BASIN	18

2.3	SAMPLE COLLECTION AND ANALYTICAL TECHNIQUES	21
2.3.1	Water samples.....	21
2.3.2	Rock samples.....	22
2.3.3	Sequential extraction techniques.....	22
2.3.4	Geochemical analysis.....	22
2.3.5	Strontium isotope analysis	24
2.4	RESULTS	24
2.4.1	Groundwater chemistry	24
2.4.2	$^{87}\text{Sr}/^{86}\text{Sr}$ isotopes of groundwater samples and lithologic samples	27
2.4.3	$\delta^{13}\text{C}$ isotopes of groundwater samples	28
2.5	DISCUSSION.....	29
2.5.1	$^{87}\text{Sr}/^{86}\text{Sr}$ of Chimayó groundwater.....	30
2.5.2	Water-rock interactions documented by $^{87}\text{Sr}/^{86}\text{Sr}$ isotopes.....	32
2.5.3	$\delta^{13}\text{C}$ isotopes.....	33
2.5.4	Multi-isotope mixing model using $^{87}\text{Sr}/^{86}\text{Sr}$ and $\delta^{13}\text{C}$ isotopes.....	34
2.5.5	Identifying reaction pathways using $^{87}\text{Sr}/^{86}\text{Sr}$ and $\delta^{13}\text{C}$ isotopes.....	36
2.5.6	Effect of decoupled CO_2 on groundwater.....	38
2.6	CONCLUSIONS.....	40
3.0	STRONTIUM ISOTOPE AND GEOCHEMICAL CHARACTERIZATION OF THE EAST SEMINOLE OIL FIELD EOR SITE, TEXAS	42
3.1	INTRODUCTION	42
3.2	STUDY AREA	48

3.2.1	Geology and hydrogeology of Central Basin Platform and formations sampled	51
3.2.1.1	Permian Basin: Central Basin Platform	51
3.2.1.2	Brine Migration in the Permian Basin	52
3.2.1.3	Permian San Andres Formation	53
3.2.1.4	Tertiary Ogallala Formation, Part of the High Plains Aquifer	57
3.2.1.5	Creataceous Duck Creek and Antler Formations.....	58
3.2.1.6	Triassic Dockum Group	59
3.3	SAMPLING	61
3.4	ANALYTICAL METHODS	64
3.5	RESULTS	65
3.5.1	Field geochemistry results.....	65
3.5.2	Organic alkalinity results.....	67
3.5.3	General geochemistry results	69
3.5.4	Strontium isotope geochemistry	72
3.6	DISCUSSION.....	75
3.6.1	Organic alkalinity	75
3.6.2	General geochemistry and isotope geochemistry.....	76
3.6.2.1	$^{87}\text{Sr}/^{86}\text{Sr}$ as a monitoring tool	76
3.6.2.2	Produced waters	78
3.6.2.3	Shallow groundwaters	84
3.7	CONCLUSIONS	86

4.0	A NEODYMIUM AND STRONTIUM ISOTOPE INVESTIGATION OF SEDIMENT SOURCES FOR THE MIDDLE DEVONIAN MARCELLUS SHALE	88
4.1	INTRODUCTION	88
4.2	RESEARCH GOALS	91
4.3	DEPOSITIONAL ENVIRONMENT, SEDIMENT SOURCES AND MINERALOGY OF THE MIDDLE DEVONIAN MARCELLUS SHALE	92
4.3.1	Depositional environment of the Marcellus Shale	93
4.3.2	Sediment sources of the Marcellus Shale	96
4.3.3	Volcanic ashes	97
4.3.4	Mineralogy of the Marcellus Shale	98
4.4	APPROACH AND METHODS.....	99
4.4.1	Sampling	99
4.4.2	Sequential extraction.....	101
4.4.3	Sample dissolution	102
4.4.4	Isotopic Analysis	104
4.5	RESULTS	105
4.5.1	Neodymium isotope geochemistry.....	105
4.5.2	Strontium isotope geochemistry	107
4.6	DISCUSSION.....	108
4.6.1	Sm-Nd systematics: Implications for post-depositional disturbances	108
4.6.2	Rb-Sr systematics: Implications for post-depositional disturbances.....	110
4.6.3	Identifying the sediment source terrane	112
4.6.4	Sediment source variation within the cores: volcanic ashes	114

4.6.5	Depositional environment and source terrane	115
4.6.6	Organic-silicate residues primary holders of Nd-Sm	116
4.7	CONCLUSIONS	116
5.0	CONCLUDING REMARKS	119
5.1	CONCLUSIONS	119
5.2	RECOMMENDATIONS FOR FUTURE WORK	121
	BIBLIOGRAPHY	122

LIST OF TABLES

Table 1. Field measurements for Chimayo well waters.....	25
Table 2. Major ion chemistry and trace elements for water samples ^a . All chemical compositions are in mg/L.....	25
Table 3. PHREEQc saturation indices for Chimayo groundwaters.....	26
Table 4. Sr isotope ratios of water samples, ammonium acetate leachates, and acetic acid leachates.....	28
Table 5. Field data for water samples collected at Emma and Seminole Oil Fields. Dr. Gwen Macpherson, University of Kansas, measured the pH, temperature, Eh, and TDS for most of these samples. All of these values as well as alkalinity were measured in the field. All samples were taken between June 3-6, 2013.	67
Table 6. Alkalinity with the contributions of organic alkalinity and the actual carbonate alkalinity to the total alkalinity. Organic alkalinity tests were not performed on shallow groundwaters and those samples not listed.	68
Table 7. Major element data for water samples collected at Emma and Seminole Oil Fields.	70
Table 8. Major cations listed in milliequivalents and the percentage that element makes of the total milliequivalents for that water sample.....	71
Table 9. Sr isotopic composition of waters at Emma and East Seminole Oil Fields.....	74

Table 10. Sm-Nd concentration isotope data for Marcellus core and volcanic ash organic-silicate residues. 107

Table 11. Sr isotope ratios of Marcellus and volcanic ash organic-silicate residue reflecting modern day values and original Sr(T) isotope ratio at time of deposition..... 108

LIST OF FIGURES

Figure 1. Geologic map of Chimayo, NM with sample well locations and major roadways identified; modified from Keating et al., 2010.	20
Figure 2. Cross section of the Chimayo region; image modified from Keating et al., 2010, which was based on previous work (Koning et al. 2002; Koning 2003).....	21
Figure 3. Piper plot of Chimayó, NM waters. CHM-05, the well with the highest CO ₂ and TDS concentrations, does not plot as a distinct end-member based on the major cation and anion chemistry. CHM-02 and CHM-03 are separated by <150 m and have different major cation compositions.	27
Figure 4. Graphs of saturation index values (SI) plotted against CO ₂ (g/L) concentration for Chimayó well waters. Squares represent calcite saturation index values and circles represent quartz saturation index values.	30
Figure 5. Strontium isotopic composition of Chimayo well water and rock leaches. Filled circles represent well water values and open circles represent values of rock leachates. An oval encompasses the ⁸⁷ Sr/ ⁸⁶ Sr range of groundwaters that can be explained by interaction with the surrounding lithosome material and the underlying limestone.	31
Figure 6. ⁸⁷ Sr/ ⁸⁶ Sr plotted against CO ₂ concentration for Chimayo well waters. Numbers next to mixing curve indicate fraction of geysering fluid added to background water. The mixing curve uses three variables (Sr concentration, ⁸⁷ Sr/ ⁸⁶ Sr, and CO ₂) of two end member waters and mixes	

these waters fractionally until the low end member has the same composition for those variables as the high end member. 33

Figure 7. Graph $\delta^{13}\text{C}$ per mil PDB vs. CO_2 (g/L). 34

Figure 8. Well water mixing diagram with $^{87}\text{Sr}/^{86}\text{Sr}$ vs. $\delta^{13}\text{C}$. Plotting the isotopic compositions of the groundwaters produces a similar mixing curve to that of $^{87}\text{Sr}/^{86}\text{Sr}$ vs. CO_2 . This figure suggests that decoupled CO_2 gas is affecting CHM-02 and CHM-03; the other Chimayó wells appear to be mixing with the high CO_2 -brackish water seen at CHM-05. 36

Figure 9. Proposed schematic cross section of area between two Chimayo wells. The cross section proposes a fault between the wells that impedes upwelling CO_2 ; the two wells have identical $^{87}\text{Sr}/^{86}\text{Sr}$ signatures, but significantly different geochemistry..... 38

Figure 10. Map showing locations of the East Seminole and Emma oil fields within the High Plains Aquifer and the Permian Basin. GIS data obtained from Bureau of Economic Geology (2008) and the USGS (2009). 44

Figure 11. Map showing geologic sub-basins and features of the Permian Basin and the immediate area. East Seminole and Emma oil fields are located within the Central Basin Platform. GIS data was obtained from Bureau of Economic Geology (2005). 46

Figure 12. Schematic of injection water mixing procedure at East Seminole oil field. Depths in figure represent the depth where representative formation samples were taken. For the Upper San Andres formation samples at the East Seminole oil field, downhole pressures were between 2200-3500 pounds per square inch (PSI) and the downhole temperatures were between 90-110°F. There is no scale intended for this image as it is just a schematic. Geologic patterns are from the USGS (2006). 50

Figure 13. Schematic column of water bearing formations, hydrocarbon reservoirs, and hydrocarbon source rocks from the Quaternary to the Precambrian in the Central Basin Platform. This figure was generated using information from multiple sources (Bassett and Bradley, 1982; Stueber et al., 1998; Bradley and Kalaswad, 2003; Dutton et al., 2005)..... 56

Figure 14. Stratigraphic column of water bearing formations from the Triassic, Cretaceous and Tertiary beneath Seminole, TX. This column was generated based on written well log descriptions from Cirrus Associates, (2011). Geologic patterns are from the USGS (2006)..... 58

Figure 15. East Seminole oil field sample locations and the formation that produces fluid at each well. Sample names are located next to well symbols..... 62

Figure 16. Map of sample locations at Emma oil field with the sampled formation listed. Sample names are located next to wells symbols. 63

Figure 17. Photograph of author sampling EM-01 with the assistance of Tabula Rasa employee. 64

Figure 18. Schematic depicting the expected flow of supercritical CO₂ after injection at the East Seminole oil field. The production wells produce from a depth of ~5350 ft. Downhole temperature ranges between 90-110°F and downhole pressure ranges from 2200-3300 psi. 77

Figure 19. Mixing models depicting (1) East Seminole produced waters mixing with Ogallala aquifer waters (2) East Seminole produced waters mixing with Santa Rosa Formation water; percentages represent the fraction of solution that is produced water. End members of this figure represent data from this study. 78

Figure 20. Graph displaying the ⁸⁷Sr/⁸⁶Sr vs. the Sr (mg/L) concentration of all samples from Emma and East Seminole Oil Fields. 79

Figure 21. Graph displaying the $^{87}\text{Sr}/^{86}\text{Sr}$ vs. the Sr (mg/L) concentration for produced water samples from this study and the $^{87}\text{Sr}/^{86}\text{Sr}$ of Upper San Andres dolomite and anhydrite leachates from Ruppel and Cander, 1988. Sr concentrations for these leachates are not accurate and were plotted for comparison of $^{87}\text{Sr}/^{86}\text{Sr}$ only. 81

Figure 22. Graph displaying the $^{87}\text{Sr}/^{86}\text{Sr}$ of produced waters in this study and the range of $^{87}\text{Sr}/^{86}\text{Sr}$ of deep-basin brines that lie beneath the Upper San Andres. Data from this study are represented by data points; data from Fisher and Kreitler, 1987 and Stueber et al., 1998 are represented by oval shaped bars. 83

Figure 23. Schematic depicting the proposed migration of Wolfcampian brine into the Upper San Andres formation at the East Seminole oil field. The brine likely followed the same flow path as oil from this source rock. Depths in this figure are approximate current depths based on those seen at the nearby Southwest Andrews area (Stueber et al., 1998). The depths of these formations at the time of migration are unknown. Geologic patterns are from the USGS (2006). 84

Figure 24. Picture of a well (OG-01) and the storage tank that holds water the well produces. .. 86

Figure 25. Map showing the geographic extent of the Middle Devonian Marcellus formation. thickness of the organic-rich portion of the Marcellus Shale. GIS data was obtained from the USGS (2002). 89

Figure 26. Map showing the thickness of the organic-rich portion of the Marcellus Shale in Pennsylvania. GIS data obtained from Pennsylvania Department of Conservation and Natural Resources. 93

Figure 27. Simplified stratigraphy of core and sedimentary sample depths from this study; lithology based on gamma ray log. 100

Figure 28. Flow chart of sequential extraction procedure for sedimentary samples. 102

Figure 29. Flow chart of silicate dissolution procedure before isotopic analysis of silicate-organic residue. 103

Figure 30. Mantle model ages [T_{DM} (Ga)] vs. $^{147}\text{Sm}/^{144}\text{Nd}$. The shale samples from this study plot clearly in the expected range for Devonian-age Appalachian Basin shales. The one limestone sample lies just outside of this range and on the projected pathway of sediments that had rare earth element redistribution. This image is modified from Lev et al., 2008..... 110

Figure 31. Strontium isotopic evolution of limestone residues (blue lines, circles) and shale residues (brown lines, squares). 111

Figure 32. Strontium isotope variations from the Greene and the Clearfield County cores..... 112

Figure 33. Depleted mantle model ages for shale and carbonate residues from the Greene County core..... 114

Figure 34. Neodymium isotope results for Marcellus shale (squares), carbonate (circle) and volcanic ashes (triangles) from this study..... 115

PREFACE

I would like to acknowledge the following individuals for their assistance in this work: Joe Graney and Jason Johnson of the University of Binghamton for providing Marcellus core samples; Jaime Toro of West Virginia University for providing volcanic ash samples; Tabula Rasa Energy Company for allowing me to sample on site and Todd Cox and John Saenz of Tabula Rasa Energy Company for assisting with the sampling process and providing background information about the wells sampled at East Seminole and Emma oil fields. For work done at the East Seminole and Emma Oil fields, I would also like to thank my field work collaborator, Dr. Gwen Macpherson, for field measurements of pH, Eh, temperature, and organic alkalinity that appear in this work. For work done at the Chimayó, NM field area, I would like to acknowledge Daniel Koning for providing unpublished geologic maps and GIS databases of the region, Elizabeth Keating and Julianna Fessenden for background information, and Nancy Kanjorski for assistance with field work and site location. I would also like to thank the Vigil family, Mike Lamb and James Roberts for well access.

It is also important to recognize and thank my committee members, Dan Bain, Ale Hakala, Bill Harbert, and Brian Stewart for their help in developing and editing this dissertation. Brian Stewart deserves extra recognition and credit for much of the Sr and Nd isotope data for my samples, which he ran on the TIMs, and for acting as a second advisor and providing additional guidance to my research.

A special thank you is due to my graduate advisor, Rosemary Capo, without whose support none of this would have been possible. Aside from the guidance she has given, which has shaped this dissertation, she has also run many of my samples for Sr and Nd isotope data on the TIMs. I greatly enjoy my work as a geologist and I credit her guidance with my professional development.

I would also like to thank members of the Capo-Stewart lab group who contributed to this study. These members include: post-doctoral researchers Andy Wall, for his assistance running the multi-collector ICP-MS for Sr isotope ratios, and Thai Phan, for his assistance running the ICP-MS for elemental concentrations; former graduate student Elizabeth Chapman and current graduate students Courtney Kolesar and Sarah Lavin for their feedback and assistance with lab procedures; and a long list of undergraduate workers who cleaned bottles, prepared samples, or assisted me in some other fashion: Megan Achilles, Emily Burt, Kelly Flannery, and Katherine Roll.

This work was supported by grants from the U.S. Department of Energy as well as the Oak Ridge Institute for Science and Education Fellowship.

Dedication

This work is dedicated to my family, large and small, but especially to my mother, Ann, my sister, Christine, and Djuna, for their unwavering support.

1.0 INTRODUCTION

Geologic carbon storage and unconventional gas drilling are both activities that change the physical and chemical state of the geologic formations that they target. Both cause increases in formation pressure that can result in the displacement of deep-seated brines and an increase in formation porosity and permeability. These brines have the potential to travel along porous pathways and interact with adjacent or overlying fluids. Aside from the physical changes in the formation, the formation can dissolve and new minerals can precipitate. The reactions that occur between the anthropogenic fluids and the overlying seal rock are also important, as this seal rock provides the pressure necessary for successful carbon storage and recovery of hydrocarbons. If seal rock integrity is compromised, the result could be a permeable pathway for upward fluid migration.

Detecting movement of deeper waters into shallow aquifers may be possible with isotopic characterizations of deep reservoir water, the shallower groundwaters, and the rock formations that hold these waters. Formation isotopic composition can also be used to understand the formation's depositional history. Developing a more comprehensive understanding of the origin of sediments and the post-depositional history for a hydrocarbon reservoir could aid in depositional models and impact future fossil fuel exploration. The application of Sr to target formations for carbon sequestration can provide insight into potential fluid-rock interactions and mixing of displaced fluids, while the application of Nd isotopes to unconventional reservoirs,

such as the Marcellus shale, can provide an insight into how such a unique unit was deposited and the diagenetic and thermal events that followed its deposition.

1.1 GEOLOGIC CO₂ SEQUESTRATION

One of the key issues in the feasibility of CO₂ sequestration is the storage permanence of CO₂ once it is injected into a deep subsurface reservoir. In order to be an effective greenhouse gas mitigation strategy, almost all of the sequestered CO₂ (>99%) would have to stay in the targeted reservoir formation (Hebson and Gobble, 2005). In order to attain the DOE's goal of 99% storage permanence, the CO₂ that is injected must stay in the storage formation either by mineralization, structural traps, or the presence of stratigraphic seal rocks overlying the formation (Griffith et al., 2011; DOE 2012). The latter two types of traps represent physical barriers to fluid migration, while mineralization would rely on chemical reactions within the reservoir to ensure storage permanence. The ability to sequester CO₂ permanently relies heavily on understanding how CO₂-fluids will affect these physical and chemical traps.

Adding to the complexity of sequestration is that once CO₂ reaches a certain pressure and temperature, it transforms to a supercritical fluid instead from the gas phase typical at surface pressure and temperature. The Earth's subsurface usually exceeds this pressure (72.9 atm) and temperature (31.1°C) at depths exceeding approximately 2600 ft (DOE, 2012). The fluid dynamics of supercritical CO₂ dictate its movement through a formation and the storage capacity of a formation. Once injected, buoyant supercritical CO₂ will sit on top of native formation water and migrate upslope beneath the cap rock and can become trapped by two fluid dynamic related processes: (1) capillary trapping and (2) solubility trapping. As the plume of CO₂ travels,

capillary trapping will hold residual CO₂ in the pore space of the formation. The buoyant plume will also begin to dissolve into the native reservoir water beneath it and the resulting solution sinks to the bottom of the formation, as it is denser than the original native water (Szulczewski, 2012). CO₂ that does not dissolve into the native reservoir water will remain buoyant and could flow out of the target reservoir via permeable pathways (Birkholzer et al., 2011).

While understanding the physical principles of supercritical CO₂ allows prediction of how CO₂ travels in the formation, chemical reactions involving CO₂-fluids and the overlying seal rock may also create permeable pathways that could act as conduits to buoyant CO₂. Previous work has shown that CO₂-induced dissolution of calcite and iron hydroxide minerals could create pathways through seal rocks for upwelling CO₂ and other fluids at sequestration sites (Kharaka et al., 2006a, 2006b, 2009). The effects of this upwelling CO₂ on an aquifer could be negative, as increased CO₂ has been shown to lower pH, increase the total dissolved solid (TDS) levels, and mobilize metals (Kharaka, 2010). Some of the previous research on the geochemical effects of upwelling CO₂ on groundwater have involved experimental test fields where CO₂ has been injected on a short time scale (days-years) into a shallow aquifer. Experimental work has shown that natural analogs sites may display more long term geochemical reactions than lab work meant to simulate those conditions (Pearce et al., 1996). Natural analog sites offer the opportunity to study the long term effects of upwelling CO₂ on groundwaters where CO₂ has been upwelling into the aquifer on geologic time scales (Evans et al., 2004).

1.1.1 Natural Analogs for CO₂ Sequestration

Natural analog sites for CO₂ sequestration are sites with large accumulations of CO₂ in a geologic formation. They are located in various regions throughout the world, but are often

associated with geothermal activity, like the Bravo Dome in the Rio Grande Rift (Pearce et al., 1996). While some of these formations do not release CO₂ into overlying strata, others are leaking CO₂ (Stevens et al., 2001a). This release of CO₂ can occur via natural pathways like low permeability faults or caprocks, as well as along anthropogenic boreholes (Shipton et al., 2004; Evans et al., 2004). These sites where CO₂ is being released are natural analogs for leaking geologic storage reservoirs; in the remainder of this dissertation, the phrase ‘natural analog’ will refer to only those leaking reservoirs.

Previous work on natural analog sites has included analysis of major ion concentrations and stable isotopic compositions for surface and groundwaters (Evans et al., 2004; Keating et al., 2010). This work has constrained possible flow paths of upward migrating fluids and modeling of potential chemical reactions occurring. For example, in Chapter 2, ⁸⁷Sr/⁸⁶Sr ratios are used to complement geochemical and stable isotope (δ¹³C) data in further developing the understanding of CO₂ migration pathways and testing the viability of ⁸⁷Sr/⁸⁶Sr as a monitoring tool for CO₂ leakage.

1.1.2 CO₂ Enhanced oil recovery

CO₂ enhanced oil recovery (EOR) is known as a miscible flooding technique. When CO₂ is injected into a formation, it forms a homogeneous solution with oil still present in the reservoir (Thomas, 2008). The process results in a solution that is less viscous than normal oil and a recovery of 5 to 20% of the original oil in the formation (Stevens, 2001b). In 1972, SACROC oil field in the Permian basin was the first site to apply CO₂ enhanced oil recovery techniques. This

technique has become common in the Permian basin, which has more than 60 active CO₂ EOR fields (Tenaska, 2011).

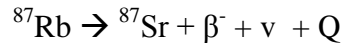
The use of supercritical CO₂ for enhanced oil recovery is an economically viable method of CO₂ sequestration (Stevens et al., 2001b). The seal rocks that kept the oil in place act as barriers to upward CO₂ migration.

1.2 BLACK, ORGANIC-RICH SHALE DEPOSITION: SEDIMENT SOURCE AND POST-DEPOSITIONAL HISTORY

Although black, organic-rich shales are an important part of current domestic energy production, there remain important questions regarding their deposition and post-depositional history. The sediment source and burial history may have an effect on a formation's characteristics, such as its porosity and the type of natural gas which it produces. The Middle Devonian Marcellus shale is one of the many black, organic-rich shales that have attracted exploration companies interested in extracting its natural gas. The characteristics of the Marcellus Formation vary across its areal extent, including quality and quantity of natural gas that the formation produces (Milliken et al., 2013). The sediment source and post-depositional history may have some effect on these varying characteristics. Gaining insight into the sediment source and the post-depositional history of the Marcellus Formation will enhance our understanding of how deposition occurred on a localized level and how black, organic-rich shale deposition occurs in general.

1.3 STRONTIUM ISOTOPE SYSTEM

$^{87}\text{Sr}/^{86}\text{Sr}$ isotopes of a groundwater or lithologic unit provide insight into the water or the rock's strontium source. Strontium has four stable isotopes: ^{84}Sr , ^{86}Sr , ^{87}Sr , and ^{88}Sr . Only one, ^{87}Sr , is formed by a radioactive decay process, which occurs when ^{87}Rb decays to ^{87}Sr through the beta-decay process (Shand et al., 2009):



In this equation the variables represent a beta particle (β^-), an anti-neutrino (ν), and the decay energy (Q) (Faure and Mensing, 2005).

Although ^{87}Rb has a half-life of 48.8 billion years, ^{87}Rb decay will enrich nearby rocks with a measurable amount of ^{87}Sr . Potassium bearing minerals have high Rb concentrations, which results in the rock surrounding these minerals to have an elevated ^{87}Sr . Because of this, rocks with high potassium bearing mineral contents, like granites, will also have high $^{87}\text{Sr}/^{86}\text{Sr}$ ratios (Gosz and Moore, 1989). The two most important factors that contribute to a rock's $^{87}\text{Sr}/^{86}\text{Sr}$ is its original rubidium concentration and its age, as older rocks with high rubidium concentrations tend to have the highest $^{87}\text{Sr}/^{86}\text{Sr}$ ratios (Graustein, 1989).

1.3.1 Sr isotopes applied to water-rock interaction

Determining the degree of mixing that is occurring in a subsurface system offers many challenges. Proximal waters, whether lateral or horizontally adjacent, may be separated by an impermeable layer or may be in communication via a porous fault or dissolved calcite vein. Geochemical and trace element data can help characterize and classify a water, but certain elemental similarities may obscure any evidence of mixing.

Strontium isotopes provide the opportunity to better document mixing and dissolution reactions when there are distinct $^{87}\text{Sr}/^{86}\text{Sr}$ ratios in the study area. The $^{87}\text{Sr}/^{86}\text{Sr}$ ratio of a groundwater reflects the geologic source of strontium (Gosz and Moore, 1989) and the strontium signature of a water is dependent upon its history of rock interaction as well as its history of mixing with other subsurface waters. When a water comes into contact with a rock unit, mineral dissolution or ion exchange reactions can pass the $^{87}\text{Sr}/^{86}\text{Sr}$ of the rock onto the water (Frost and Toner, 2004).

A modern day example is the ocean, which has a $^{87}\text{Sr}/^{86}\text{Sr}$ of ~ 0.7092 . This value is higher than the average of its two main inputs, hydrothermal fluids from oceanic vents (~ 0.703) and global river water (~ 0.711) because the strontium flux from the river water is a larger fraction of flux to the ocean (Veizer et al., 2003). The ability to identify unique strontium sources allows strontium isotopes to characterize potentially occurring chemical reactions, like dissolution of carbonates, and also to quantify the contributions of waters with distinct $^{87}\text{Sr}/^{86}\text{Sr}$ ratios to the resulting mixture. Strontium isotope ratios may be reset or fractionated by sedimentary cycle occurrences, such as fluid alteration or metamorphism, which is why the more robust Sm-Nd system, with rare earth elements more resistant to chemical weathering, can be used to complement Rb-Sr data well.

Strontium isotope mixing models are used in Chapters 2 and 3 of this work. These mixing models produce the $^{87}\text{Sr}/^{86}\text{Sr}$ and Sr concentration of a solution based on two end member mixing. The two end members have distinct $^{87}\text{Sr}/^{86}\text{Sr}$ values and Sr concentrations that are used to indicate the degree of mixing that has occurred between the two end members. The mixing model in Chapter 2 creates a mixing curve using CO_2 concentration as well as $^{87}\text{Sr}/^{86}\text{Sr}$ and Sr concentrations. This mixing curve uses strontium isotopes to accurately depict mixing that is

occurring in the aquifer between high CO₂, high TDS waters and low CO₂, low TDS waters. The mixing model in Chapter 3 depicts how the ⁸⁷Sr/⁸⁶Sr of groundwaters would change if they were mixed with produced waters from an underlying oil reservoir. Overall, this work displays that isotope mixing models can accurately represent mixing that is happening now and that they can also be used to model future scenarios.

1.3.2 Sr isotopes applied to lithologic depositional history

Strontium isotopes of the bulk composition of a rock are indicative of the strontium that was available around the rock when it formed. This has allowed for extremely informative work that resulted in the creation of a ⁸⁷Sr/⁸⁶Sr curve for Phanerozoic waters and modeling of the formation of modern continental crust (Burke et al., 1982; Godderis and Veizer, 2000). Since the ⁸⁷Sr of a rock is always increasing due to decay of ⁸⁷Rb, the ⁸⁷Sr/⁸⁶Sr value of any rock must be corrected for time in order to accurately identify the isotopic ratio at the time of the rock's deposition (Faure and Mensing, 2005):

$$^{87}\text{Sr}/^{86}\text{Sr} = (^{87}\text{Sr}/^{86}\text{Sr})_0 + (^{87}\text{Rb}/^{86}\text{Sr}) * (e^{\lambda t} - 1)$$

In this equation, ⁸⁷Sr/⁸⁶Sr is the modern isotope signature, (⁸⁷Sr/⁸⁶Sr)₀ represents the ⁸⁷Sr/⁸⁶Sr at the time of mineral formation, ⁸⁷Rb/⁸⁶Sr is the modern concentration of these isotopes, λ is the decay constant, and t is the time since deposition. This method can be applied to rocks where the time of deposition can be constrained stratigraphically or with another dating method.

However, if the rock lost or gained Rb or Sr over time after deposition, the calculated value for ⁸⁷Sr/⁸⁶Sr at the time of mineral formation would be skewed. For example, when a metamorphic event or a fluid flow event affects a rock, its concentration of rubidium and strontium can be affected. Metamorphic activity, specifically hydrothermal fluid migration

related to metamorphic activity, has been shown to preferentially mobilize Sr relative to Rb from the rock formation. This Sr mobilization increases the ratio of Rb/Sr and the $^{87}\text{Sr}/^{86}\text{Sr}$ (Evans, 1991). If hydrothermal fluid-rock interactions did occur post-deposition, the estimated $^{87}\text{Sr}/^{86}\text{Sr}$ at the time of deposition should be elevated to levels above those of natural sedimentary depositional fluxes. The sensitivity of bulk rock measurements of $^{87}\text{Sr}/^{86}\text{Sr}$ to post-depositional processes makes it an important tool in interpreting the evolution of a rock's geochemical history.

1.4 NEODYMIUM ISOTOPE SYSTEM

1.4.1 Nd isotopes applied to lithologic depositional history

Neodymium and samarium are both rare earth elements that are incorporated into a rock during mineral crystallization. Rare earth elements are more resistant to weathering and diagenetic alteration than the Rb-Sr system, which means it is more likely that Sm-Nd isotopic values will reflect the time of mineralization (Faure and Mensing, 2005). Samarium has seven isotopes and one of them, ^{147}Sm , decays to ^{143}Nd via α (alpha) emission:



In this equation, E is the decay energy. The half-life of ^{147}Sm has is 106 billion years.

Based on the half-life and measurements of current Sm-Nd isotopes of the rock sample, the approximate time of mineral crystallization can be calculated:

$$^{143}\text{Nd}/^{144}\text{Nd} = (^{143}\text{Nd}/^{144}\text{Nd})_0 + (^{147}\text{Sm}/^{144}\text{Nd})_0 * (e^{\lambda t} - 1)$$

In this equation, $^{143}\text{Nd}/^{144}\text{Nd}$ and $^{147}\text{Sm}/^{144}\text{Nd}$ are the current isotopic values of the rock, $(^{143}\text{Nd}/^{144}\text{Nd})_0$ is the signature at the time of mineralization, λ is the decay constant, and t is the time of crystallization or deposition. Despite the robust nature of the Sm-Nd system, post-depositional fluid-rock interactions have been known to affect the distribution of these rare earth elements and in the case of some Appalachian shales, elevate $^{147}\text{Sm}/^{144}\text{Nd}$ (Lev et al., 2008). This change in $^{147}\text{Sm}/^{144}\text{Nd}$ would alter the modern measured Sm-Nd isotope values and the estimated time of crystallization or deposition, which is based on the following model mantle age equation (DePaolo, 1981):

$$T_{\text{DM}} = (1/\lambda) * \left[\frac{1 + \left[\frac{(^{143}\text{Nd}/^{144}\text{Nd})_{\text{Measured}} - (^{143}\text{Nd}/^{144}\text{Nd})_{\text{CHUR}}}{(^{147}\text{Sm}/^{144}\text{Nd})_{\text{Measured}} - (^{147}\text{Sm}/^{144}\text{Nd})_{\text{CHUR}}} \right]}{1} \right]$$

T_{DM} is the mantle model age in this equation and ‘CHUR’ refers to the ‘chondritic uniform reservoir’ reference standard. The $^{143}\text{Nd}/^{144}\text{Nd}$ values of chondritic meteorites are fairly homogeneous and have not been affected by magmatic processes, making their average $^{143}\text{Nd}/^{144}\text{Nd}$ value an appropriate reference standard.

Sm-Nd isotope data is also reported in this study using reported using epsilon (ϵ) notation:

$$\epsilon_{\text{Nd}}(T) = \left[\frac{^{143}\text{Nd} / ^{144}\text{Nd}_{\text{sample}}(T)}{^{143}\text{Nd} / ^{144}\text{Nd}_{\text{CHUR}}(T)} - 1 \right] 10^4$$

Here T is the age of crystallization or deposition, and CHUR is the chondritic uniform reservoir, thought to represent bulk Earth values. Post-depositional water-rock interaction that disturbed the Sm/Nd ratio would be reflected in T_{DM} and $\epsilon_{\text{Nd}}(T)$ values that would reflect the age of disturbance rather than the age of initial mantle crystallization.

1.5 RESEARCH OBJECTIVES AND APPROACH

Natural isotope tracers have been used to characterize fluid-rock interaction in geologic environments and to determine the origin of dissolved solids in ground and surface water systems. Through analysis of waters from monitoring wells, natural isotope tracers can be an important complement to standard geochemical and geophysical tools used to track groundwater movement or CO₂ migration, and use of natural tracers avoids potential issues that can arise with an introduced tracer (Davis et al., 1980). Radiogenic natural isotopes, like Sr, have been used to identify groundwater inputs and to quantify the contribution of groundwater, brine, seal rock and aquifer interactions in short term water-rock interactions (Banner, 2004; Choi et al., 2010).

Radiogenic natural isotopes, like Nd and Sr, of bulk rock compositions have been used to identify sediment sources and post-depositional events, which are both related to long-term geologic activity (Nelson and DePaolo, 1988; Lev et al., 2008). Overall, this study applies both Sr and Nd to understand short-term and long-term subsurface rock and fluid interactions, including brine migration and post-depositional disturbances. Specifically, the goals of this study are (1) to apply Sr and C isotopes to understand how upwelling CO₂-fluid interacts with a shallow aquifer, (2) to analyze the Sr isotopic composition of a set of formations and test its feasibility as a monitoring tool for CO₂ leakage, and (3) to apply Sr and Nd isotopes to a formation containing black, organic-rich shales in order to gain a better understanding of its sediment source and depositional history.

1.6 ORGANIZATION OF THIS DISSERTATION

This study is focused on the use of Sr and Nd isotopes to track water-rock interactions that occur both on a short time scale, like salinization of an aquifer, and on the geologic time scale, like post-depositional metamorphism. This study investigates diverse geologic settings in order to assess the viability of these isotope systems in varying conditions. Results from this study are presented in Chapter 2, Chapter 3, and Chapter 4.

The first part of this dissertation centers on the application of Sr isotopes as a natural tracer of potential CO₂ leakage impacts to a shallow groundwater aquifer (Chapter 2). This section focuses on a field area with naturally occurring high CO₂ groundwaters in Chimayó, New Mexico. The CO₂ migrates into the aquifer from depth via fractures and faults due its geologic setting within the Rio Grande rift. This upwelling CO₂ makes this a natural analog site for the waters that overlie a leaky geologic carbon storage reservoir. Water samples and lithologic samples help document interactions between deeply sourced upwelling CO₂-fluids and the Tertiary aquifer. This chapter shows that Sr isotopes are extremely sensitive to the intrusion of deep-sourced saline waters, and could be a sensitive monitor of brine displacement by CO₂ injection.

The second part of this dissertation is a site characterization of a water flooded enhanced oil recovery (EOR) field in the East Seminole oil field that will be transitioning to an active CO₂-based EOR site (Chapter 3). Waters were sampled from the producing formation at East Seminole and the groundwaters that lie above the area where active CO₂ injection will take place. Geochemical and Sr isotope characterization of produced waters and overlying groundwaters at East Seminole will allow determination of the feasibility of using Sr isotopes as

a monitoring and verification tool at this particular site. They also will provide insight into the evolution of produced water over time.

The third part of this dissertation involves application of Sr and Nd isotopes to the sediment sources and post-depositional history of Middle Devonian Marcellus Formation samples. This study focuses on determining where Marcellus sediment originated from and what, if any, metamorphism or fluid migration affected the limestone and shale core samples from Pennsylvania and New York that span the Middle Devonian (Chapter 4).

2.0 SR ISOTOPE TRACKING OF CO₂ SOURCE AND MIGRATION PATHWAYS AT A NATURAL ANALOG SITE FOR GEOLOGIC CARBON STORAGE: CHIMAYÓ, NEW MEXICO

2.1 INTRODUCTION

In response to concerns that anthropogenic emissions of greenhouse gasses are spurring climate change, there has been an increased focus on the capture and storage of carbon dioxide (CO₂) in geologic formations. This process involves the injection of supercritical CO₂ into geologic formations such as oil and gas reservoirs, saline formations, or unmineable coal seams (Plasynski et al., 2009). The feasibility of this strategy relies on our ability to understand the effects of high-CO₂ fluids on both the storage formation and the impermeable rocks that form natural barriers to fluid migration. Although experimental work has documented potential mineralization processes (Kaszuba et al., 2005), other work suggests that host rock mineral dissolution or well-bore cement dissolution could create pathways for CO₂ migration from depth to overlying geologic units (Kharaka et al., 2006a). Impermeable rocks capping geologic carbon-sequestration reservoirs could also react with supercritical CO₂, potentially compromising the integrity of the seal rock (Kaszuba et al., 2003). Seal rock failures and mineral dissolution reactions could create potential migration pathways to local shallow aquifers serving as domestic and industrial water sources. This migration of CO₂ could result in the dissolution of carbonates and other aquifer

minerals, changes in pH, and ion-exchange reactions that could mobilize toxic trace metals such as uranium, arsenic and lead (Kharaka et al., 2010; Zheng et al 2009). The ability to monitor these reactions will allow us to detect groundwater impairment and identify that upwelling CO₂ is the cause of this impairment.

The successful storage of anthropogenic CO₂ in geologic formations requires sensitive monitoring of the geochemical and mineralogical interactions of storage units, their formation waters, and associated aquifers and brines potentially affected by injection of supercritical CO₂. Naturally occurring high CO₂ groundwaters can serve as analogs for post-CO₂ injection conditions, providing sites to develop and optimize geochemical tools that rapidly detect potential migration of CO₂ affected waters. Additionally these sites can quantify the contribution of groundwater, brine, seal rock, and aquifer interactions related to the injection of supercritical CO₂. Through analysis of waters from monitoring wells, trace element and isotopic systems can identify changes spurred by injection of supercritical CO₂, including changes in processes such as dissolution or precipitation reactions and the migration of brines.

Chimayó, New Mexico is a natural analog site that displays the potential effects of high concentrations of CO₂ on groundwater. Work by Cumming (1997) and Keating et al. (2010, 2011, 2013) shows the area is a site of long-term water-CO₂-rock interaction, including deep-sourced brines, CO₂ from non-hydrothermal sources, and shallow aquifers. Additionally, groundwaters of the Tertiary age Tesuque aquifer exhibit signs of long-term exposure to CO₂ infiltration. As a result, many residents of Chimayó have switched over to a community water system and abandoned their private wells (Cumming 1997). The impaired groundwater in the region is believed to be the result of the mixing of shallow groundwater with high CO₂-saline fluids that migrate along faults and fractures that cross-cut the region (Cumming 1997; Grauch,

2009; Keating et al., 2010).. Waters in the region can have elevated levels of dissolved CO₂, including a geysering well with 1.8 g/L CO₂. This study combines isotopic and geochemical characterization of local groundwater with sequential chemical extraction experiments on aquifer sediments, enhancing characterization of subsurface chemical reactions and groundwater mixing processes occurring in this natural analog system.

Natural isotope tracers are an important complement to standard geochemical and geophysical tools used to track CO₂ migration through analysis of waters from monitoring wells. In situations where the public does not want a tracer introduced to the groundwater system, the use of naturally-occurring isotope signatures to detect CO₂ migration could be preferable to the use of an introduced tracer such as chlorofluorocarbons (CFCs) (Hinkle and Snyder, 1997). Natural isotope tracers are already present in some geologic settings and are a viable alternative to introduced geochemical tracers. If there are variations between the natural isotope ratios of shallow groundwaters and deep, upwelling fluids, natural isotope tracers have the potential to be a valuable tool for scientists monitoring the safe storage of CO₂.

Variations in natural isotope ratios have successfully identified groundwater inputs and quantified the contribution of groundwater, brine, seal rock, and aquifer interactions at other sites (Banner 2004). For example, light stable isotope systems (e.g., oxygen, hydrogen, carbon) have illustrated changes in processes such as dissolution or precipitation of carbonate cements in response to CO₂ injection (Lewicki et al, 2013; Wilkinson et al. 2009), and migration of brines into adjacent aquifers due to supercritical CO₂ injection (Kharaka et al., 2006a, 2006b, 2009). Recently the combination of light stable isotope systems with naturally-occurring noble gas isotopes (e.g., helium, neon, argon) have served as a tracer of CO₂ migration at natural analog sites (Gilfillan et al., 2011; Lollar and Ballentine, 2009).

To date, there are limited studies exploring the application of strontium (Sr) isotopes to monitoring subsurface reactions related to carbon sequestration (Quattrocchi et al., 2006). Ultimately, the use of natural multi-isotope systems can enhance our understanding of short and long-term risk assessment at geologic storage sites. Furthermore, these systems can aid in the development of new geochemical tools necessary for long term monitoring of CO₂ storage permanence. In this study, we apply Sr and carbon (C) isotopes to identify deep and shallow groundwater-brine-CO₂ interactions at a naturally high CO₂ system in the Rio Grande Rift area near Chimayó, NM in the southwestern U.S.

This study addresses issues critical to the long-term storage of CO₂ in geologic formations such as (1) the relationship between high-CO₂ fluid-rock interaction and aquifer water quality, (2) mechanisms involved in the transport of dissolved CO₂ into shallow aquifers, and (3) the migration of deep brines displaced by CO₂. Dissolved CO₂ and other chemical species such as chloride vary significantly in the region (Keating et al. 2010, 2011); this study uses a multi-isotope approach to identify the sources of shallow groundwater, brine, and CO₂ in the Chimayó area in order to explain some of this geochemical heterogeneity. We also examine the relevant lithologic units to consider mineral scale water-rock interactions. This work involved both petrologic characterization and fluid-rock leaching experiments. The goals of this investigation are to (1) quantify the extent of interaction and mixing between deep-sourced CO₂-bearing brackish waters and aquifer groundwater (2) identify and quantify processes of water-rock interaction associated with CO₂ introduction; and (3) test the sensitivity of Sr and C isotopes as a monitor for CO₂ containment during geologic carbon injection and storage through early detection of CO₂ leakage and brine migration.

2.2 GEOLOGY AND HYDROGEOLOGY OF THE ESPAÑOLA BASIN

The town of Chimayó is located in north-central New Mexico and is approximately 95 kilometers (km) northwest of Albuquerque, New Mexico. The Tesuque aquifer was once a source of drinking water for the town's residents, but due to concerns about the overall quality of the water, many residents have switched to a community water system and abandoned their private wells (Cumming, 1997; Keating et al., 2010). The Tesuque Formation, which holds the aquifer of the same name, is located in the Española basin, a basin created as a result of the Rio Grande rift. The Rio Grande Rift is an extensional geologic feature that spans over 1,000 km from Colorado to Mexico and was created during two phases of extension in the Oligocene (30 Ma) and the Miocene (10-16 Ma) (Keller and Baldrige, 1999). The Rio Grande Rift is active and widens the rift zone ~2.5 cm every 40 years (Kelly, 2012). The eastern margin of the Española basin is marked by the Sangre de Cristo Mountains and late Cenozoic high angle faults that penetrate Tertiary basin fill and Precambrian basement rocks (Vernon and Riecker, 1989). Previous work suggests these high angle faults may act as conduits for deeply sourced CO₂ (Cumming, 1997; Keating et al., 2010).

The Tesuque formation is a basin fill deposit created by Neogene uplift and erosion of Precambrian-aged sediments from Sangre de Cristo Mountains (Galusha and Blick, 1971; Keller and Baldrige, 1999). This formation is dominated by alluvial-fluvial units, but also contains some lacustrine and ash tuff layers (Cavazza, 1986). Earlier literature divided the Tesuque Formation into five subcategories (Galusha and Blick, 1971), however this study will use the two subcategories defined by Cavazza, 1986.

The two main sedimentary units within the Tesuque Formation are defined as Lithosome A and Lithosome B. While most of the sediments in these two units originate from the erosion of

igneous and metamorphic Precambrian rocks of the Sangre de Cristo Mountains, they differ both mineralogically and petrologically. Lithosome B has a higher lithic content and those lithics have a higher volcanic content ($L_v/L=0.62$) in Lithosome B than those from Lithosome A ($L_v/L=0.18$) (Cavazza 1986).

Stratigraphically, the Tesuque formation lies unconformably atop Pennsylvanian carbonate strata and Precambrian basement rocks. The basal layer of the Tesuque Formation is composed of coarse- to fine-grained arenite sandstones (65-82 ft thick) which grade upward into the arkosic sandstones (QFL: 55% quartz, 38% feldspars, and 7% lithic fragments) that dominate the aquifer (Cavazza, 1986). These arkosic sandstones are then divided into the two units previously discussed, Lithosome A and Lithosome B. Displacement caused by the abundant number of faults throughout the study area, in addition to the intertonguing of these two units throughout the Tesuque aquifer, allows wells of the same depth to tap into different lithosomes within the 6 km² study area (Figure 1).

Tesuque formation beds dip at low angles to the west and groundwater flows as it flows from east to west as it generally follows the direction of the dipping beds (Figure 2; Frenzel 1995). Precipitation in the region ranges from 20-64 cm/yr depending upon elevation, and the aquifer is predominantly recharged through the Sangre de Cristo Mountains (Keating et al., 2010).

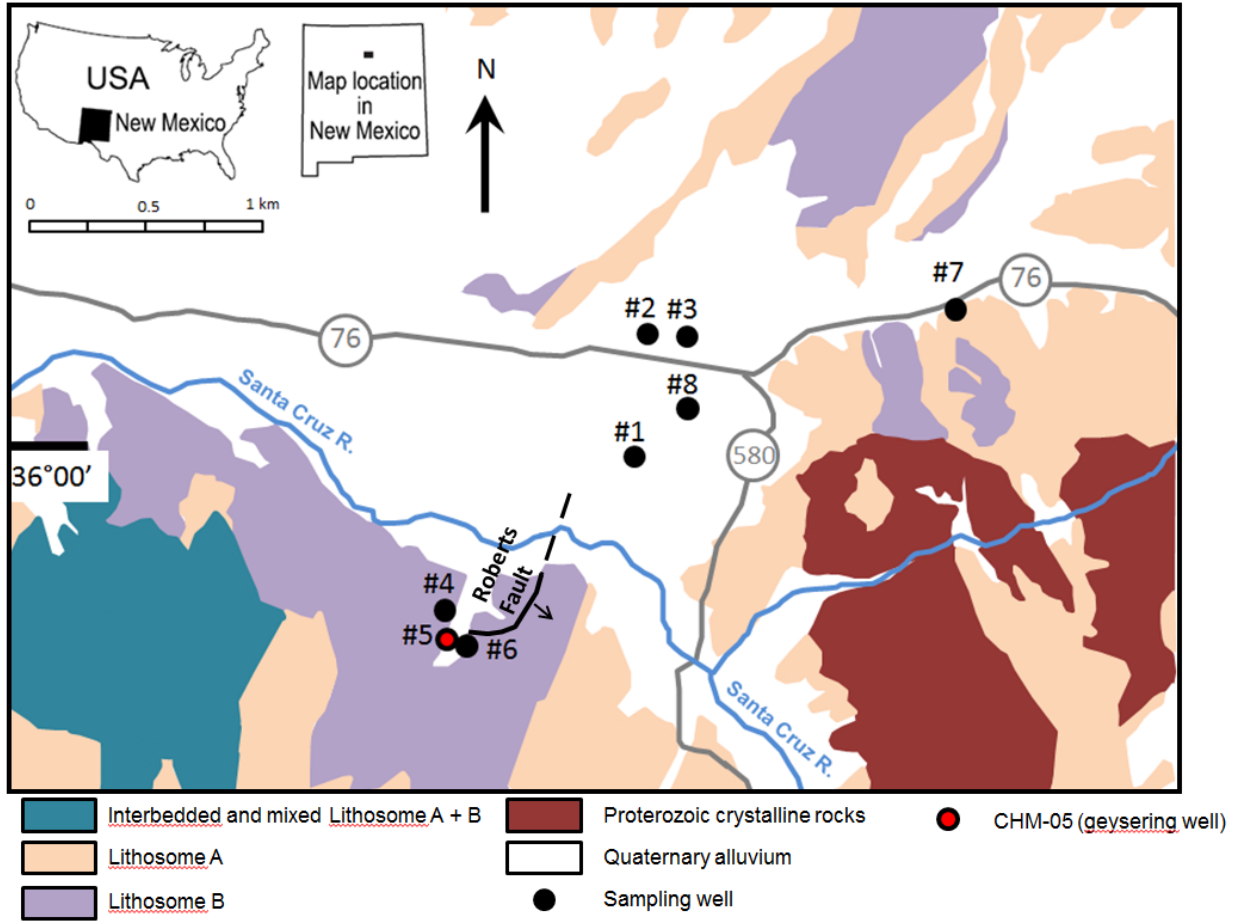


Figure 1. Geologic map of Chimayo, NM with sample well locations and major roadways identified; modified from Keating et al., 2010.

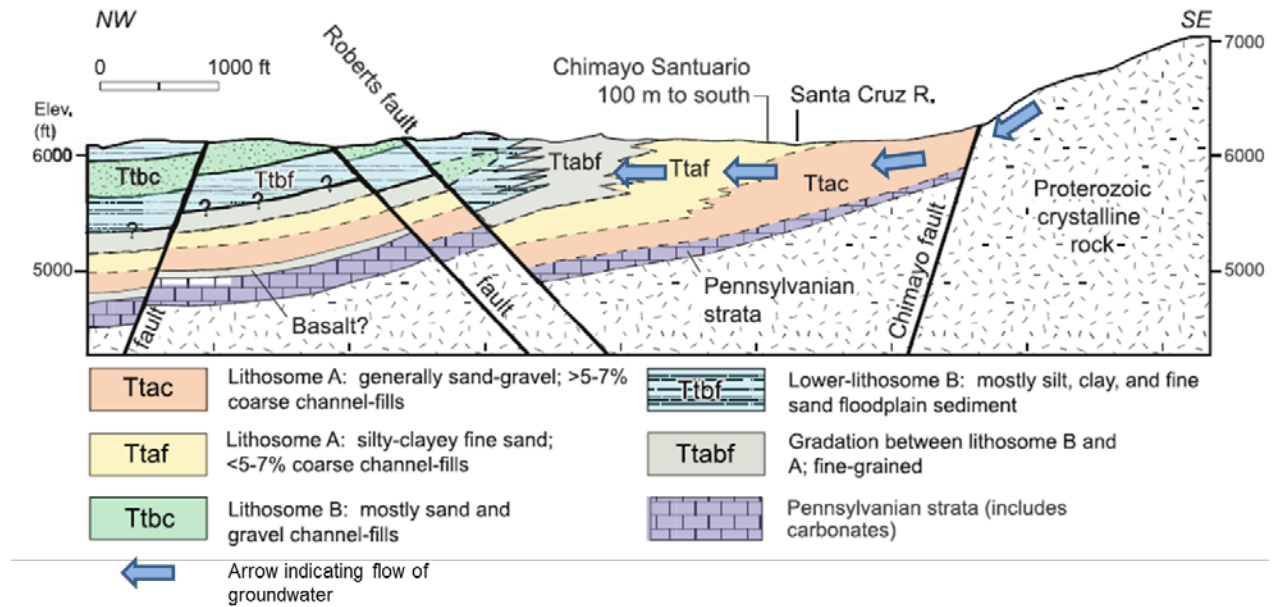


Figure 2. Cross section of the Chimayo region; image modified from Keating et al., 2010, which was based on previous work (Koning et al. 2002; Koning 2003).

2.3 SAMPLE COLLECTION AND ANALYTICAL TECHNIQUES

2.3.1 Water samples

Water samples were taken in August 2009 from home wells and irrigation wells in Chimayó, New Mexico. Most of the water was collected at outdoor spigot heads, but three of the well waters were retrieved using a bailer. At all sites, samples were not collected until both water pH and temperature values stabilized. Alkalinity measurements were made in the field using a Hach digital titrator. Samples were filtered using a 0.45 micron filter, stored in acid cleaned polypropylene bottles, and acidified within eight hours after collection.

2.3.2 Rock samples

Samples, representative of Lithosomes A and B of the Tesuque Formation, were collected from road cuts and river cut banks (Keating et al., 2010). Samples of Paleozoic limestone were collected from outcrops at Nambé Falls, 17.9 km south of the Chimayó town center.

2.3.3 Sequential extraction techniques

Lithosome samples were crushed using a rock hammer, passed through a 2 mm sieve, and separated using a splitter. Approximately 2 g of sample were weighed and then subjected to a sequential extraction process modified from that of Spivak-Birndorf et al., 2012. Exposure to a water leach removed water-soluble lithologic components, primarily sulfates and salts, from lithosome samples. Next, an ammonium acetate (pH buffered ~ 8.14) step leached exchangeable cations from clays. Finally, a 4% acetic acid leach targeted carbonate material within the sample.

Non-weathered surfaces of Paleozoic limestones were obtained by using a rock crusher to halve the rock 7-8 times until a chemically unaltered piece of limestone was produced. The non-weathered piece of limestone was then crushed using a rock hammer, passed through a 2 mm sieve, and separated using a splitter. Approximately 0.1 g of sample was dissolved with 4% acetic acid.

2.3.4 Geochemical analysis

Unfiltered samples for anion determination were kept on ice or refrigerated until analysis by ion chromatography (IC) at NETL-Pittsburgh. IC QA/QCs included multiple runs of samples, each

set returning a percent deviation of less than 1%, and matrix spikes. Samples for elemental analysis were filtered in the field using 0.45 micron filters and acidified at the Los Alamos National Laboratories within eight hours of collection, and subsequently analyzed at NETL-Pittsburgh using a Perkin Elmer Optima 3000 ICP-OES. QA/QCs for the ICP-OES samples included duplicates to test the reproducibility of the sample analyses, as well as spikes that exhibited a recovery percentage of greater than 95%, except for Cr (92.3%) and Cu (89.1%). CO₂ measurements used in this study came from samples that were immediately capped and stored in clean, 200-mL plastic bottles and analyzed for dissolved CO₂ using a CarboQC (Anton Paar), using methods discussed in Vesper and Edenborn (2012).

Saturation indices for the well waters were determined using PHREEQc (USGS, 2002). PHREEQc is a low temperature, aqueous geochemistry modeling program designed by the United States Geological Survey. One of the basic functions of the PHREEQc modeling program is the generation of saturation indices (SI) for given solutions (USGS, 2002). A saturation index describes whether a water is undersaturated or supersaturated with respect to a certain compound or mineral. The goal of modeling this system is to gain a better understanding of the groundwater-rock dissolution-precipitation reactions in the Tesuque aquifer. A key variable in this specific system is the influence of CO₂. The concentration of CO₂ may have an influence on the saturation indices of many minerals, but especially carbonate minerals that are more susceptible to dissolution, like calcite (CaCO₃) and siderite (FeCO₃).

2.3.5 Strontium isotope analysis

For groundwater and leachate samples, aliquots were taken from samples so that ~5 µg of Sr was collected. These aliquots were then placed in Teflon-vials and evaporated to dryness in a high-efficiency particulate air-filtered hood. Dried samples were redissolved in 3 M HNO₃ and then passed through a SrSpec resin under clean lab conditions (Moody, 1982).

All ⁸⁷Sr/⁸⁶Sr isotopic compositions were determined using a Finnigan MAT 262 thermal ionization mass spectrometer at the University of Pittsburgh. Each sample was measured for a total of 100 ratios.

2.4 RESULTS

2.4.1 Groundwater chemistry

The pH measurements for groundwater samples were circumneutral (6.37-8.62), and temperatures ranged from 14 to 20°C (Table 1). Well waters displayed a wide range of TDS and alkalinity concentrations. Major ion concentrations and trace element results (Table 2) also exhibited wide ranges of elemental concentrations (e.g., iron (Fe) ranges from 3 to 30,000 µg/L). The results for the Chimayó groundwaters show that three of the wells had uranium concentrations greater than the EPA maximum contaminant level (MCL) of 30 µg/L. Ion chemistry data were used to generate saturation indices for the Chimayó well waters using PHREEQc (Table 3).

Cation and anion data was plotted on a Piper diagram, and anions in all eight of the wells were dominated by bicarbonate (HCO_3^-) (Figure 3). Samples from these wells plotted between Ca-HCO_3 and Na-HCO_3 waters, with half being Ca-Na-HCO_3^- waters. The geysiring well (CHM-05) has the highest concentrations of Ca, Na, and CO_2 , but does not plot as a distinct outlier based on its water type.

Table 1. Field measurements for Chimayo well waters.

Well	Temp °C	pH	TDS ppm	Alkalinity mg/L (as HCO_3^-)	CO_2 g/L	Well Depth (ft)	Latitude	Longitude
CHM-01	16.8	7.20	300	411	0.10	ND	35.997	-105.935
CHM-02	17.2	6.76	1030	1040	0.30	75	36.004	-105.939
CHM-03	16.5	6.37	1490	2290	1.31	155	36.004	-105.938
CHM-04	16.6	6.42	320	366	0.27	110	35.993	-105.944
CHM-05	14.9	6.49	>2000	4120	1.83	280	35.991	-105.943
CHM-06	15.8	6.92	1110	1210	0.19	120	35.992	-105.944
CHM-07	19.3	8.62	234	171	<0.05	80	36.005	-105.919
CHM-08	14.2	7.15	336	418	0.10	135	35.998	-105.932

Table 2. Major ion chemistry and trace elements for water samples^a. All chemical compositions are in mg/L.

Well	Ca	Na	K	Fe	Mg	Sr	U ^b	Cl	SO_4	NO_3	F	Br
CHM-01	87.3	12.1	5.56	0.15	20.7	1.52	1.10E-02	5.17	6.57	<0.2	<0.2	<0.2
CHM-02	0.460	493	6.29	<0.0003	0.982	3.84E-02	0.50	171.31	70.42	9.29	<0.2	<0.2
CHM-03	123	487	13.8	0.33	116	7.93	8.70E-02	52.18	82.95	<0.2	<0.2	<1
CHM-04	64.4	48.5	5.63	0.09	10.7	0.46	1.17E-02	29.70	17.82	1.20	<0.2	<0.2
CHM-05	439	956	33.5	6.54	248	6.23	0.20	579.45	193.39	<1	<0.2	2.45
CHM-06	125	294	7.86	26.68	27.0	1.20	7.51E-03	228.67	26.66	<1	4.00	1.37
CHM-07	5.16	91.5	0.713	0.08	0.031	0.15	2.96E-02	28.91	43.49	4.46	6.24	<1
CHM-08	71.0	19.7	2.87	14.57	19.8	1.46	1.10E-02	13.56	12.16	<0.2	<0.2	<0.2

^a Most concentrations measured by ICP-OES

^b Concentrations measured by ICP-MS

Table 3. PHREEQc saturation indices for Chimayo groundwaters.

	CHM-01	CHM-02	CHM-03	CHM-04	CHM-05	CHM-06	CHM-07	CHM-08
Anhydrite	-2.92	-4.09	-2.46	-2.58	-1.45	-2.32	-3.14	-2.61
Aragonite	-1.63	-3.03	-0.72	-1.85	0.48	-0.68	-3.46	-1.61
Barite	0.01	---	---	-0.27	0.09	-0.52	-0.14	-1.22
Calcite	-1.48	-2.88	-0.57	-1.70	0.63	-0.53	-3.32	-1.46
Chalcedony	0.14	0.07	0.36	0.22	0.73	0.32	-0.05	0.27
Dolomite	-3.45	-5.54	-0.59	-4.05	1.11	-1.67	-8.67	-3.61
Fe(OH) ₃ (a)	-3.31	-3.83	-1.32	-3.62	0.38	-0.07	-4.43	-1.56
Goethite	2.28	1.78	4.26	1.97	5.90	5.49	1.25	3.93
Gypsum	-2.68	-3.85	-2.21	-2.34	-1.21	-2.08	-2.90	-2.36
Halite	-8.72	-5.66	-6.19	-7.33	-5.01	-5.74	-7.06	-8.13
Hematite	6.53	5.53	10.49	5.90	13.77	12.94	4.49	9.83
Quartz	0.60	0.52	0.82	0.68	1.19	0.78	0.39	0.73
Siderite	-2.08	-3.00	-0.80	-2.34	0.72	0.74	-2.89	-0.28
Talc	-13.14	-15.45	-6.45	-13.97	-3.59	-10.04	-23.83	-13.41
CO ₂ (g L ⁻¹)	0.10	0.30	1.34	0.27	1.827	0.19	0.03	0.10

***Saturation indices were calculated using each sample's chemical and CO₂ composition.**

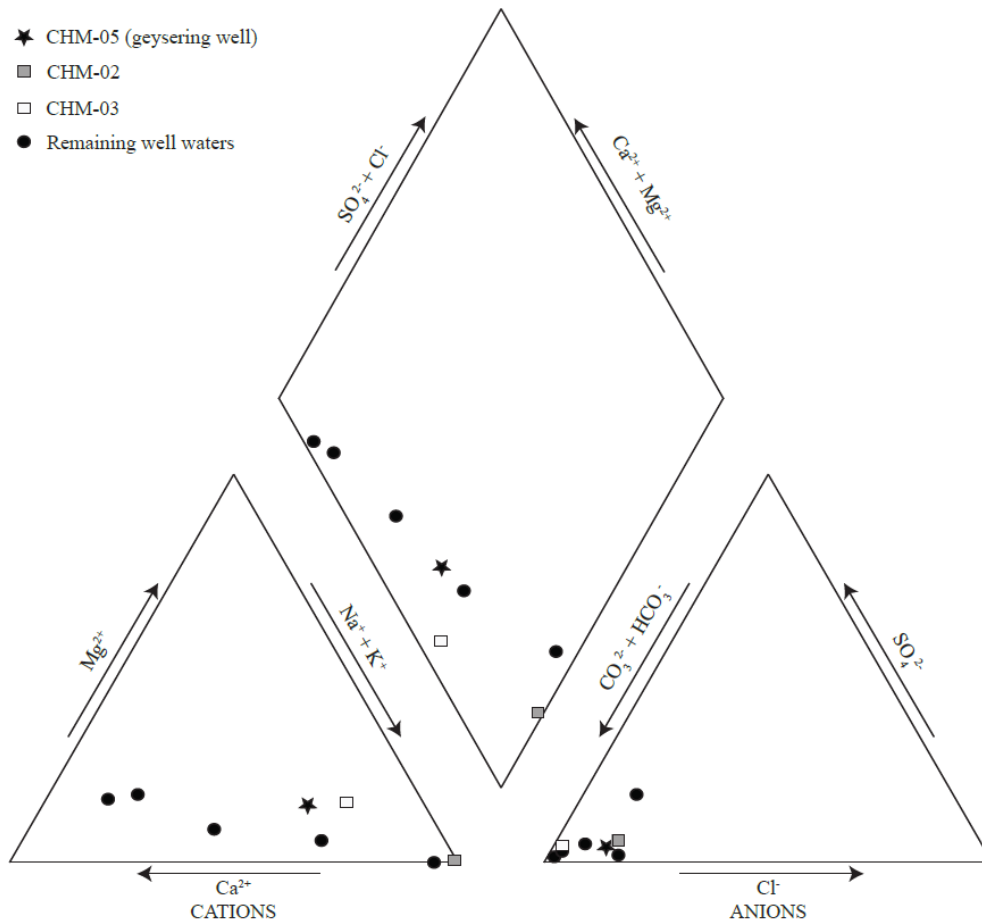


Figure 3. Piper plot of Chimayó, NM waters. CHM-05, the well with the highest CO_2 and TDS concentrations, does not plot as a distinct end-member based on the major cation and anion chemistry. CHM-02 and CHM-03 are separated by <150 m and have different major cation compositions.

2.4.2 $^{87}Sr/^{86}Sr$ isotopes of groundwater samples and lithologic samples

Despite their spatial proximity, well waters in the Chimayó area exhibit large variations in $^{87}Sr/^{86}Sr$, with isotopic compositions ranging from 0.7098 to 0.7176 (Table 4). The lowest $^{87}Sr/^{86}Sr$ values belonged to two neighboring wells, CHM-02 and CHM-03, located within 50 meters of one another.

$^{87}Sr/^{86}Sr$ values for ammonium acetate and acetic leachates ranged from 0.7082-0.7147 (Table 4). Acetic and ammonium acetate leachates from Lithosome A had the most radiogenic

values (0.7137-0.7147, respectively). One of the Pennsylvanian limestone samples from Nambé Falls had the lowest isotopic leachate value (0.7082).

Table 4. Sr isotope ratios of water samples, ammonium acetate leachates, and acetic acid leachates.

Sample Name	$^{87}\text{Sr}/^{86}\text{Sr}$		
Groundwaters			
CHM-01	0.710649	±	0.000009
CHM-02	0.709795	±	0.000009
CHM-03	0.709780	±	0.000010
CHM-04	0.715372	±	0.000008
CHM-05	0.717641	±	0.000008
CHM-06	0.714475	±	0.000010
CHM-07	0.712592	±	0.000009
CHM-08	0.712072	±	0.000009
Ammonium Acetate Leachates			
Fine Lithosome A	0.710777	±	0.000012
Coarse Lithosome A	0.714718	±	0.000008
Lithosome B	0.711641	±	0.000008
Cemented Lithosome B	0.711466	±	0.000012
Acetic Acid Leachates			
Fine Lithosome A	0.710759	±	0.000008
Coarse Lithosome A	0.713692	±	0.000010
Lithosome B	0.710912	±	0.000008
Cemented Lithosome B	0.711169	±	0.000007
Paleozoic Limestone: Stop #4 (Top of Ls)	0.711687	±	0.000008
Paleozoic Limestone: Stop #1 (Lower Ls)	0.708198	±	0.000009
Paleozoic Limestone: Stop #2 (Middle Ls)	0.710973	±	0.000009

2.4.3 $\delta^{13}\text{C}$ isotopes of groundwater samples

Carbon isotope values of dissolved inorganic carbon (DIC) were measured for seven of the eight sample wells. The carbon isotope values ranged from -15.5 to 4.5 per mil. The geysering well reported the only positive $\delta^{13}\text{C}$ value. The lower $\delta^{13}\text{C}$ values of the remaining six samples have negative $\delta^{13}\text{C}$ signatures (-15.1 to -1.6).

2.5 DISCUSSION

The Chimayó groundwater chemistry plots between Ca-HCO₃ and Na-HCO₃ waters on a Piper plot (Figure 3). The water well (CHM-05) with distinctively high elemental concentrations was a Ca-Na-HCO₃ water. CHM-05 is an artesian spring that was created when the overlying seal rock was punctured during the drilling of a water well. Due to CO₂ over pressuring, the resultant well periodically geysers; hence, this water is referred to as the ‘geysering well’ in this paper. This well (CHM-05) is believed to have a deeper source (Cumming, 1997; Keating et al., 2010) but it does not have distinctive major cation-anion chemistry when displayed on a Piper plot (Figure 3). Water from this well (plotted between the other local groundwaters (Ca-HCO₃ and Na-HCO₃ waters), suggesting more complex mixing (relative to two end-member mixing) occurring between this deep sourced, geysering brackish water (CHM-05) and the remaining shallow aquifer waters.

Elemental results were modeled for saturation indices using PHREEQc. The PHREEQc saturation results suggest that the geysering well water (CHM-05) is oversaturated in respect to most modeled minerals, including all of the carbonates (Table 3). These results are consistent with observed siderite precipitation at the geyser mouth. If this water is oversaturated with respect to carbonates, it is unlikely that deep sourced brine is interacting with shallow aquifer carbonates, despite the water’s (CHM-05) observed high CO₂ concentration (1.34 g/L).

Positive saturation indices for most minerals, except evaporates, suggest that despite high levels of CO₂, the high elemental concentrations of CHM-05 are not the result of dissolution reactions with shallow aquifer lithology. The remaining seven wells have negative saturation indices for calcite but positive values for quartz (Figure 4), indicating these waters preferentially undergo carbonate dissolution reactions rather than silicate dissolution reactions.

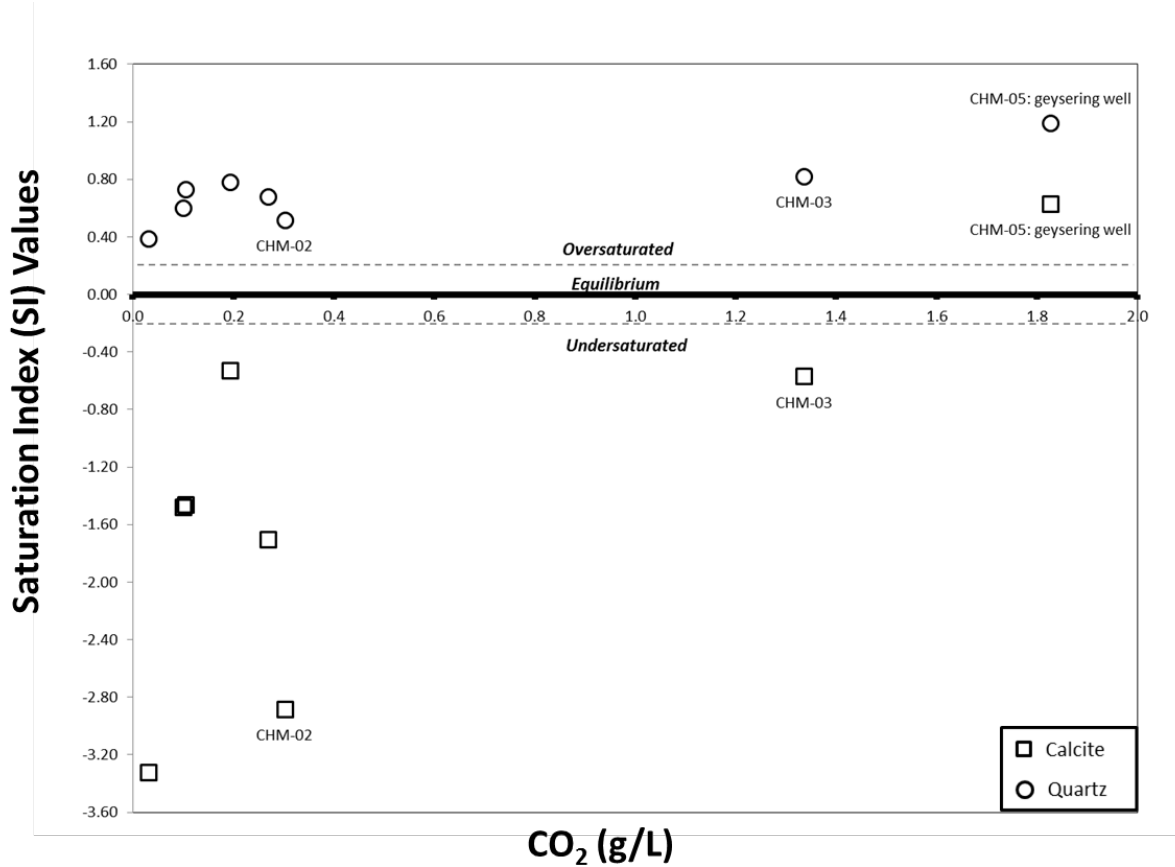


Figure 4. Graphs of saturation index values (SI) plotted against CO₂ (g/L) concentration for Chimayó well waters. Squares represent calcite saturation index values and circles represent quartz saturation index values.

2.5.1 ⁸⁷Sr/⁸⁶Sr of Chimayó groundwater

Results of strontium isotopic analysis are shown in Table 4. Despite their spatial proximity (Figure 1), well waters in the Chimayó area exhibit large variations in ⁸⁷Sr/⁸⁶Sr (0.7098-0.7176) (Figure 5) and CO₂ concentration (0.03-1.83 g/L). In general, high TDS, high CO₂ samples have high ⁸⁷Sr/⁸⁶Sr. In particular, the geysering well (CHM-05) has the most radiogenic strontium (⁸⁷Sr/⁸⁶Sr = 0.71764) and the highest CO₂ concentrations.

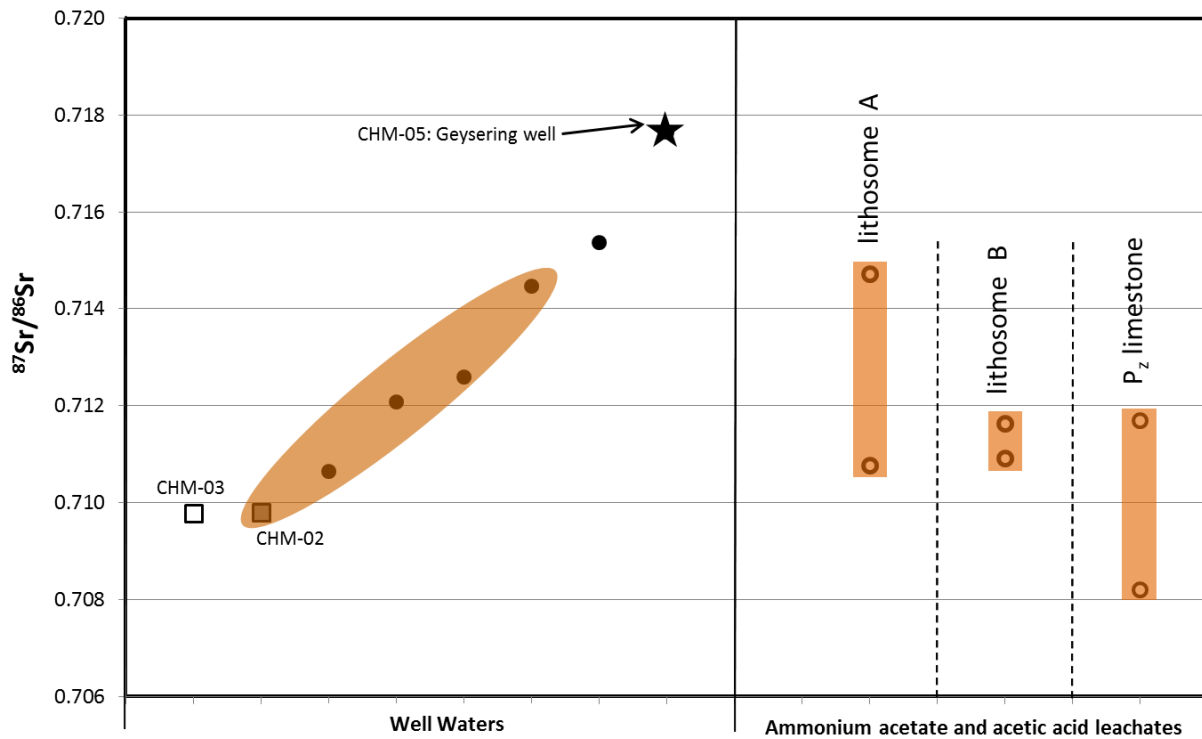


Figure 5. Strontium isotopic composition of Chimayo well water and rock leaches. Filled circles represent well water values and open circles represent values of rock leachates. An oval encompasses the $^{87}\text{Sr}/^{86}\text{Sr}$ range of groundwaters that can be explained by interaction with the surrounding lithosome material and the underlying limestone.

While there is not a strong correlation of $^{87}\text{Sr}/^{86}\text{Sr}$ values with geographic location, the highest measured ratios do tend to cluster around the southern portion of the Roberts fault, where entrainment of deep-sourced brackish water is thought to be greatest (Keating et al., 2010, 2013). The highest $^{87}\text{Sr}/^{86}\text{Sr}$ value belongs to the geysering well (CHM-05), located near the southern portion of Robert's Fault. The high $^{87}\text{Sr}/^{86}\text{Sr}$ (0.7176) for the geysering well (CHM-05) is consistent with derivation of high- CO_2 waters from deeper levels in the crust, where it likely interacted with high $^{87}\text{Sr}/^{86}\text{Sr}$ Proterozoic crystalline basement rocks ($^{87}\text{Sr}/^{86}\text{Sr} \sim 0.730$, Vezier et al., 2003). The lowest $^{87}\text{Sr}/^{86}\text{Sr}$ groundwater values, like those seen at CHM-01, CHM-02 and

CHM-03 (Table 4 and Figure 5), may result from interactions with Paleozoic limestones, which have $^{87}\text{Sr}/^{86}\text{Sr}$ leachate values between 0.70820-0.71169.

2.5.2 Water-rock interactions documented by $^{87}\text{Sr}/^{86}\text{Sr}$ isotopes

The relatively wide range of leachate $^{87}\text{Sr}/^{86}\text{Sr}$ values (Figure 5) reflects the heterogeneous nature of the Tesuque Formation lithosomes, which contain quartz, feldspar, clays, carbonates and lithic fragments, and the underlying Pennsylvanian limestones which include marly, clay-rich units. Six of the wells (CHM-01, CHM-02, CHM-03, CHM-06, CHM-07, and CHM-08) fall within this leachate range (0.7082-0.7147), and thus the interaction of infiltrating water with lithosome minerals, carbonate cement and underlying limestone could explain most of the low- CO_2 Chimayó water chemistry. CO_2 -related dissolution of carbonate cement in the Tesuque aquifer or the underlying Pennsylvanian limestone could factor into why six of these wells have $^{87}\text{Sr}/^{86}\text{Sr}$ values similar to the heterogeneous Tesuque aquifer.

With the exception of one well (CHM-03), wells with lower $^{87}\text{Sr}/^{86}\text{Sr}$ ratios (0.709-0.713) tend to have lower CO_2 concentrations. These wells are generally lower in TDS, and should represent aquifer waters relatively unaffected by brine and CO_2 . We can take the low $^{87}\text{Sr}/^{86}\text{Sr}$, low CO_2 wells as the “unaffected” end member and look at the effects of mixing with the high- CO_2 , high TDS geysering well (CHM-05) (Figure 6). This well has an $^{87}\text{Sr}/^{86}\text{Sr}$ of 0.7176, significantly higher than the lithosome leachates. Depending on the exact position of the end members, we can explain the intermediate composition waters by mixing of unaffected groundwater with 1-10% of the high- CO_2 brine (Figure 6). We see that Sr isotopes are quite sensitive to small amounts of brine interaction, due to the high Sr concentration and large

difference in isotopic composition of the brine. Two wells (CHM-02 and CHM-03) are outliers on this mixing curve and will be further analyzed using a multi-isotope mixing model.

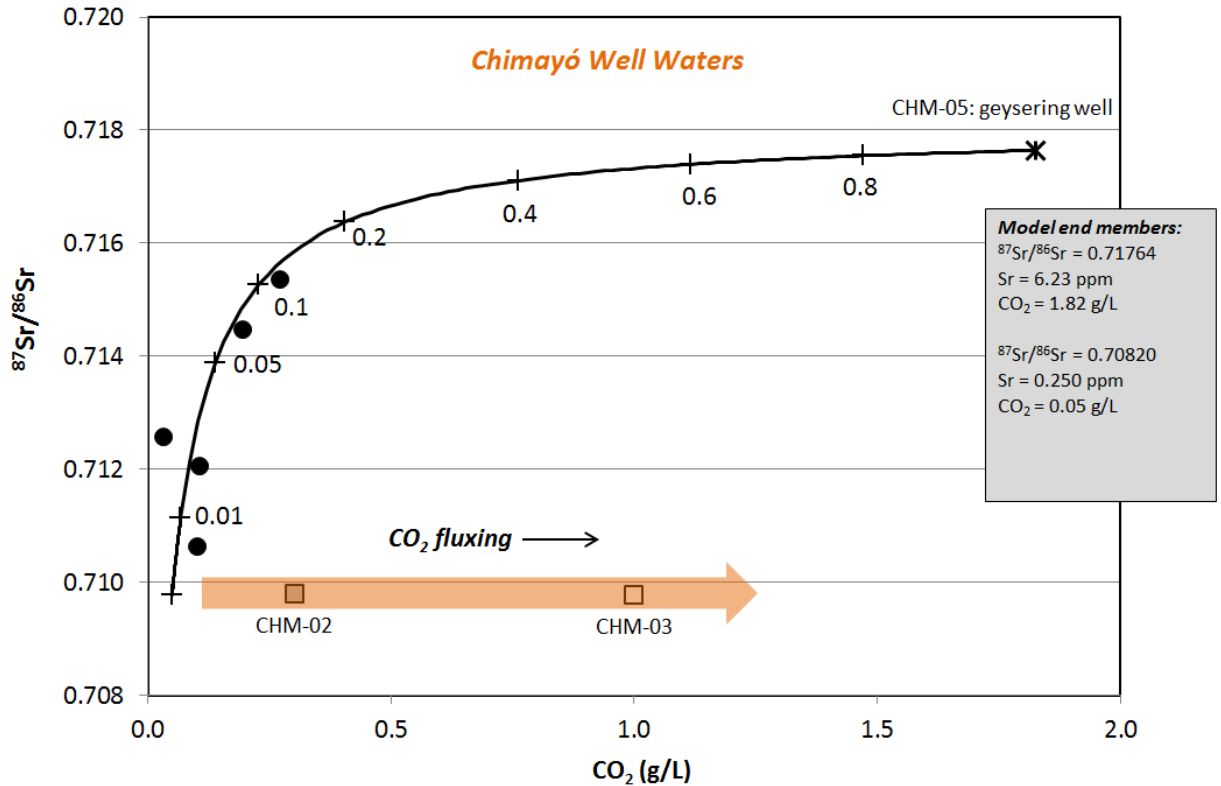


Figure 6. $^{87}\text{Sr}/^{86}\text{Sr}$ plotted against CO_2 concentration for Chimayó well waters. Numbers next to mixing curve indicate fraction of geysering fluid added to background water. The mixing curve uses three variables (Sr concentration, $^{87}\text{Sr}/^{86}\text{Sr}$, and CO_2) of two end member waters and mixes these waters fractionally until the low end member has the same composition for those variables as the high end member.

2.5.3 $\delta^{13}\text{C}$ isotopes

The geysering well has a $\delta^{13}\text{C}$ that lies well outside the range of the other Chimayó groundwaters. A plot of $\delta^{13}\text{C}$ vs. CO_2 shows a positive correlation between these two measurements (Figure 7). Previous experimental work has demonstrated the ability to track CO_2 migration in groundwaters with $\delta^{13}\text{C}$ (Kharaka et al., 2009). The $\delta^{13}\text{C}$ data from Chimayó groundwaters suggests that introducing CO_2 from the same source as the geysering well may

increase the $\delta^{13}\text{C}$ of a well water, and that at this natural analog site $\delta^{13}\text{C}$ may be a sensitive indicator of CO_2 migration from a deep source.

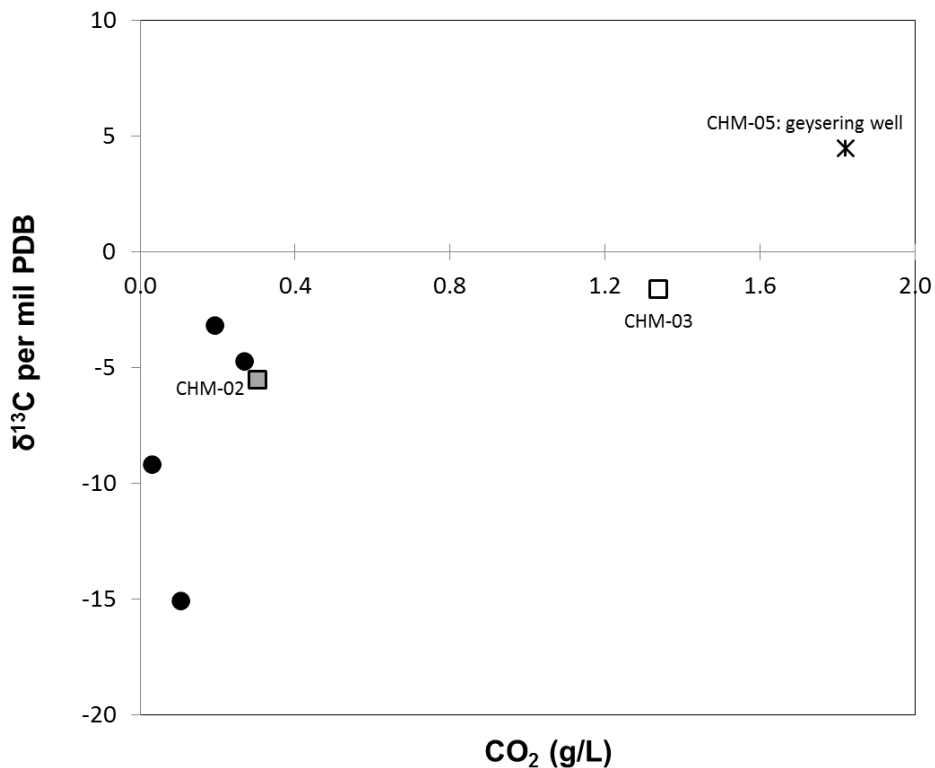


Figure 7. Graph $\delta^{13}\text{C}$ per mil PDB vs. CO_2 (g/L).

2.5.4 Multi-isotope mixing model using $^{87}\text{Sr}/^{86}\text{Sr}$ and $\delta^{13}\text{C}$ isotopes

A mixing curve using $^{87}\text{Sr}/^{86}\text{Sr}$ and $\delta^{13}\text{C}$ (Figure 8) indicates that while most of the waters appear to be mixing with the geysering brackish water, there are two outliers, similar to the mixing curve using $^{87}\text{Sr}/^{86}\text{Sr}$ and CO_2 (Figure 6). These two outliers, CHM-02 and CHM-03, exhibit nearly identical $^{87}\text{Sr}/^{86}\text{Sr}$ even though their $\delta^{13}\text{C}$ increases with CO_2 , similar to the overall trend.

This trend suggests that the geysiring well's distinctive $\delta^{13}\text{C}$ signature, likely the result of deeply sourced CO_2 , is being mixed to varying degrees with all of the waters, including CHM-02 and CHM-03.

This multi-isotope mixing model suggests that while deeply sourced CO_2 is raising the $\delta^{13}\text{C}$ of both CHM-02 and CHM-03, this CO_2 is traveling without geysiring brackish water. The low $^{87}\text{Sr}/^{86}\text{Sr}$ values of CHM-02 and CHM-03 indicate they are not mixing with the high $^{87}\text{Sr}/^{86}\text{Sr}$ signature found in the brackish water. Previous work (Cumming, 1997; Keating et al., 2010) has suggested that there are two modes of CO_2 transport into the Chimayó aquifer: (1) CO_2 dissolved in brackish water that is carried up along faults and fractures and (2) diffuse migration of CO_2 into shallow aquifers. This multi-isotope mixing model indicates that that $^{87}\text{Sr}/^{86}\text{Sr}$ and $\delta^{13}\text{C}$ can identify wells where the latter CO_2 transport mechanism is occurring, an objective that could not be accomplished using the major cation and anion geochemistry of Chimayó wells.

The diffusion of CO_2 , referred to as 'CO₂ fluxing' in Figure 6 and Figure 8, from this upwelling brackish water likely occurs at a deep impermeable lithologic barrier that separates waters like CHM-02 and CHM-03 from the rest of the aquifer. Although the Roberts Fault apparently acts as a conduit for high- CO_2 fluid migration, faults in the area have been known to impede groundwater flow (Grauch et al. 2009), such as when cement precipitation from groundwater flow creates a hydrologic barrier (Mozley and Goodwin, 1995). CO_2 could have decoupled from the brine at heavily cemented faults either at depth, so that the CO_2 is traveling a distance to the aquifer, or within the aquifer itself. The data suggest that the anomalous wells (CHM-02 and CHM-03) that were excluded from the mixing curves represents local CO_2 fluxing that is decoupled from the brine carrier fluid, which would have otherwise greatly elevated the $^{87}\text{Sr}/^{86}\text{Sr}$ ratios of these waters. This CO_2 infiltration would lead to an increase in the $\delta^{13}\text{C}$ values

and significant dissolution of the surrounding aquifer lithology, which would increase TDS, as observed, while maintaining the same $^{87}\text{Sr}/^{86}\text{Sr}$ isotopic ratio.

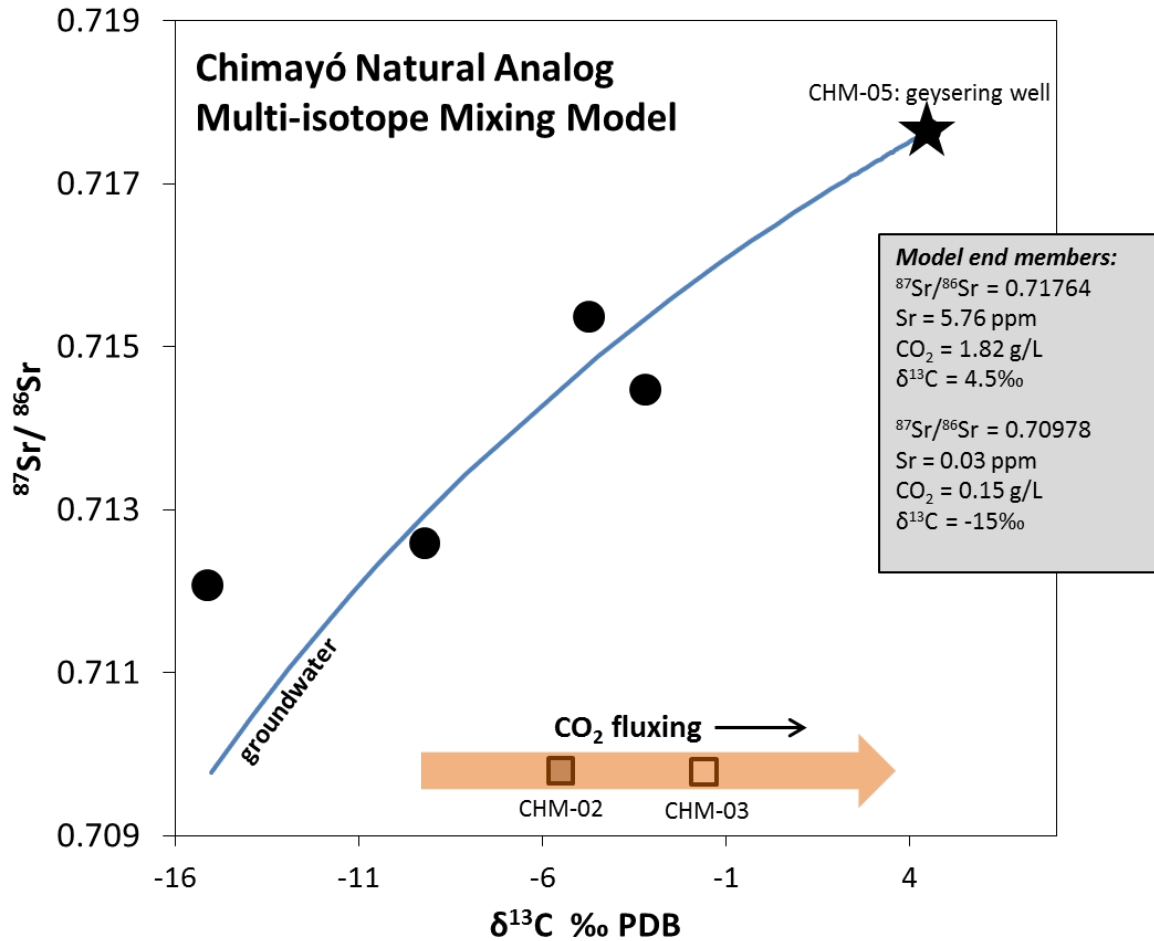


Figure 8. Well water mixing diagram with $^{87}\text{Sr}/^{86}\text{Sr}$ vs. $\delta^{13}\text{C}$. Plotting the isotopic compositions of the groundwaters produces a similar mixing curve to that of $^{87}\text{Sr}/^{86}\text{Sr}$ vs. CO₂. This figure suggests that decoupled CO₂ gas is affecting CHM-02 and CHM-03; the other Chimayó wells appear to be mixing with the high CO₂-brackish water seen at CHM-05.

2.5.5 Identifying reaction pathways using $^{87}\text{Sr}/^{86}\text{Sr}$ and $\delta^{13}\text{C}$ isotopes

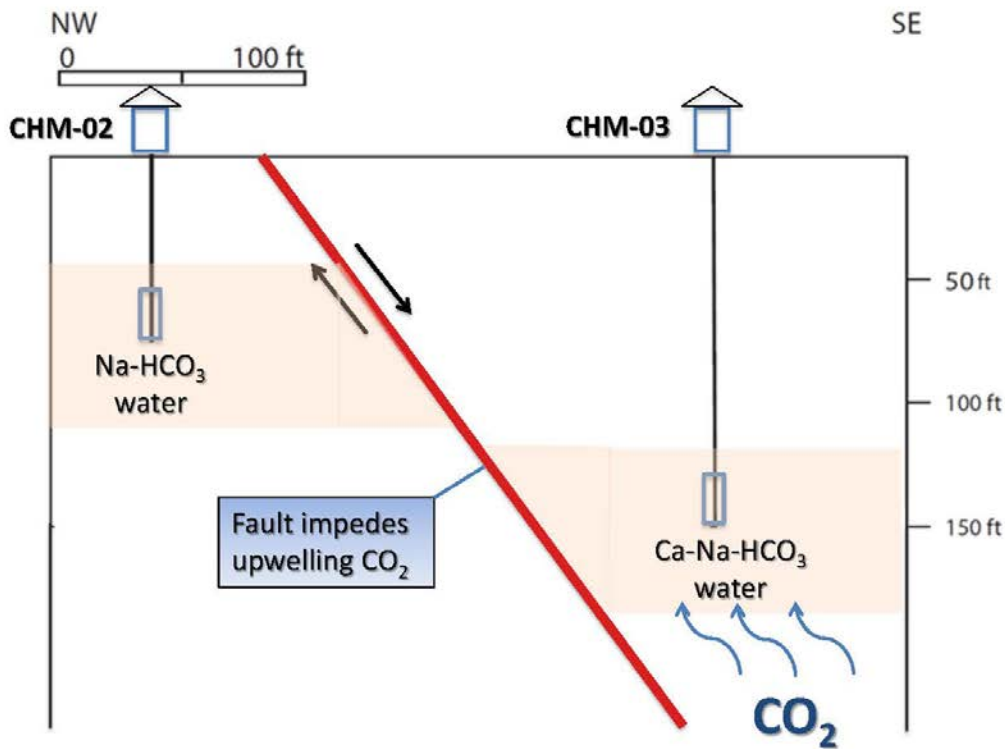
The two wells (CHM-02 and CHM-03) that fall outside the mixing trends (Figure 6 and Figure 8) appear to be affected by CO₂, with CO₂ concentrations above background values. However

$^{87}\text{Sr}/^{86}\text{Sr}$ values in these wells are much lower than that of the geysering well (CHM-05). Based on the $^{87}\text{Sr}/^{86}\text{Sr}$ mixing curve (Figure 6), these wells appear to have almost no interaction with the geysering brackish water and its high $^{87}\text{Sr}/^{86}\text{Sr}$ of 0.7176. These two well samples are separated by a short distance (<150 m) and yield essentially identical $^{87}\text{Sr}/^{86}\text{Sr}$ of 0.70979 ± 1 .

However, the concentration of dissolved CO_2 in CHM-03 is higher by a factor of >4 compared to that of CHM-02. CHM-03, a Ca-Na- HCO_3 water, also shows significant enrichments in dissolved solids, especially alkaline earth elements (Ca, Mg, Sr) and different $\delta^{13}\text{C}$ values when compared to CHM-02, a Na- HCO_3 water. The data suggest that the aquifers tapped by both wells (CHM-02 and CHM-03) are separated by a CO_2 -resistant barrier. In order to tap a sustainable water source, CHM-03 was drilled 75 ft deeper than CHM-02 (Table 1). The nearly identical $^{87}\text{Sr}/^{86}\text{Sr}$ values indicate that the Sr for both wells is being derived from similar carbonates, but the distinct differences in $\delta^{13}\text{C}$ values, CO_2 concentrations, and major and trace geochemistry suggest that the wells are not in direct communication. Therefore it is likely that a barrier separates these two wells.

The presence of a barrier in this region would not be surprising. The Tesuque aquifer is variably unconfined, with clay lenses resulting in artesian wells, like the geysering well, in certain locations. However, it is also possible that a normal fault separates these wells and impedes the upwelling of CO_2 from CHM-03 to CHM-02 (Figure 9). A normal fault would explain the offset in depths to a sustainable water source (Table 1). Previous work has shown that faulting can cause aquifer compartmentalization in the Española Basin (Grauch et al., 2009). Based on $^{87}\text{Sr}/^{86}\text{Sr}$ values, major and trace element concentrations, and CO_2 concentrations, it is likely that in between these two proximal wells is an impermeable normal fault that limits the flow of groundwater and the flow of CO_2 from CHM-03 into CHM-02. There is no evidence of

the fault, like fault gouge material or a difference in vegetation, between the two wells. The Rio Grande Rift is an area of active rifting, but it is possible that this fault is no longer active or that the low spreading rate (2.5 cm/40 years) does not result in a visible surface delineation (Kelley, 2012).



1

Figure 9. Proposed schematic cross section of area between two Chimayo wells. The cross section proposes a fault between the wells that impedes upwelling CO₂; the two wells have identical ⁸⁷Sr/⁸⁶Sr signatures, but significantly different geochemistry.

2.5.6 Effect of decoupled CO₂ on groundwater

Previous work (Keating et al, 2010) has suggested that CO₂-brine fluid negatively affects the groundwater in Chimayó; the results in this study suggest that CO₂ decoupled from the brackish

fluid may also have a negative effect on groundwater quality. The two wells (CHM-02 and CHM-03) that exhibit the decoupled CO₂ signature have uranium (U) concentrations above the EPA MCL and TDS concentrations above the EPA secondary drinking water standards (Table 1 and 2). The geysering well (CHM-05) also has high U and TDS concentrations, but the Sr isotope data suggest that this high CO₂-high TDS water is not in communication with these wells. It is therefore unlikely that high U concentrations in CHM-02 and CHM-03 are a result of mixing with the high TDS, geysering well. Positive saturation indices suggest that the source of the U in CHM-05 is likely native to this brackish water (Table 3). These indices imply that the upwelling, geysering brackish water is more likely to precipitate material than dissolve materials from the surrounding aquifer matrix. Conversely, U in the CHM-02 and CHM-03 waters likely results from dissolution reactions spurred by the migration of decoupled CO₂. The concentration of CO₂ in groundwaters has been shown to have an effect on the water's pH and the dissolution of uranium carbonate complexes (Langmuir, 1978; Gómez et al., 2006). The migration of decoupled CO₂ may increase the concentration of trace elements, like uranium, in this compartment of the aquifer by enhancing dissolution of the surrounding aquifer matrix.

Isotopic data suggests this process may be occurring in the groundwaters of Chimayó, specifically at CHM-02 and CHM-03, thus impairing groundwater quality. ⁸⁷Sr/⁸⁶Sr values indicate there is no intrusion of the geysering brackish water from CHM-05, yet CHM-02 and CHM-03 still have higher TDS levels (>1000 ppm) than most of the wells. High TDS levels in these wells likely results from enhanced mineral dissolution caused by the migration of decoupled CO₂. This enhanced mineral dissolution may be releasing trace elements, like U, into the groundwater surrounding CHM-02 and CHM-03, while wells that are slightly mixing with the geysering brackish water actually have lower TDS and trace element concentrations.

2.6 CONCLUSIONS

Waters with distinct CO₂ and TDS characteristics in the Chimayó region of New Mexico can be distinguished in part based on their Sr and C isotopic composition, with high-TDS, high-CO₂ waters having high ⁸⁷Sr/⁸⁶Sr and δ¹³C isotopic signatures indicative of entrainment of CO₂ associated with Proterozoic crystalline basement rocks. Sr and C isotopes corroborate previous work (Cumming, 1997; Keating et al., 2010) that suggested CO₂ migrates into the shallow Chimayó aquifer via two mechanisms: (1) dissolved in brine and transported along fracture or fault conduits, and (2) via fluxing of CO₂ gas independent of a brine carrier fluid. Shallow subsurface water-rock reactions with high-CO₂ fluids can result in dissolution of carbonate cement. This dissolution causes an increase in aquifer TDS and can impair water quality. We found evidence for carbonate dissolution in the Tesuque aquifer; the elevated TDS is part of the reason that Chimayó residents have closed some of these wells and switched to another source of drinking water.

This study also demonstrates that Sr and C isotope systematics of well waters and associated rocks can track groundwater-brine-CO₂-rock interaction within lithologically complex strata. We find reasonable correspondence between Sr isotope ratios and background aquifer waters, and likely aquifer matrix, in addition to evidence for the migration of deep-sourced brines into shallower aquifers, as suggested by Cumming (1997) and Keating et al. (2010; 2013). ⁸⁷Sr/⁸⁶Sr ratios are extremely sensitive to even small amounts of brine mixing with freshwater systems. Our results show that mixing of a small amount (1-10%) of fluid from the geysiring brackish well with shallow aquifers causes a distinguishable shift in ⁸⁷Sr/⁸⁶Sr. Sr isotopes are extremely sensitive to intrusion of deep-sourced saline waters in this case, and may in general be a very sensitive means of monitoring brines displaced by CO₂ injection. Combining Sr and C

isotopes not only reinforced earlier findings of two CO₂ transport mechanisms at Chimayó, but also indicated that certain wells (CHM-02 and CHM-03) are impacted solely by one mechanism, diffuse CO₂ migration. Diffuse CO₂ migration may also be contributing to water quality degradation in Chimayó, as both of the wells affected by this mechanism, CHM-02 and CHM-03, had U concentrations above the EPA MCL and TDS concentrations above the EPA secondary drinking water standard. Major and trace element data alone could not identify this mechanism, but complementing the elemental data with Sr and C isotope data helped to identify waters where this mechanism occurs and its effects on groundwaters.

Naturally occurring (non-radioactive) isotopes of elements such as strontium combined with stable isotope analysis can be used to identify CO₂ injection-related subsurface interactions between groundwater, brine and the solid aquifer matrix that signal either CO₂ migration (and future release) or effective sequestration of CO₂. Conservative isotope tracers such as ⁸⁷Sr/⁸⁶Sr ratios have potential as a monitoring tool to verify containment or identify transport mechanisms and pathways of injected CO₂ and associated brines. Multi isotope tools can quantify reaction progress within a reservoir and other subsurface geologic systems, aiding in identifying changes in groundwater-rock interaction due to intrusion of CO₂. Additionally, these tools can quantify the relative contributions of CO₂ intrusions even when there is no entrainment of deeper sourced waters. The use of multiple isotopic systems at Chimayó suggests that while some deeper faults can act as conduits for CO₂ to migrate into certain wells (CHM-05), some faults also appear to act as impermeable barriers to the mixing of adjacent well waters (CHM-02 and CHM-03). Such sensitive indicators are an important complement to geochemical and geophysical tracking of large-scale CO₂ migration, and can also aid in storage site risk assessment.

3.0 STRONTIUM ISOTOPE AND GEOCHEMICAL CHARACTERIZATION OF THE EAST SEMINOLE OIL FIELD EOR SITE, TEXAS

3.1 INTRODUCTION

Compressed CO₂ has been used for decades as a means of enhanced oil recovery (EOR). Although water is typically used as the flooding fluid following primary production from a reservoir formation, it does not liberate hydrocarbons with lithophilic bonds to reservoir grains. Use of compressed gas increases pore pressure and extracts oil that is sorbed to sediments within the reservoir formation. Conventional oil production results in removal of 20 to 40% of the original oil in place. The EOR process extracts an additional 5 to 20% of the original oil in the formation, and the CO₂ is trapped in the formation (Stevens, 2001b). The use of CO₂ EOR has been proposed as an economical way to sequester greenhouse gas emissions and expand domestic oil production (DOE, 2008). Despite this possibility, there is the possibility that CO₂ EOR could result in the contamination of overlying groundwaters.

The East Seminole oil field, located in Gaines County, Texas (TX) is an oil field that taps into the Upper San Andres dolomite reservoir rock (Figure 10). The top of the Upper San Andres is at a depth of ~5300 ft at East Seminole oil field. Outside of Andrews, TX, 43 miles to the south of Seminole, the Emma oil field also taps into the Upper San Andres formation that is at a shallower depth of ~4200 ft at this location. The unit has a maximum thickness in excess of 1500

ft (Ramondetta, 1982a). Wolfcamp basinal clastics and carbonates are the source rock for nearby San Andres reservoirs in the Midland Basin (Figure 11) and they are the likely source rock for the Upper San Andres oil reservoir in the Central Platform Basin. Anticlines flank the center of the basin and act as structural traps for the oil that migrated mostly through vertical fractures to reach the Upper San Andres. There are also anhydrite lenses within the formation that reduce porosity (Gray, 1989). Secondary porosity in the reservoir rock was created during diagenesis and dolomitization by hypersaline brines (Gray, 1989).

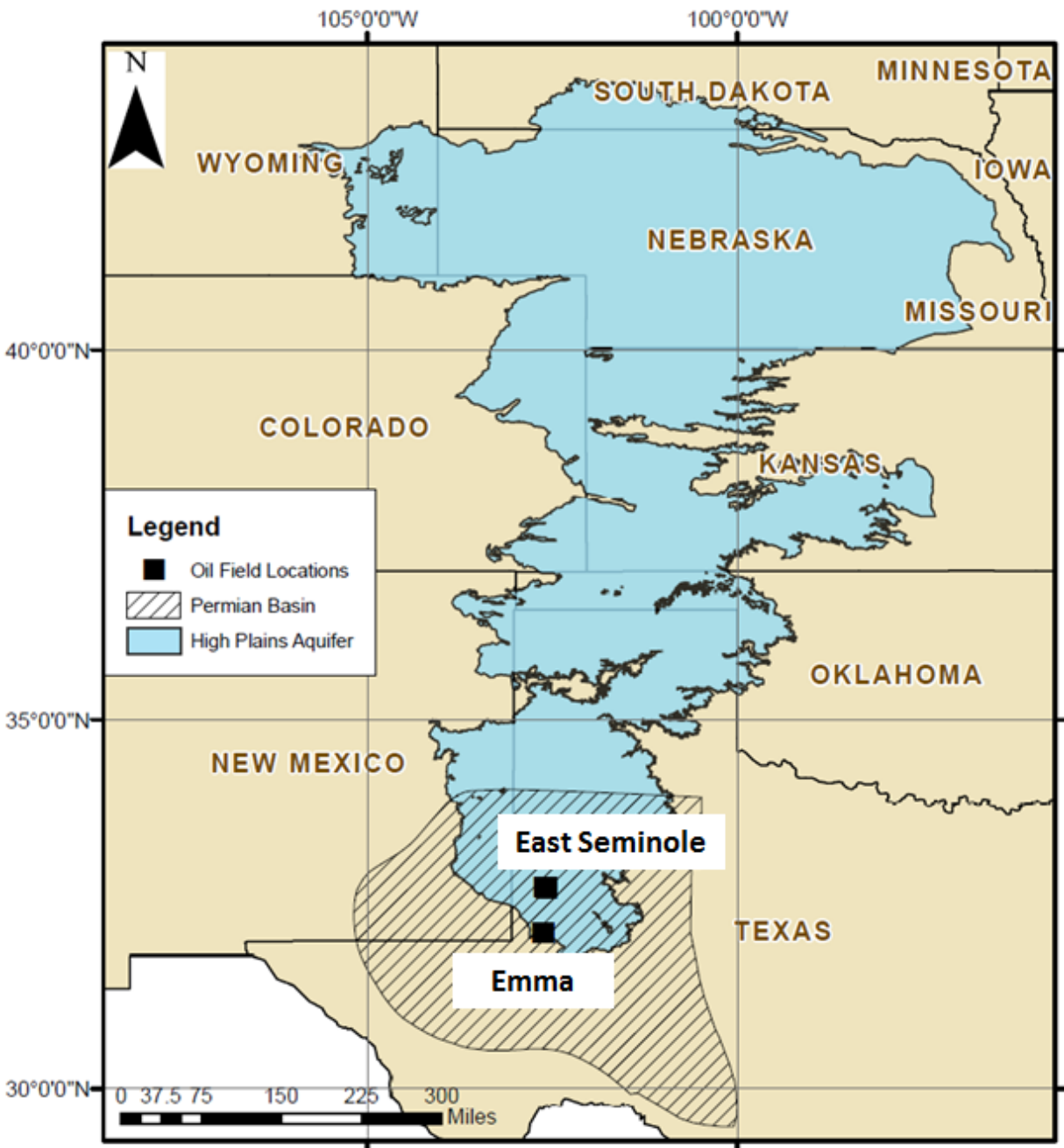


Figure 10. Map showing locations of the East Seminole and Emma oil fields within the High Plains Aquifer and the Permian Basin. GIS data obtained from Bureau of Economic Geology (2008) and the USGS (2009).

Water flooding of the East Seminole field began in 1987. Since the total volume of oil produced at the field is only 22% of the estimated 24 million barrels of oil in place, the site is now a target for EOR by CO₂ flooding, which is projected to remove an additional 15% of the

original oil in the formation. Injected water in the current water flooding phase is sourced from the Triassic Santa Rosa formation, which sits at a depth of ~1500 ft. The waters involved in the injection and production process have not been thoroughly geochemically analyzed. The only previously reported water chemistry data are chloride concentrations for the original formation water (20,240 mg/L), the injection water (2,000 mg/L), and breakthrough at wellbore (8,948 mg/L) (Gray, 1989). The waters in this study were sampled prior to injection of CO₂ at the East Seminole oil field. Previous work analyzed core samples of Upper San Andres dolomite and anhydrite for ⁸⁷Sr/⁸⁶Sr (Ruppel and Cander, 1988). This active CO₂ EOR site provides an opportunity to characterize the geochemistry of Upper San Andres produced waters and the overlying Santa Rosa and Ogallala groundwaters before CO₂ injection begins. This baseline testing will assess the viability of a natural isotope tracer (⁸⁷Sr/⁸⁶Sr) as a monitoring and verification tool at the East Seminole oil field.

The Emma oil field is not a site of active water injection. There were attempts to water flood the field in the 1960s and then again in the 1990s, but water flooding did not increase oil production and was ceased soon after it began. Oil is the only hydrocarbon produced from both the Emma and East Seminole fields, but they both have high H₂S content in the gas that comes up with the oil. The Emma field's gas content (~13% H₂S) is similar to that of East Seminole (~11% H₂S). There is also a significant amount of FeS in the produced water at the Emma field, but not any at the East Seminole site. This FeS may be the result of reactions with the metal drill pipes at the Emma field or geochemical differences in the produced water between the fields.

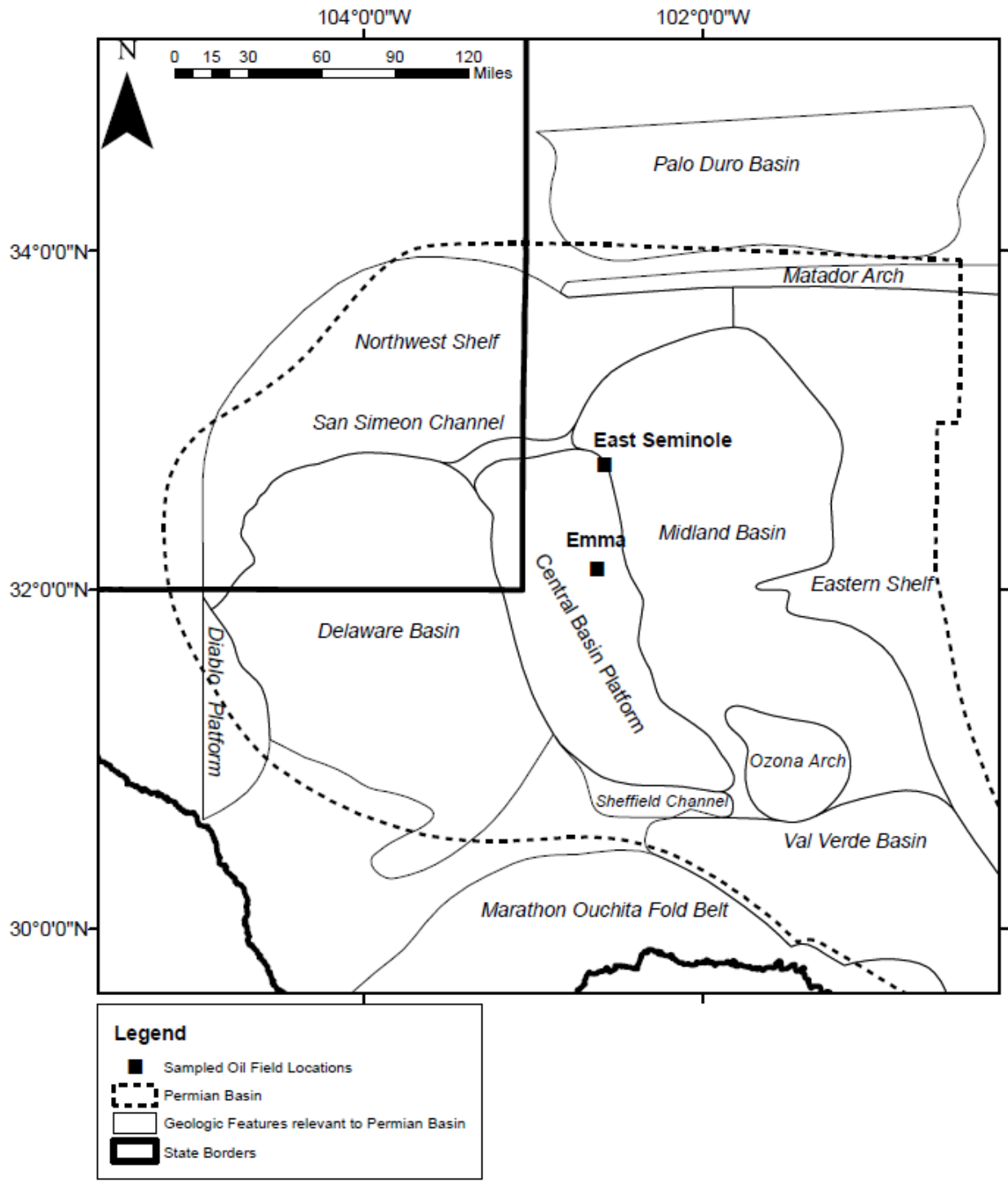


Figure 11. Map showing geologic sub-basins and features of the Permian Basin and the immediate area. East Seminole and Emma oil fields are located within the Central Basin Platform. GIS data was obtained from Bureau of Economic Geology (2005).

Production levels are low at both fields. The produced fluid at the Emma field San Andres wells is ~1.6-4.7% oil; the remainder is considered ‘produced water,’ which is the fluid analyzed in this study. The produced water in this study was sampled from oil-water separators that were located next to each well head. The East Seminole field produces more oil and has an oil-water fraction (1-12%) that spans a larger range. CO₂ flooding is projected to begin at East Seminole in the fall of 2013 with a response in production expected three months to one year after injection begins.

The Ogallala aquifer (Figure 10) is the source of drinking water and irrigation water for peanut and cotton farming that occurs in Gaines County (Wheeler et al., 2006). There are several water quality issues concerning the Ogallala in this region. In the southern panhandle of Texas, the aquifer has high total dissolved solid levels (400 to >3000 mg/L) and incidences of perchlorate levels elevated above 150 µg/L (Mehta et al., 2000; Rajagopalan et al., 2006). The city of Seminole is dealing with two specific issues involving the Ogallala: (1) high levels of arsenic (0.3-164 µg/L) in regional aquifer waters and (2) farming irrigation combined with exceptional drought conditions resulting in well draw down of ~4 ft/yr in some West Texas locations (Dutton et al, 2001; Scanlon et al., 2009; Johnson et al., 2009; Heim, 2013). This has resulted in exploratory drilling into the Triassic Santa Rosa formation (depth ~1500 ft) to supplement current Ogallala drinking supplies.

This study involved obtaining groundwater and produced water samples and characterizing these samples using Sr isotopes. The main activities involved:

- 1) Water sampling to characterize Upper San Andres formation water pre-water flooding conditions (Emma oil field)

- 2) Water sampling to characterize formation water post-water flooding and pre-CO₂ injection (East Seminole oil field)
- 3) Geochemical and isotopic site characterization with an emphasis on identifying relevant water-rock-CO₂ reactions and assessment of the sensitivity of the Sr isotope method to identify and quantify changes in the hydrologic system with increased CO₂ interaction.

The first goal of this investigation is to assess the sensitivity of Sr isotopes as a monitor for CO₂ containment during geologic carbon injection in a carbonate-based petroleum reservoir. This site will provide the opportunity to develop Sr mixing models to investigate what the effects of upwelling fluids displaced by CO₂ injection might have on the overlying Ogallala aquifer and the Santa Rosa formation. The second goal is to compare the geochemical and isotopic data of the produced waters from two different oil fields that produce from the same formation. This will give us insight into the brine migration history of these two oil fields.

3.2 STUDY AREA

Water samples from this study were taken from a variety of wells, including producing oil wells at two separate oil fields, industrial wells, and residential wells. Producing oil wells were sampled at the East Seminole oil field and the Emma oil field, located in the Permian basin of West Texas (Figure 10). Twelve of the thirteen production wells sampled produce oil from the Upper San Andres dolomite, which is deeper at the Emma oil field (5300 ft) than at the East Seminole field (4200 ft). At the Emma oil field, another production well was sampled that produces oil from the Cowden-Glorieta sandstone, a formation that is ~1400 ft beneath the Upper San Andres.

There are six Ogallala groundwater well samples in this study. All of the samples lie either directly above the proposed CO₂ injection flooding area or are outside of the proposed flooding zone. Three of these groundwater wells are residential drinking wells and two are irrigation wells. Tabula Rasa Energy owns and operates the other well and uses the water for industrial purposes, including dust control on surrounding dirt roads.

Two of the samples are injection waters that are injected into the Upper San Andres at East Seminole oil field as part of the water flooding EOR that has been occurring there since 1988 (Figure 12). These water samples are a mixture of East Seminole production waters and Santa Rosa formation waters. These injection wells are composed mainly of East Seminole production waters (~75%), with enough Santa Rosa water (~25%) to reduce the viscosity of the water so it can be injected into the formation once again.

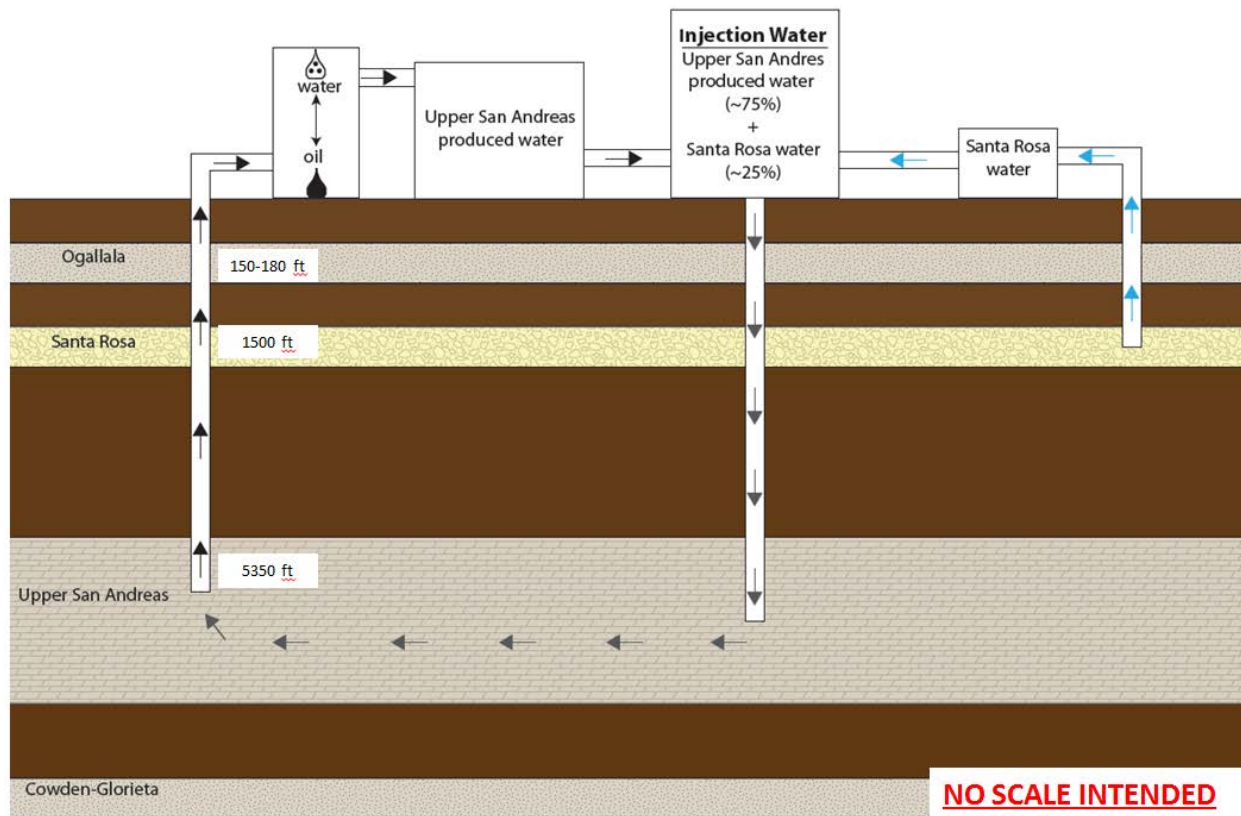


Figure 12. Schematic of injection water mixing procedure at East Seminole oil field. Depths in figure represent the depth where representative formation samples were taken. For the Upper San Andreas formation samples at the East Seminole oil field, downhole pressures were between 2200-3500 pounds per square inch (PSI) and the downhole temperatures were between 90-110°F. There is no scale intended for this image as it is just a schematic. Geologic patterns are from the USGS (2006).

These samples of production well waters, the groundwaters overlying those producers, and the injection water used on site, provide an opportunity to characterize the geochemistry and isotope geochemistry before CO₂ injection begins. The diversity of these samples also allows the opportunity to estimate the effects that CO₂ flooding will have on the reservoir formation and its production waters, as well as the effect that upwelling CO₂ and displaced production fluids could have on the overlying groundwaters.

3.2.1 Geology and hydrogeology of Central Basin Platform and formations sampled

3.2.1.1 Permian Basin: Central Basin Platform

The Permian Basin features numerous sub-basins and other geologic features that play a crucial role in oil generation and production (Figure 11). All of the samples in this study are located within the Central Basin Platform, a mix of carbonate and siliciclastic-carbonate platform deposits that were deposited during the Guadalupian (Ward et al., 1986; Kerans et al., 1994). The Permian Basin formed when Precambrian basement rocks began to subside as part of asymmetrical structural depression near the edge of the North American plate (Ward et al., 1986). Paleozoic sediments filled the Delaware and Midland basins (Figure 11) and then during the Early Permian (~299 Ma), carbonates on the edges of both of basins formed and eventually formed barriers that precluded contact with the sea, creating the Central Basin Platform (Ward et al., 1986).

The physical separation of the Delaware and Midland basins resulted in important depositional changes across the Permian Basin. From the Early Permian (~299 Ma) till the end of the Guadalupian (~260 Ma), the Delaware and Midland basins were sites of siliciclastic deposition, while carbonate deposition took place on the platforms and shelf environments (Figure 11) (Ward et al., 1986). These carbonate deposits, including the San Andres, Grayburg, and Seven Rivers formations, would later become the primary reservoirs for Permian Basin oil production when oil migrated from a source rock, likely the Wolfcamp, into these carbonates (Ramondetta, 1982b; Cowan and Harris, 1986; Dutton et al., 2005).

3.2.1.2 Brine Migration in the Permian Basin

Previous work has divided the stratigraphic units of the Permian Basin into the upper aquifer, the evaporate confining unit, deep basin brine aquifer, and the basement aquiclude (Bassett and Bentley, 1982; Dutton, 1987; Stueber et al., 1998; Mehta et al., 2000). In this study, we sample two formations from the upper aquifer (Ogallala and Santa Rosa) and two from the evaporate confining unit (Upper San Andres and Cowden-Glorieta). While there are no samples from formations in the deep basin brine aquifer, previous work suggests that the high hydraulic heads in the Wolfcamp and Pennsylvanian deep basin brines could result in fluid migration into overlying Permian formations (Bentley, 1981; Langmuir and Melchoir, 1985).

The origin of deep basin brines in the Permian Basin has multiple suggested origins (Bassett and Bentley, 1982; Knauth and Beeunos, 1986; Dutton, 1987; Bein and Dutton, 1993; Stueber et al., 1998). Bassett and Bentley (1982) suggested that the brines in the Wolfcamp and other deep basin formations are the result of regional groundwater flow interacting with surrounding anhydrite lithology. They concluded that meteoric waters recharged outcrops in New Mexico in the Late Cretaceous and that eastward groundwater flow flushed out the connate brine in the Wolfcamp and other deep basin formations. Chemical and isotopic analyses of these deep basin brines have led others to conclude that some of these brines are native. Dutton (1987) found that preservation of ancient connate brines better explains the δD and $\delta^{18}O$ of the San Andres Formation relative to groundwater reaction pathways.

The brines may have origins different from regional groundwater and preserved connate brine. Other work has suggested that the current brines in the deep basin aquifer are the result of meteoric water and seawater mixing during deposition or early diagenesis (Knauth and Beeunos,

1986). Other work has suggested that this mixing was regional and that in some regions, connate brines persist (Eastoe et al., 1999).

Brine migration is also an issue in the upper aquifer, as salinization of groundwaters is common in the High Plains, a location where water scarcity is also a concern (Wheeler et al., 2006). Previous work has shown that natural salinization of groundwaters does occur, but in an area where oil production is common, it is important to clearly display that the salinization is not the result of oil and gas production processes (Mehta et al., 2000). This previous work by Mehta et al. (2000) concluded that paleorecharge waters interacting with Upper Permian salts resulted in Ogallala salinization and that migration or discharge of oil-reservoir brines were not the cause of salinization.

Previous researchers analyzed Permian Basin brines and their respective lithologies for $^{87}\text{Sr}/^{86}\text{Sr}$ (Fisher and Kreitler, 1987; Ruppel and Cander, 1988; Bein and Dutton, 1993; Stueber et al., 1998). Three of these works (Fisher and Kreitler, 1987; Bein and Dutton, 1993; Stueber et al., 1998) sampled brines from the San Andres as well as from Pennsylvanian and Devonian formations. Ruppel and Cander (1988) analyzed the leachates of core samples from San Andres Formation. These core samples were taken at the Emma oil field, so they are representative of the host rock at that location. This previous research provides a background for comparison for the results from this study.

3.2.1.3 Permian San Andres Formation

The San Andres Formation is predominantly a carbonate facies with a lateral extent that covers most of the Permian basin. Previous work identified a widespread karstic unconformity as the divider between the Upper San Andres and the Lower San Andres (Kerans et al., 1994). This boundary is not confining and fluids between the formations may interact. Produced waters in

this study come from a porous dolomite facies within the Upper San Andres. Aside from this dolomite facies, formation lithologies include anhydrite, limestone, salt, and red bed units (Ramondetta et al., 1982). The San Andres is present at depths from 5000-6500 ft in the Seminole region and the wells sampled in this study are of a depth of ~5350 ft. The San Andres Formation is not as deep at the Emma oil field, where producing wells are at a depth of 4200 ft.

The Upper San Andres sediments were deposited during the Guadalupian epoch (270-260 Ma) in the Permian basin region. Eustatic sea level change was common in the basin during the Permian period, resulting in the deposition of marine shales and carbonates along with shoreline sandstones and sabkha related salts and evaporites. A rise in sea level made the eastern part of the Permian basin a carbonate shelf during the early Guadalupian. When the sea level in the basin eventually lowered, the recently deposited carbonate muds were subjected to aerial exposure and dessication. This created porous pathways in the mud where an influx of meteoric water caused the dolomitization of the formation (Ramondetta et al., 1982).

It is also possible that seawater caused the dolomitization following the subaerial exposure and dessication. Stable isotope data suggests that seawater brines have caused the dolomitization of the San Andres Formation (Ruppel and Cander, 1988). These dolomites have a $^{87}\text{Sr}/^{86}\text{Sr}$ ratio (0.7067), similar to the minimum values seen for Permian seawater, suggesting that the San Andres was dolomitized shortly after it was deposited when the sea levels rose (Ruppel and Cander, 1988).

The hydrocarbons present in the San Andres dolomite migrated vertically to this reservoir from Wolfcampian (299-280 Ma) shales (Ramondetta, 1982b). Anhydrite beds of the San Andres act as non-permeable seal rocks for the porous dolomite reservoir (Ramondetta et al., 1982a). The anhydrites of the San Andres formation are a source of sulfur for connate brines,

although degraded organics and reduction of Permian sulfate can also contribute to sulfur (Lueth et al., 2005). This sulfur is present as H₂S gas in oil produced from the Upper San Andres formation at both East Seminole and Emma oil fields.

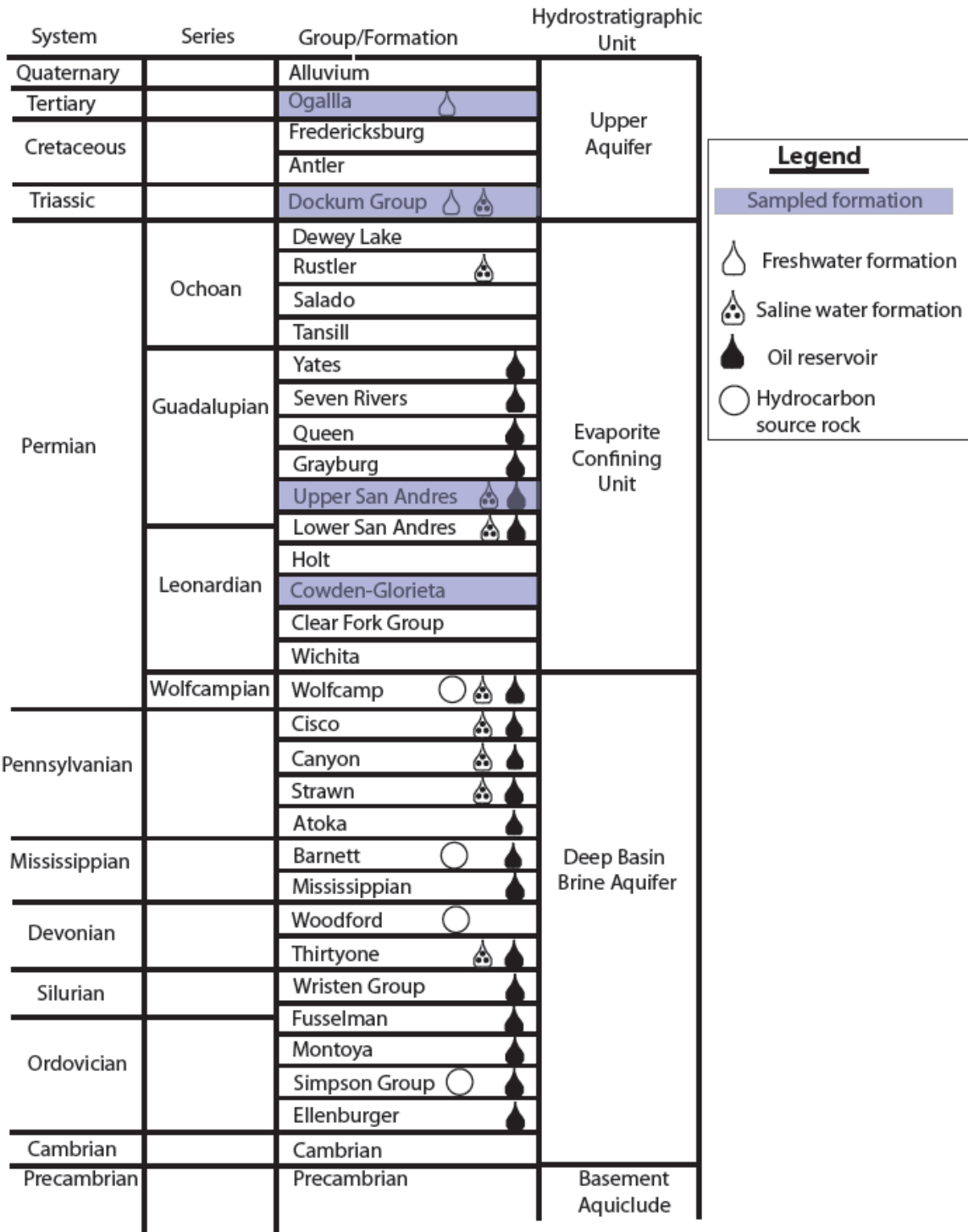


Figure 13. Schematic column of water bearing formations, hydrocarbon reservoirs, and hydrocarbon source rocks from the Quaternary to the Precambrian in the Central Basin Platform. This figure was generated using information from multiple sources (Bassett and Bradley, 1982; Stueber et al., 1998; Bradley and Kalaswad, 2003; Dutton et al., 2005).

3.2.1.4 Tertiary Ogallala Formation, Part of the High Plains Aquifer

The sampled groundwater wells tap water from the Ogallala aquifer, which has a thickness of ~200 ft in the area and is a reliable water source for wells drilled to depths between 120 and 180 ft (Figure 14). The Ogallala aquifer is part of the High Plains Aquifer, which sits under 8 states, covers more than 450,000 km², and serves as an irrigation source and a drinking water source for the 2.3 million people within its extent (Figure 10) (Sophocleous, 2010). According to drilling logs, the top of the Ogallala consists of a 30 ft caliche caprock that confines the lower sandstone water-bearing segment of the formation (Figure 14) (Cirrus Associates, 2011).. The East Seminole oil field is in a semiarid climate and receives 350 mm/year of rainfall, of which an estimated 11±2 mm/yr recharges this Tertiary aquifer (Nativ, 1992; Wood and Sanford, 1995). In addition to rainfall recharge that travels primarily from the Rocky Mountains, playa lakes are believed to be the primary source of recharge for the Ogallala aquifer in the Permian Basin (Nativ, 1992; Wood and Sanford, 1995).

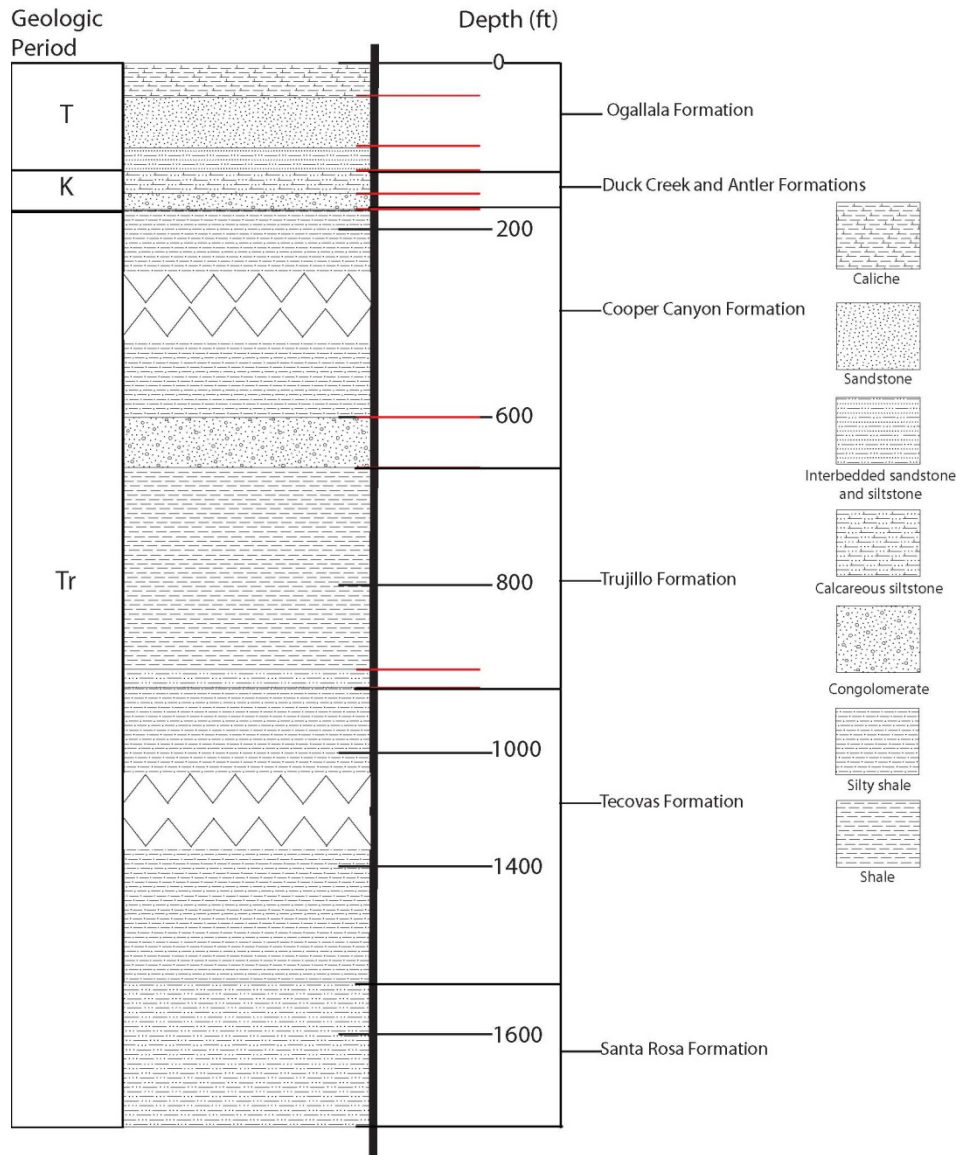


Figure 14. Stratigraphic column of water bearing formations from the Triassic, Cretaceous and Tertiary beneath Seminole, TX. This column was generated based on written well log descriptions from Cirrus Associates, (2011). Geologic patterns are from the USGS (2006).

3.2.1.5 Cretaceous Duck Creek and Antler Formations

Beneath the Tertiary Ogallala is a 50-ft layer of Cretaceous limestones, shales, and conglomerates that are not ubiquitous throughout the Permian Basin. The limestone and shale layers may be part of the Fredericksburg Formation, an aquifer in some regions. The

conglomerate is potentially part of the Antlers Formation (Cirrus Associates, 2011). The Cretaceous aquifers of the region, including the Fredericksburg Formation, have a higher potentiometric surface than the Ogallala aquifer. Previous work has shown that it is reasonable to believe that upward flow through permeable contacts is possible and that sections of the Ogallala aquifer with higher salinity levels are often underlain by Cretaceous strata, suggesting that permeable contacts exist between the two (Nativ, 1992).

3.2.1.6 Triassic Dockum Group

The Triassic Dockum Group, a set of reddish-brown sandstones and conglomerates that host brackish to saline waters (Bradley and Kalaswad, 2003), has been identified as beginning at 175 ft beneath the surface of Seminole and terminating at a depth around 1750 ft (Figure 14) (Cirrus Associates, 2011). Despite its depth and total dissolved solid levels that can range between 5,000-60,000 mg/L, Dockum Group groundwater is being considered to complement current water supplies because of drawdown in the Ogallala aquifer due to pumping irrigation wells beyond sustainable yields and severe drought conditions (Dutton et al, 2001; Johnson et al., 2009; Heim, 2013). Researchers have begun to study the viability of a wind-powered water desalinization plant that would treat water from the Dockum Group for the Seminole municipal water supply (Clayton et al., 2013).

The critical water shortage has also resulted in the drilling of a test well in Seminole that penetrates the Dockum Group. Drilling logs from this test well indicate that the upper Dockum group is composed mostly of mudstones that separate its waters from the overlying Ogallala (Cirrus Associates, 2011). Mudstones and siltstones are the first ~350 ft of the Dockum Group in Seminole and although these may partially confine the Dockum Group, previous work has shown that the potentiometric surface of the Dockum is higher than that of the Ogallala in the region

(Nativ, 1992). Evidence of communication between the two formations has been shown in pockets of the Permian basin where mixed-cation- HCO_3 water, typical of the Ogallala aquifer, has been shown to shift to Na-HCO_3 water, which is common in the Dockum aquifer (Nativ, 1992). This Triassic formation may receive groundwater input from outcrop locations, but it is unlikely that this recharge is significant (Nativ, 1992; Bradley and Kalaswad, 2003).

The Dockum Group produces water at three different depths: the Copper Canyon Formation (540-650'), the Tecovas Formation (890-920'), and the Santa Rosa Formation (1610-1770') (Figure 14). Although the majority of Dockum sediments were deposited in varying lacustrine, fluvial and deltaic environments in a closed basin, the basal Santa Rosa is believed to have been deposited in a fluvial system that flowed east-to-west. The other two water bearing formations consist of siltstones and claystones that were deposited in a floodplain environment and they lie at the top of fining upward depositional sequences (Lehman and Chatterjee, 2005).

While the term 'Santa Rosa' is used colloquially for any part of the Dockum group that produces water, the depth (~1500 ft) of the sampled well indicates that this water actually originates from that formation (Cirrus Associates, 2011). The Santa Rosa formation is sandstone and conglomerate formation composed predominantly of quartzose grains that were deposited in a stream environment (Lehman and Chatterjee, 2005). The Santa Rosa formation has a maximum thickness of 130 ft and lies at the base of the Dockum Group, which is the only Triassic group to outcrop in Texas (Bradley and Kalaswad, 2003). The remainder of the overlying Dockum group is composed of mudstones, siltstones, and massive sandstones (Lehman and Chatterjee, 2005).

3.3 SAMPLING

Water samples were collected in June 2013 (Figure 15 and Figure 16). Thirteen of the water samples came from production wells that required the help of a Tabula Rasa production foreman, who would check the well head pressure and then open the valve when the researchers were ready to sample (Figure 17). A similar process was required for the injection well waters and the Santa Rosa water well. The remaining six wells were groundwater wells used either for irrigation, industrial purposes, or drinking water. They were all screened at a depth of <200 ft below the surface and samples were taken directly from the well head. All samples were collected in a two gallon plastic carboy (Figure 17) that was thoroughly rinsed with the sample water twice before an actual sample was collected. All samples were filtered with an EnviroTech 0.45 μm filter using a peristaltic pump. Production and injection well samples were first filtered using glass wool to remove as much oil as possible. The other samples were not filtered with glass wool because they did not have any visible oil content. New peristaltic tubing was used for each production and injection well sample. The same peristaltic tubing was used for each groundwater well. This tubing was rinsed with ~250 mL of the next groundwater sample before any sample collection took place. The carboys used to collect production and injection samples were cleaned with Dawn soap mixed with water from Tabula Rasa WSW #1 and then rinsed three times with water from Tabula Rasa WSW #1. The carboys were thoroughly rinsed with the groundwater samples three times before sample collection occurred.

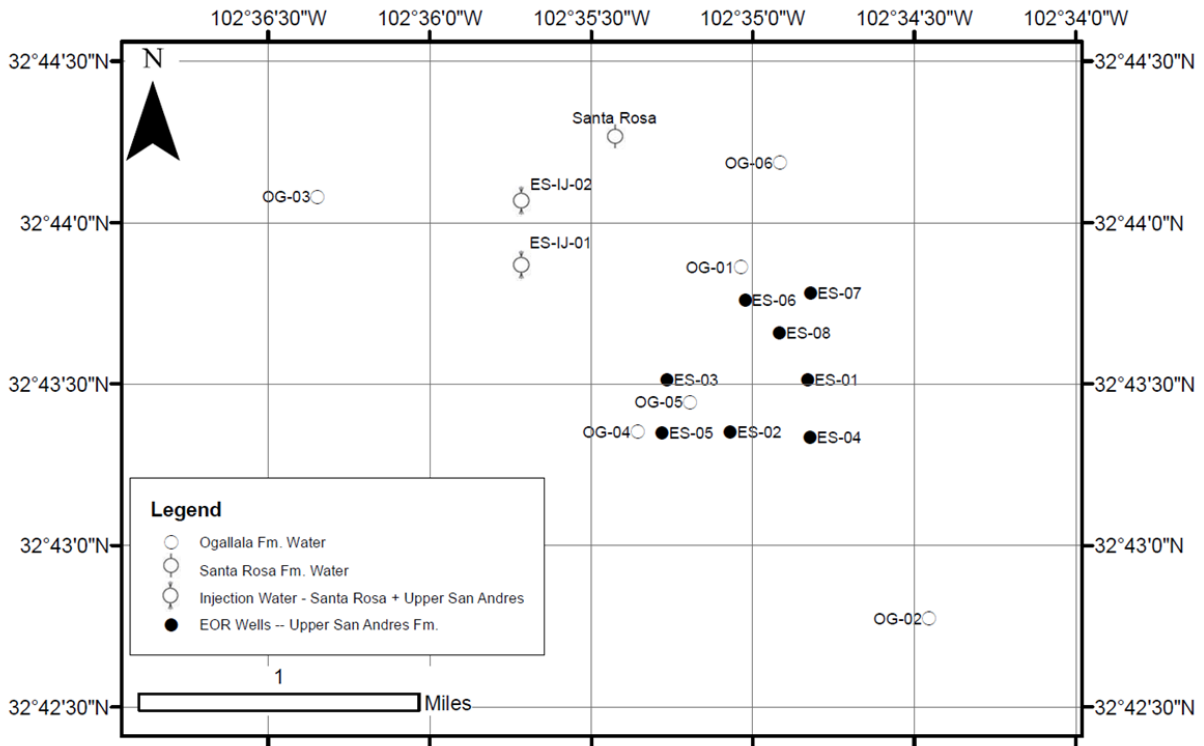


Figure 15. East Seminole oil field sample locations and the formation that produces fluid at each well. Sample names are located next to well symbols.

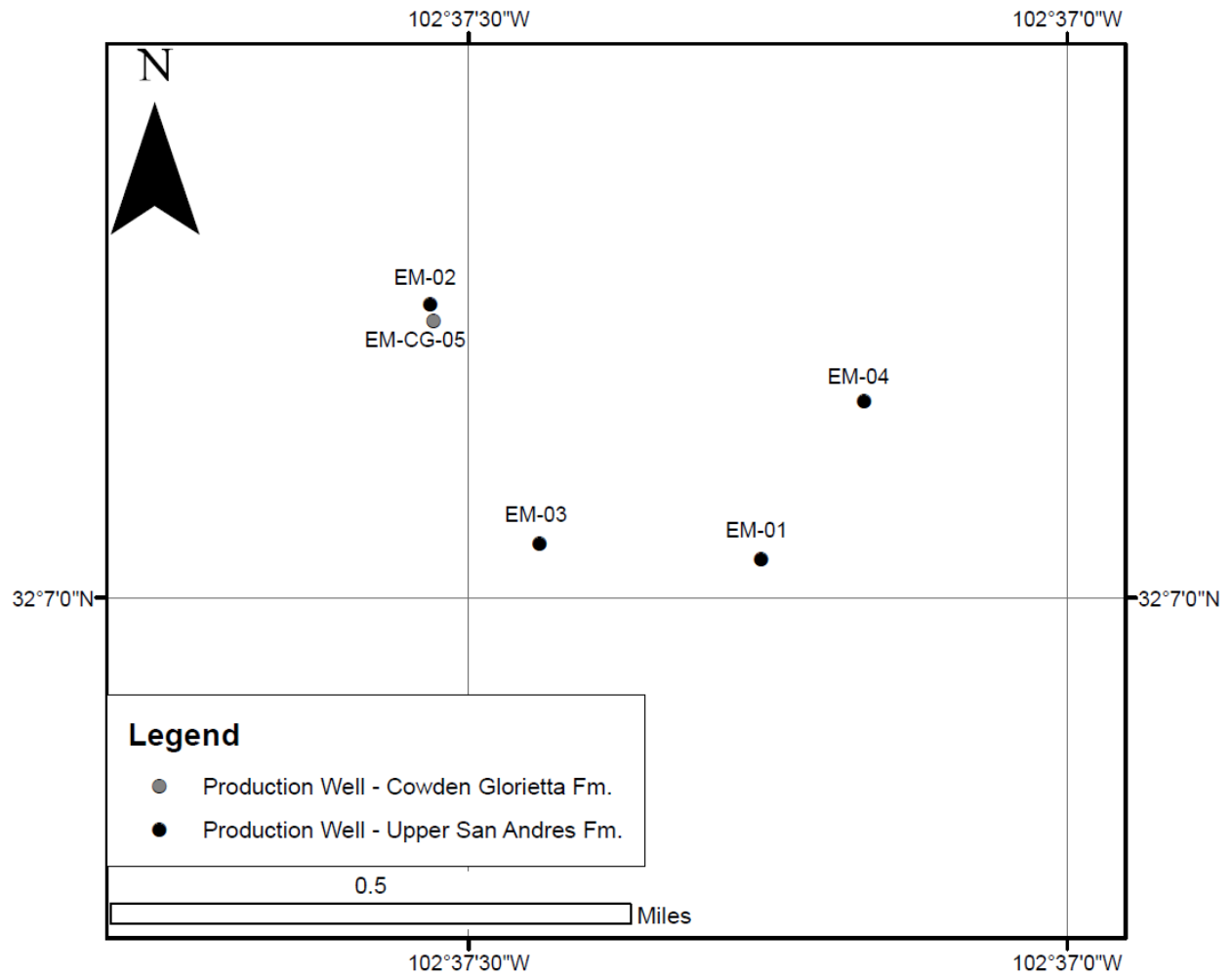


Figure 16. Map of sample locations at Emma oil field with the sampled formation listed. Sample names are located next to wells symbols.



Figure 17. Photograph of author sampling EM-01 with the assistance of Tabula Rasa employee.

3.4 ANALYTICAL METHODS

For production and injection wells, the samples were taken as soon as possible to a field lab station, where pH, reduction potential (E_H), total dissolved solids (TDS), temperature, and alkalinity were measured. OG-01 was treated in a similar matter. For all other Ogallala and Santa Rosa groundwaters, pH, E_H , and TDS were measured in a flow-through cell.

Alkalinity measurements were made using a Hach digital titrator. Due to time constraints in the field, reverse alkalinity tests were done a few hours after sampling to determine the

contribution of organic alkalinity to the total alkalinity. This test used the same solution that had already been titrated with acid using the Hach digital titrator. The method, based on that of Muller and Bleie (2008), involved bubbling N₂ gas through the solution to remove CO₂ gas and then titrating the sample with 0.10 M NaOH in a closed cell.

After filtration, samples were placed in zip-lock bags and placed on ice for sample preservation and prevention of bottles rupture via degassing H₂S, the sample bottles were kept on ice throughout transport to Pittsburgh, PA, where they were acidified to 2% HNO₃ by weight.

These samples were then measured for major cations and Sr, 2013 by ICP-OES at the University of Pittsburgh. Based on these Sr concentrations, a volume of solution that contained approximately 2 µg of Sr was aliquoted for each sample. This aliquot was dried down, dissolved in 8N ultrapure nitric acid, and put through Eichrom® Sr resin columns to isolate Sr from the rest of the sample. The column set up, elution, and cleaning process was modeled after the high throughput method described by Wall et al. 2013. Concentrated nitric was then added to each of the Sr solutions so that they were 2% HNO₃ by volume and these samples were then analyzed by MC-ICP-MS. The NIST 987 standard was analyzed concurrently with the other samples and produced an average ⁸⁷Sr/⁸⁶Sr ratio was 0.710278 ± 0.000009 (2σ).

3.5 RESULTS

3.5.1 Field geochemistry results

Field measurements are listed in Table 5. The wells have been categorized based on well depth, location, or water use. Emma oil field produced waters are from the conventional oil field. The

TDS levels for these wells (53,000-75,000 ppm) indicate that they are saline waters. These TDS levels are double those for the East Seminole oil field (12,000-32,000 ppm) where an active water injection is occurring. The alkalinity values (601-871 mg/L as CaCO₃) for Emma produced waters are also lower than the values for the Seminole wells (925-1426 mg/L as CaCO₃). The pH values for both Emma (6.38-6.53) and East Seminole (6.25-6.58) fell in a narrow range and were circumneutral, save for Emma 1013R (5.89).

Injection waters are a mixture of East Seminole produced waters and Triassic Santa Rosa Formation waters. These injection waters are used to flood the East Seminole oil fields. The TDS levels (22,000-29,000 ppm) were within the range of produced waters at East Seminole, as were their alkalinity (1098-1133 mg/L as CaCO₃) and pH values (6.4-6.5). The Santa Rosa Formation water had a much lower alkalinity value (305.5 mg/L as CaCO₃), a higher pH (7.99), and a lower TDS (4225 ppm) than the injection waters.

Most of the Ogallala groundwaters pHs between 6.93-7.33 and alkalinity values between 140-238 mg/L as CaCO₃. One Ogallala well had a higher TDS (2990 ppm) than of the other groundwaters (767-2145 ppm). This well (OG-01) is used by Tabula Rasa Energy for industrial purposes on site, including dust control. Despite an elevated TDS, this water had a pH (6.91) and alkalinity (161 mg/L as CaCO₃) similar to its neighboring Ogallala groundwaters.

Table 5. Field data for water samples collected at Emma and Seminole Oil Fields. Dr. Gwen Macpherson, University of Kansas, measured the pH, temperature, Eh, and TDS for most of these samples. All of these values as well as alkalinity were measured in the field. All samples were taken between June 3-6, 2013.

Sample	Depth (ft)	pH	Temperature °C	Eh mV	TDS ppm	Alkalinity (mg/L as CaCO ₃)
East Seminole oil field produced waters						
ES-01	5350	6.30	30.4	-178	28000	1342
ES-02	5350	6.49	31.8	-170	12000	1124
ES-03	5350	6.41	36.3	-185	16500	925.2
ES-04	5350	6.50	34.1	-184	17000	1252
ES-05	5350	6.26	36.1	-166	20000	1145
ES-06	5350	6.58	27.7	-137	30000	1387
ES-07	5350	6.28	28.1	-167	32000	1426
ES-08	5350	6.51	34.2	-158	ND	1084
Emma oil field produced waters						
EM-01	4200	5.89	23.8	-160	72000	732.3
EM-02	4200	6.53	31.9	-172	65000	826
EM-03	4200	6.38	27.8	-164	75000	601.2
EM-04	4200	6.51	27.6	-181	67000	871.4
EM-CG-05	5600	6.46	29.5	-150	53000	712.4
Injection water used at East Semionle oil field (mix of Santa Rosa Fm water and East Seminole produced water)						
ES-IJ-01	NA	6.37	28.1	-157	22000	1133
ES-IJ-02	NA	6.45	28.1	-186	29000	1098
Santa Rosa formation water						
Santa Rosa	1500	7.99	28.5	-52	4225	305.3
Ogallala formation water						
OG-01 (industrial)	180	6.91	29.1	405	2990	161.1
OG-02 (irrigation)	174	6.93	19.3	ND	2015	140.0
OG-03 (irrigation)	150	7.15	21.8	486	1268	173.7
OG-04 (residential)	153	7.28	19.5	341	767	238.4
OG-05 (residential)	180	7.03	20.3	477	1560	181.3
OG-06 (residential)	180	7.33	19.8	319	2145	167.0

3.5.2 Organic alkalinity results

Organic alkalinity results are reported in Table 6. Due to the high oil content of certain sampled wells, organic alkalinity was measured. Despite the differences in total alkalinity values, produced waters from East Seminole and Emma oil fields had small fractions of organic alkalinity. The estimated percentages of carbonate alkalinity for East Seminole (90.8-94.3%) and

Emma (83.2-94.8%) produced waters are similarly high. The injection waters also had similar carbonate contributions between 91.6-92.5%. The one formation water which did appear to have a higher organic alkalinity contribution was the Santa Rosa Formation water, where the estimated percentage of carbonate alkalinity was ~60%. None of the Ogallala aquifer wells were tested for organic alkalinity because they did not contain any visible oil molecules.

Table 6. Alkalinity with the contributions of organic alkalinity and the actual carbonate alkalinity to the total alkalinity. Organic alkalinity tests were not performed on shallow groundwaters and those samples not listed.

Sample	Depth (ft)	Total alkalinity meq/L as CaCO ₃	Organic alkalinity † meq/L as CH ₃ COO ⁻	Carbonate alkalinity meq/L as CaCO ₃	% Carbonate alkalinity
East Seminole oil field produced waters					
ES-01	5350	26.8	1.98	24.8	92.6
ES-02	5350	22.5	ND	NA	NA
ES-03	5350	18.5	3.10	15.4	83.2
ES-04	5350	25.0	1.95	23.1	92.2
ES-05	5350	22.9	2.86	20.0	87.5
ES-06	5350	27.7	2.07	25.6	92.5
ES-07	5350	28.5	1.47	27.0	94.8
ES-08	5350	21.7	2.12	19.5	90.2
Emma oil field produced waters					
EM-01	4200	14.6	0.949	13.7	93.5
EM-02	4200	16.5	0.949	15.6	94.3
EM-03	4200	12.0	1.10	10.9	90.8
EM-04	4200	17.4	1.29	16.1	92.6
EM-CG-05	5600	14.2	1.25	13.0	91.2
Injection water used at East Semionle oil field (mix of Santa Rosa Fm water and East Seminole produced water)					
ES-IJ-01	NA	22.6	1.69	20.9	92.5
ES-IJ-02	NA	21.9	1.85	20.1	91.6
Santa Rosa formation water					
Santa Rosa	1500	6.10	2.44	3.7	60.0

† By Dr. Gwen Macpherson, University of Kansas

3.5.3 General geochemistry results

Produced waters from the Emma oil field had the highest concentrations of all seven elements measured (Table 7). Although anion results were not available at the time of this dissertation, the waters were characterized based on their major cation content (Table 8). Emma oil field produced waters are dominated by Na-cations, like most of the waters sampled in this study, and received minor cation contributions from Ca (7-11% of total cation charge) and Mg (5-7%). Sodium concentrations were between 15,600-20,100 mg/L for these samples. Produced waters from the East Seminole oil field were also Na waters, although the concentrations of Na (5,928-11472 mg/L) were much lower than seen in the Emma oil field.

Table 7. Major element data for water samples collected at Emma and Seminole Oil Fields.

Sample Name	Depth (ft)	Ca	K	Mg	Na	P	Si	Sr
mg/L								
East Seminole oil field produced waters								
ES-01	5350	920.6	265	290	8951.0	68.2	7.32	26.4
ES-02	5350	829.2	203	226	5514.0	74.8	7.14	21.3
ES-03	5350	888.7	191	209	6143.2	59.0	6.18	21.7
ES-04	5350	802.1	218	218	5927.5	79.5	6.56	23.4
ES-05	5350	930.0	264	368	6604.3	82.9	7.59	25.0
ES-06	5350	892.7	295	308	7772.4	88.3	7.85	28.6
ES-07	5350	447.3	331	336	8256.7	87.6	3.20	15.4
ES-08	5350	1170	303	319	11472	73.1	7.75	29.4
Emma oil field produced waters								
EM-01	4200	2335	584	695	19624	155	8.93	73.9
EM-02	4200	2027	549	685	20124	153	7.86	59.8
EM-03	4200	1955	593	781	17575	173	10.4	77.5
EM-04	4200	1587	527	638	15556	157	8.11	52.4
EM-CG-05	5600	1385	466	510	18536	163	5.89	40.8
Injection water used at East Semionle oil field (mix of Santa Rosa Fm water and East Seminole produced water)								
ES-IJ-01	NA	693.7	184	215	5355.9	68.8	5.47	21.6
ES-IJ-02	NA	885.7	265	234	7130.5	81.5	8.77	24.6
Santa Rosa formation water								
Santa Rosa	1500	16.80	5.74	11.0	1194.3	3.37	6.25	0.73
Ogallala formation water								
OG-01 (industrial)	180	338	14.1	224	343.03	28.6	74.2	10.1
OG-02 (irrigation)	174	83.85	9.03	122	243.44	11.2	32.7	3.02
OG-03 (irrigation)	150	56.36	7.43	82.2	104.84	4.59	24.8	2.16
OG-04 (residential)	153	33.31	4.20	37.8	117.65	4.50	27.2	1.14
OG-05 (residential)	180	67.82	8.48	110	123.00	7.59	29.9	2.33
OG-06 (residential)	180	101	12.0	164	144.96	12.2	29.2	4.14

East Seminole injection waters were similar to East Seminole produced waters, but the injection waters were more dilute, with Na concentrations in the range of 5,356-7,131 mg/L. The Na still was ~80% of the milliequivalents for major cations. It also received minor cation contributions from Ca (12%) and Mg (6%). Santa Rosa formation water had an even lower concentration of Na (1194 mg/L), but a scant amount of Ca and Mg compared to Na. This water also would be considered a Na-dominated water.

Ogallala aquifer waters were the only waters that did not have Na as the dominant cation. These waters are from depths of <180 ft and are groundwater drinking and irrigation sources. These waters had substantially lower Na concentrations (105-343 mg/L) than the other deeper well samples (Table 3). One well (OG-01) had nearly equal proportions of Ca-Mg-Na (Table 8). This water is from the same depth as the other Ogallala wells, which are Na-Mg based waters with contributions from Ca (17-20%) always being less than Mg (31-50%).

Table 8. Major cations listed in milliequivalents and the percentage that element makes of the total milliequivalents for that water sample.

Sample Name	Depth (ft)	Ca		K		Mg		Na		Total
		mEQ	%	mEQ	%	mEQ	%	mEQ	%	mEQ
East Seminole produced waters										
ES-01	5350	46.0	10	7	1	24	5	389.3	83	466.6
ES-02	5350	41.4	14	5	2	19	6	239.8	79	305.5
ES-03	5350	44.4	13	5	1	17	5	267.2	80	334.2
ES-04	5350	40.1	12	6	2	18	6	257.8	80	322.0
ES-05	5350	46.5	13	7	2	30	8	287.3	77	371.4
ES-06	5350	44.6	11	8	2	25	6	338.1	81	416.2
ES-07	5350	22.4	5	8	2	28	7	359.1	86	418.0
ES-08	5350	58	10	8	1	26	4	499	84	592
Emma oil field produced waters										
EM-01	4200	117	11	15	1	57	5	854	82	1044
EM-02	4200	101	10	14	1	56	5	875	83	1048
EM-03	4200	98	10	15	2	64	7	764	81	943
EM-04	4200	79	10	13	2	52	6	677	82	823
EM-CG-05	5600	69	7	12	1	42	5	806	87	930
Injection water										
ES-IJ-01	NA	34.7	12	5	2	18	6	233.0	80	290.5
ES-IJ-02	NA	44.3	12	7	2	19	5	310.2	81	381.0
Santa Rosa formation water										
Santa Rosa	1500	0.84	2	0.15	0	0.9	2	51.9	96	53.9
Ogallala formation water										
OG-01 (industrial)	180	17	33	0.4	1	18	36	14.92	29	50.82
OG-02 (irrigation)	174	4.19	17	0.23	1	10	40	10.59	42	25.14
OG-03 (irrigation)	150	2.82	20	0.19	1	6.8	47	4.56	32	14.38
OG-04 (residential)	153	1.66	17	0.11	1	3.1	31	5.12	51	10.02
OG-05 (residential)	180	3.39	19	0.22	1	9	50	5.35	30	18.02
OG-06 (residential)	180	5	20	0.3	1	14	53	6.31	25	25.29

3.5.4 Strontium isotope geochemistry

The strontium isotope data is presented in Table 9. Emma oil field samples consist of produced waters from the Upper San Andres formation (EM-01 to EM-04) and the Cowden-Glorieta sandstone (EM-CG-05). These Upper San Andres formation produced waters from the Emma oil field had the highest $^{87}\text{Sr}/^{86}\text{Sr}$ (0.7098-0.7105) and the highest Sr concentrations of Sr [52.4-73.9 mg/L] of any sample (Table 9). EM-CG-05, from the Cowden-Glorieta sandstone, had a lower ratio (0.7085) and strontium concentration [40.8 mg/L] than the produced waters from the overlying Upper San Andres formation.

East Seminole produced waters all had markedly lower $^{87}\text{Sr}/^{86}\text{Sr}$ [\sim 0.7079] compared to the Emma oil field values. The East Seminole produced waters, all from the Upper San Andres formation, also had $^{87}\text{Sr}/^{86}\text{Sr}$ values that fell in such a tight range that they have the same value to the fourth decimal place. The strontium concentrations varied between 15.4-29.4 mg/L. The East Seminole produced waters appear to be quite different than those of the Emma oil field, especially since all of the samples except one are produced waters from the Upper San Andres formation.

The critical difference between these waters is that Emma oil field samples come from a conventional field, as opposed to East Seminole samples, which from a water flooded EOR field. This means that it is important to consider the chemistry of the injection water that floods East Seminole. The injection waters at East Seminole had $^{87}\text{Sr}/^{86}\text{Sr}$ of \sim .7079 and Sr concentrations [21.6-24.6 mg/L] that were similar to those seen in East Seminole produced waters. The injection waters and the East Seminole produced waters have the same $^{87}\text{Sr}/^{86}\text{Sr}$ to the fourth decimal place (\sim 0.7079) and cannot be discerned via in the strontium isotope data.

Santa Rosa formation water has a slightly higher $^{87}\text{Sr}/^{86}\text{Sr}$ (0.7084) but a much lower Sr concentration [0.73 ppm] than East Seminole produced waters. The Santa Rosa formation water does have a higher $^{87}\text{Sr}/^{86}\text{Sr}$, but with a strontium concentration that is 30 times less than that of the injected water, it affects the $^{87}\text{Sr}/^{86}\text{Sr}$ of the East Seminole produced waters minimally.

Injection waters and Santa Rosa formation waters both had $^{87}\text{Sr}/^{86}\text{Sr}$ ratios that were approximately the same or slightly higher than that of East Seminole produced waters. Therefore, there were no waters injected into the East Seminole field that would lower its $^{87}\text{Sr}/^{86}\text{Sr}$ ratio. Taking into account these results, the original formation waters at East Seminole may have had a different, lower $^{87}\text{Sr}/^{86}\text{Sr}$ than that of the produced waters at Emma Oil field, despite the fact that they are believed to produce from the same section of the San Andres formation.

Ogallala formation waters had $^{87}\text{Sr}/^{86}\text{Sr}$ (0.7086-0.7087) that were slightly elevated to those in the Santa Rosa (0.7084) and those in the East Seminole produced waters (0.7079) (Table 5). While the geochemistry of one Ogallala formation water (OG-01) was distinct from the others, its strontium isotope ratio was nearly identical to the other Ogallala waters. OG-01 also had a much higher Sr concentration [10.1 mg/L] than the other waters from the same formation. Despite the higher Ca and Sr concentrations (Table 7) in OG-01 relative to other Ogallala waters and the difference in major cation constituents (Table 8), these waters have nearly identical $^{87}\text{Sr}/^{86}\text{Sr}$ signatures. This suggests that both groups of water have a similar source of Sr.

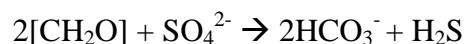
Table 9. Sr isotopic composition of waters at Emma and East Seminole Oil Fields.

Sample Name	Depth (ft)	$^{87}\text{Sr}/^{86}\text{Sr}$		Sr mg/L
East Seminole oil field produced waters				
ES-01	5350	0.707883	± 0.000010	26.4
ES-02	5350	0.707914	± 0.000008	21.3
ES-03	5350	0.707917	± 0.000010	21.7
ES-04	5350	0.707886	± 0.000010	23.4
ES-05	5350	0.707924	± 0.000010	25.0
ES-06	5350	0.707953	± 0.000010	28.6
ES-07	5350	0.707905	± 0.000008	15.4
ES-08	5350	0.707893	± 0.000010	29.4
Emma oil field produced waters				
EM-01	4200	0.710513	± 0.000008	73.9
EM-02	4200	0.710006	± 0.000008	59.8
EM-03	4200	0.710587	± 0.000008	77.5
EM-04	4200	0.709776	± 0.000008	52.4
EM-CG-05	5600	0.708509	± 0.000010	40.8
Injection water used at East Seminole oil field (mix of Santa Rosa Fm water and East Seminole produced water)				
ES-IJ-01	NA	0.707934	± 0.000010	21.6
ES-IJ-02	NA	0.707939	± 0.000010	24.6
Santa Rosa formation water				
Santa Rosa	1500	0.708403	± 0.000010	0.73
Ogallala formation water				
OG-01 (industrial)	180	0.708667	± 0.000008	10.1
OG-02 (irrigation)	174	0.708639	± 0.000008	3.02
OG-03 (irrigation)	150	0.708646	± 0.000008	2.16
OG-04 (residential)	153	0.708613	± 0.000010	1.14
OG-05 (residential)	180	0.708665	± 0.000008	2.33
OG-06 (residential)	180	0.708669	± 0.000008	4.14

3.6 DISCUSSION

3.6.1 Organic alkalinity

Organic alkalinity is not a significant contributor to the total alkalinity of any of the produced waters. This is despite the strong H₂S content of these wells and the possibility that H₂S is a by-product of microbial activity in the subsurface. The sulfate reduction to H₂S in the San Andres formation is occurring via microbial activity or thermally driven processes (Goldhaber, 2005). Previous work has shown that in oil fields deeper (6,000-10,000 ft) than East Seminole or Emma, SO₄ reduction to H₂S is likely the result of bacterially driven sulfate reduction (Cai et al., 2005). Anaerobic sulfate reduction has also been shown to transform organics and anions in the following manner (Jobson et al., 1979, Cai et al., 2002):



The H₂S enrichment in the Upper San Andres is likely the result of this anaerobic process, as microbes from recharge water degraded hydrocarbons (Ramondetta, 1982b).

Interestingly, the only well with a significant component of organic alkalinity is from the Santa Rosa well. The Santa Rosa water may be a source of additional organics for the microbes in the San Andres formation, although they would only be providing a small amount given the split of Santa Rosa in the injection water. The estimated split of Santa Rosa-to-produced water in the injection water is 25% Santa Rosa formation water to 75% produced water.

3.6.2 General geochemistry and isotope geochemistry

3.6.2.1 $^{87}\text{Sr}/^{86}\text{Sr}$ as a monitoring tool

The projected flow of injected CO_2 (Figure 18) indicates that the CO_2 plume should travel to the northwest of the injector wells and underneath the groundwaters sampled in this study. A $^{87}\text{Sr}/^{86}\text{Sr}$ mixing model was created using the average $^{87}\text{Sr}/^{86}\text{Sr}$ (0.707909) and strontium concentration (23.9 mg/L) of East Seminole produced waters as one end member and the regional groundwaters as the other (Figure 19). One mixing model curve mixes the average East Seminole produced water with Ogallala waters (average $^{87}\text{Sr}/^{86}\text{Sr}$ =0.708646; average [Sr] = 2.56 mg/L). This curve shows that even slight mixing (5-10% of East Seminole produced water) would lower the $^{87}\text{Sr}/^{86}\text{Sr}$ of the water. The extremely tight $^{87}\text{Sr}/^{86}\text{Sr}$ range of the Ogallala waters (~0.7086-0.7087) means that even these slight shifts could indicate upwelling produced water.

The second mixing model curve uses $^{87}\text{Sr}/^{86}\text{Sr}$ (0.7084) and Sr (0.73 mg/L) of the Santa Rosa Formation water and mixes it with the average East Seminole produced water (Figure 19). Its low strontium concentration makes Santa Rosa water even more sensitive to mixing with East Seminole produced waters. Mixing 5% of East Seminole produced waters with it would cause a precipitous drop in $^{87}\text{Sr}/^{86}\text{Sr}$. Based on these mixing curves, $^{87}\text{Sr}/^{86}\text{Sr}$ could be a sensitive monitor of upward migration of East Seminole produced water in both the Santa Rosa formation and the Ogallala aquifer. However, Santa Rosa formation water does appear to be more sensitive to the intrusion of Upper San Andres produced because Santa Rosa formation water has a substantially lower Sr concentration than Ogallala water.

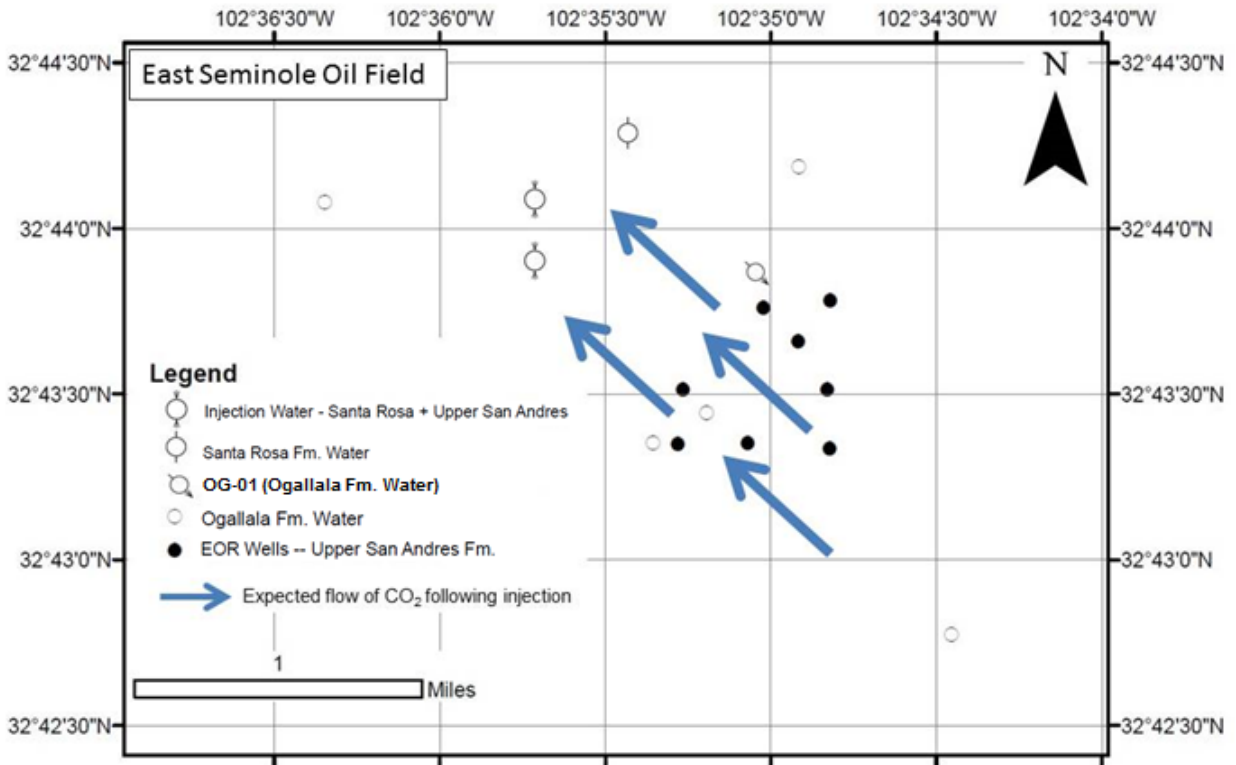


Figure 18. Schematic depicting the expected flow of supercritical CO₂ after injection at the East Seminole oil field. The production wells produce from a depth of ~5350 ft. Downhole temperature ranges between 90-110°F and downhole pressure ranges from 2200-3300 psi.

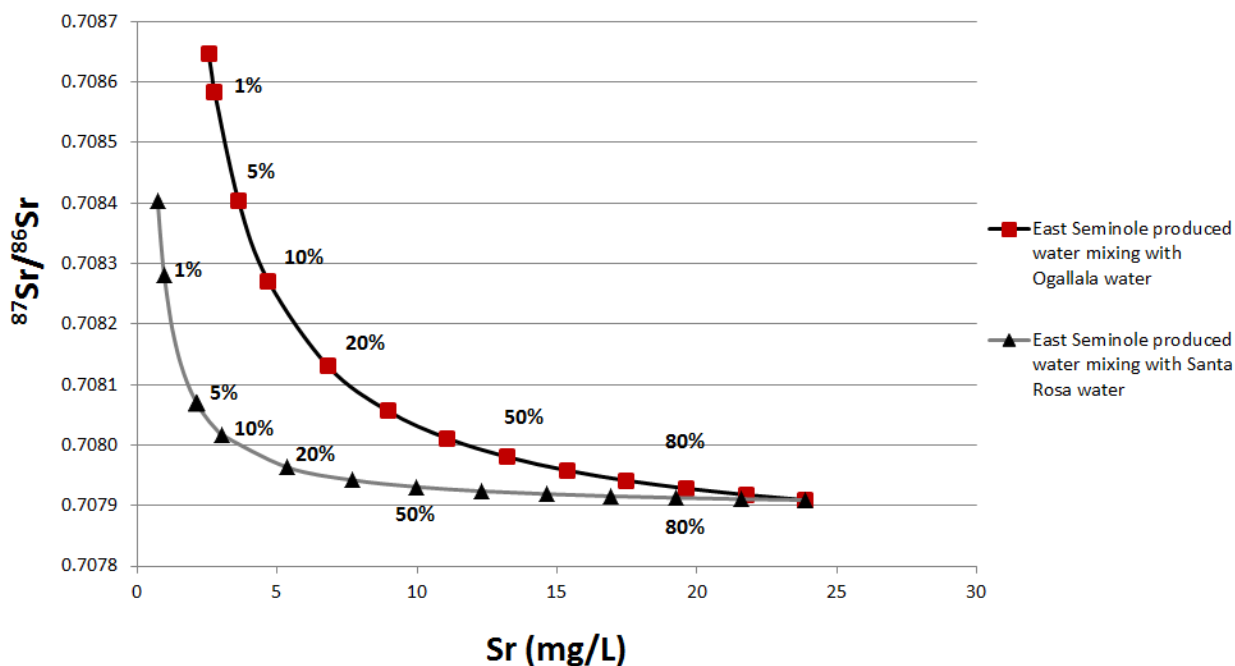


Figure 19. Mixing models depicting (1) East Seminole produced waters mixing with Ogallala aquifer waters (2) East Seminole produced waters mixing with Santa Rosa Formation water; percentages represent the fraction of solution that is produced water. End members of this figure represent data from this study.

3.6.2.2 Produced waters

The general geochemistry for the produced waters suggests that it is possible that the East Seminole Field, with its significantly lower TDS and major cation concentrations, may have at one point been similar to that of the Emma oil field. Santa Rosa formation water has much lower TDS and major cation concentrations and it could be acting to continuously dilute the formation water that it is slowly flushing out of the system. Despite this, the $^{87}\text{Sr}/^{86}\text{Sr}$ indicates that the difference between the Emma and East Seminole oil fields cannot be explained by simple dilution from water flooding and that differing brine migration histories may have caused the differences in these formation waters.

The Emma oil field has higher $^{87}\text{Sr}/^{86}\text{Sr}$ values compared with that of the East Seminole field (Figure 20). The $^{87}\text{Sr}/^{86}\text{Sr}$ strontium values for the East Seminole field are significantly lower than those of the Emma oil field, despite the fact that no components of the injection water into the East Seminole field would lower the current signature. This suggests that the Sr source for the East Seminole field is unique from the Sr source at the Emma oil field.

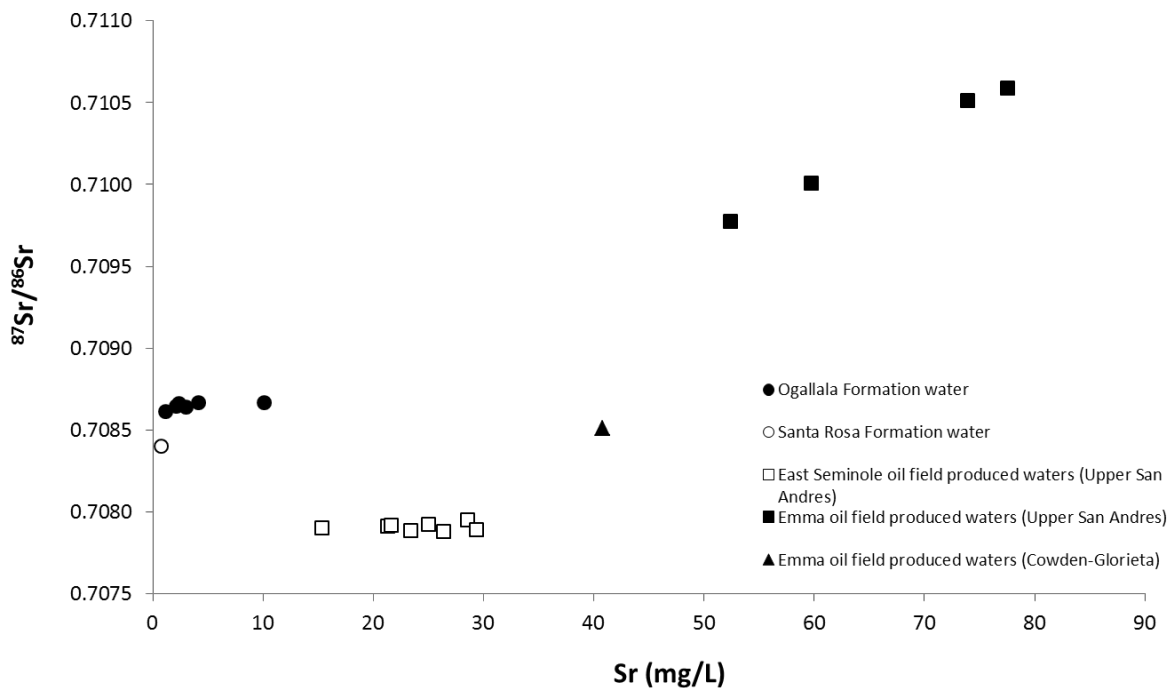


Figure 20. Graph displaying the $^{87}\text{Sr}/^{86}\text{Sr}$ vs. the Sr (mg/L) concentration of all samples from Emma and East Seminole Oil Fields.

The origin of the $^{87}\text{Sr}/^{86}\text{Sr}$ signature for the Upper San Andres formation waters at the Emma field does not appear to be derived from the surrounding Permian dolomite. Previous work (Ruppel and Cander, 1988) measured the $^{87}\text{Sr}/^{86}\text{Sr}$ ratios for the Upper Permian San Andres

dolomite (0.7067-0.7074) and anhydrite (0.7067-0.7071) from a core at the Emma field. The Emma field produced waters from this study have measured $^{87}\text{Sr}/^{86}\text{Sr}$ ratios between 0.7098-0.7106, which is well above the range of the formation's dolomites and anhydrites (Figure 21). These $^{87}\text{Sr}/^{86}\text{Sr}$ ratios also plot above Permian seawater (0.7068-0.7084) and almost all Phanerozoic seawater (0.7068-0.7093) (Burke et al., 1982; Veizer et al., 1999).

Despite water flooding in the past, the Emma oil field has not been flooded in the past twenty years, suggesting that this produced water and its $^{87}\text{Sr}/^{86}\text{Sr}$ signature is representative of the current formation water. The values reported in this study are higher than the Permian signature and suggest an influx of Sr from sedimentary continental crust ($^{87}\text{Sr}/^{86}\text{Sr} \sim 0.712$; Shields, 2007). Considering that the San Andres formation is a dolomite, the increased $^{87}\text{Sr}/^{86}\text{Sr}$ may be the result of a deep basin brine that migrated into the current reservoir rock either with a migrating oil or post oil emplacement.

Deep basin brines have $^{87}\text{Sr}/^{86}\text{Sr}$ that range from 0.7086-0.7280 and they can have Sr concentrations in excess of 600 mg/L (Figure 22). The elevated $^{87}\text{Sr}/^{86}\text{Sr}$ for the Emma produced waters indicate that migration of one of these brines into the formation is likely to have occurred at some point. Based on its proximal location and its status as a source rock, it is likely that it is a Wolfcampian brine, but this is not certain since brines from Wolfcampian, Pennsylvanian, and Devonian strata all have overlapping $^{87}\text{Sr}/^{86}\text{Sr}$ values (Figure 22). Based on the relative depths of these formations and the Wolfcamp's status as the source rock for the Upper San Andres, upward migration of Wolfcamp brine is likely the source of elevated $^{87}\text{Sr}/^{86}\text{Sr}$ in the Upper San Andres. This brine migrated either with the oil or after the oil migration and likely followed the same flow path, likely fractures and faults, into the Upper San Andres (Figure 23). Once this brine arrived in the reservoir formation, it probably interacted with the surrounding Upper San Andres

dolomite-anhydrite formation(0.7067-0.7074), which lowered the overall signature of the Upper San Andres produced water to what is seen today (0.7098-0.7106).

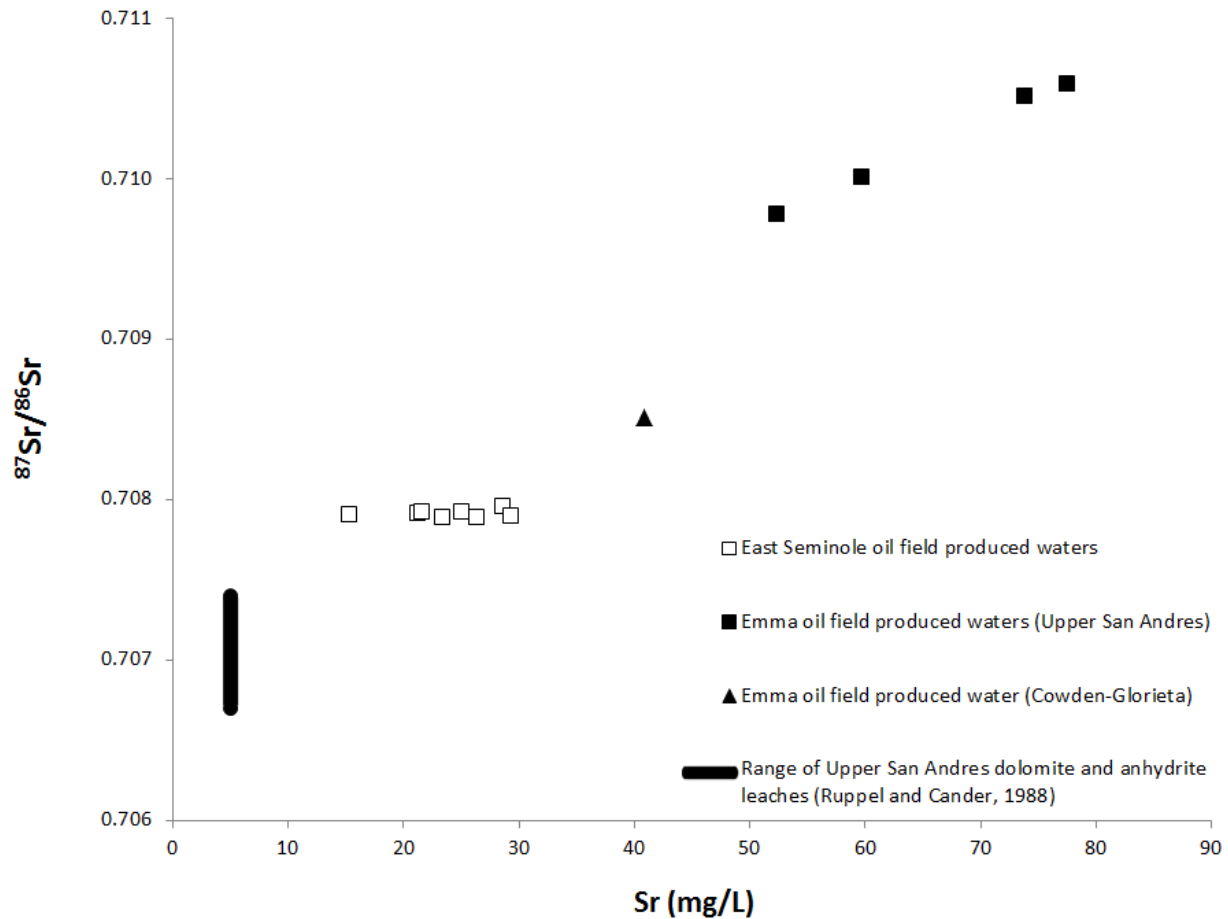


Figure 21. Graph displaying the $^{87}\text{Sr}/^{86}\text{Sr}$ vs. the Sr (mg/L) concentration for produced water samples from this study and the $^{87}\text{Sr}/^{86}\text{Sr}$ of Upper San Andres dolomite and anhydrite leachates from Ruppel and Cander, 1988. Sr concentrations for these leachates are not accurate and were plotted for comparison of $^{87}\text{Sr}/^{86}\text{Sr}$ only.

The produced water from the Cowden-Glorieta sandstone at the Emma oil field appears to receive most of its strontium from a Permian source. This produced water had a $^{87}\text{Sr}/^{86}\text{Sr}$ ~0.7085, which fell close to the range of Permian seawaters. The produced water may have interacted with Permian carbonates during its migration to this reservoir or it is also possible that there are carbonaceous Permian rocks within the sandstone reservoir itself.

The East Seminole produced waters had a narrow range of $^{87}\text{Sr}/^{86}\text{Sr}$ values (all ~ 0.7078) that were within the range of Permian seawater carbonates (0.7068-0.7084) and slightly above the range of Upper San Andres dolomite leaches (0.7067-0.7074) (Ruppel and Cander, 1988). The injection water has a higher strontium signature (0.7079), the East Seminole produced waters are likely the result of the more dilute production waters interacting with Upper San Andres formation dolomites and anhydrites.

The $^{87}\text{Sr}/^{86}\text{Sr}$ values for East Seminole and Emma oil field produced waters are distinct (Figure 21). There are two scenarios to explain this difference: (1) that the two fields always had distinct signatures due to differing brine migration histories or (2) that these waters once had similar $^{87}\text{Sr}/^{86}\text{Sr}$ values, but water flooding at East Seminole flushed out the native brine.

The Sr concentrations of the Emma field produced waters (52.4-77.5 mg/L) are nearly double that of the current East Seminole produced waters (15.4-29.4 mg/L). The water flooding that occurs at East Seminole is constant, meaning that over time, the produced waters will slowly become more dilute until water-rock reactions reach a new steady state. Once this steady state is reached and the water flooding continues under the same practice, the produced water will produce a consistent geochemistry and likely with it, a uniform $^{87}\text{Sr}/^{86}\text{Sr}$, as seen at East Seminole field.

While flushing the connate brine out of the East Seminole reservoir is a possibility, previous work suggests that the two fields always had distinct $^{87}\text{Sr}/^{86}\text{Sr}$. Stueber et al. (1998) measured the $^{87}\text{Sr}/^{86}\text{Sr}$ of six San Andres Formation waters and produced a range (0.7072-0.7078) that is similar to those seen at East Seminole (~ 0.7078). These results suggest a $^{87}\text{Sr}/^{86}\text{Sr}$ representative of the Upper San Andres dolomite may be common in this formation and that the Emma oil field experienced brine migration into its reservoir and East Seminole did not.

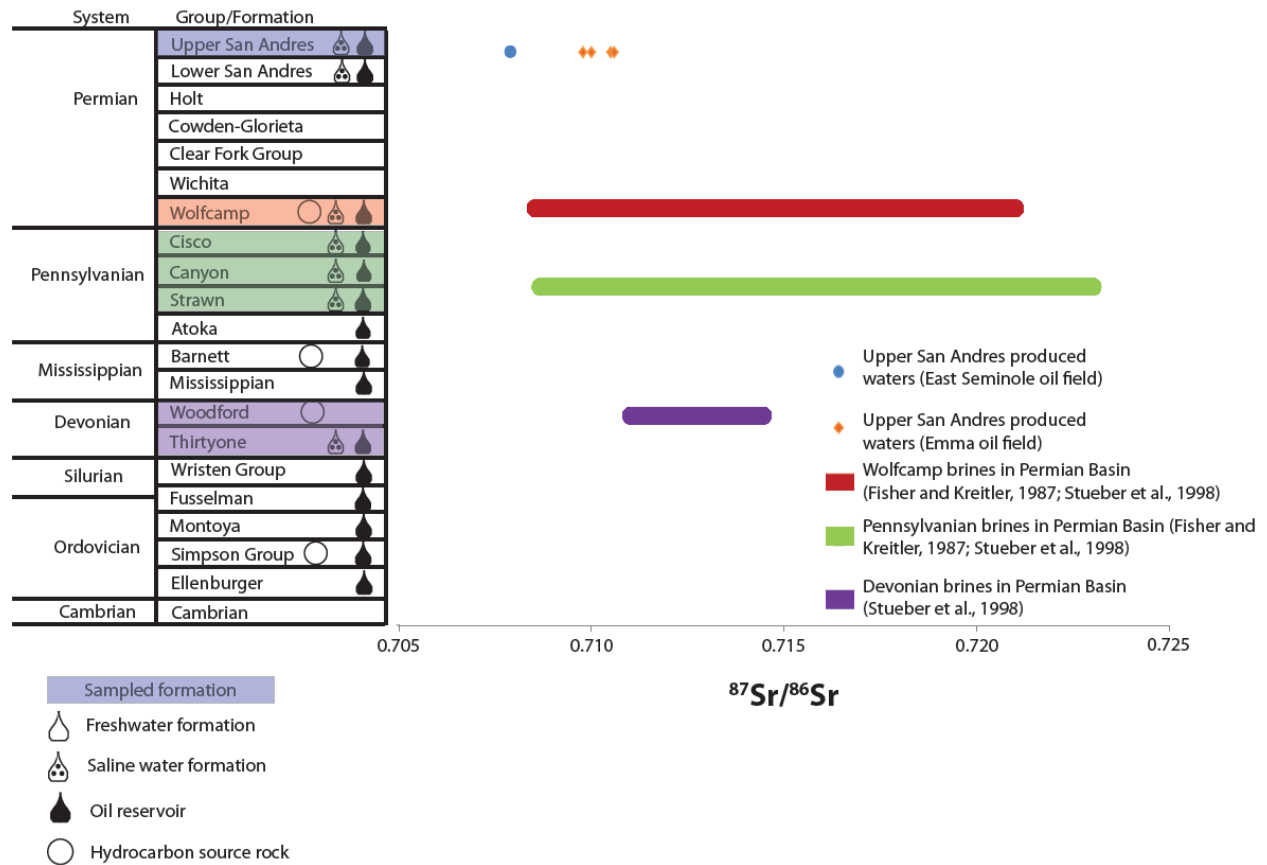


Figure 22. Graph displaying the $^{87}\text{Sr}/^{86}\text{Sr}$ of produced waters in this study and the range of $^{87}\text{Sr}/^{86}\text{Sr}$ of deep-basin brines that lie beneath the Upper San Andres. Data from this study are represented by data points; data from Fisher and Kreitler, 1987 and Stueber et al., 1998 are represented by oval shaped bars.

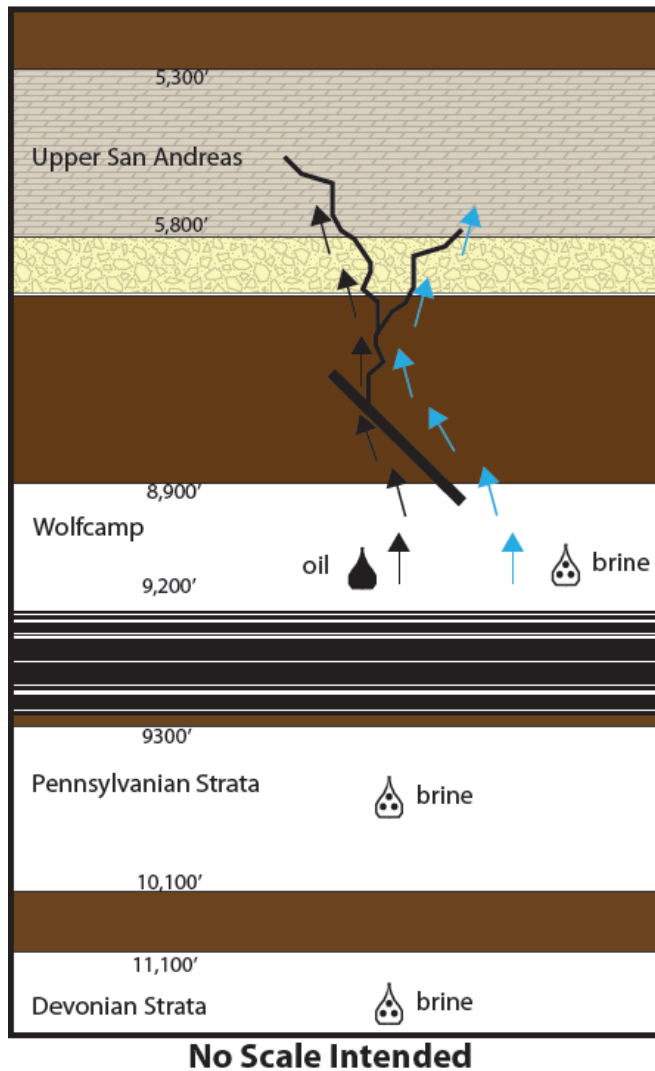


Figure 23. Schematic depicting the proposed migration of Wolfcampian brine into the Upper San Andres formation at the East Seminole oil field. The brine likely followed the same flow path as oil from this source rock. Depths in this figure are approximate current depths based on those seen at the nearby Southwest Andrews area (Stueber et al., 1998). The depths of these formations at the time of migration are unknown. Geologic patterns are from the USGS (2006).

3.6.2.3 Shallow groundwaters

The general geochemistry indicates that OG-01 is different than other Ogallala aquifer waters despite similar depths and their proximity. The well depths were confirmed to be accurate with the records of Tabula Rasa Energy. Despite having distinct geochemistries, the $^{87}\text{Sr}/^{86}\text{Sr}$ ratios of OG-01 (0.7087) and Ogallala waters (0.7086-0.7087) were similar. These ratios are similar to

those of Tertiary seawater carbonates. Unfortunately these are not distinct from Triassic carbonate values, making it difficult to determine if mixing with Triassic Dockum Group waters (Santa Rosa well, $^{87}\text{Sr}/^{86}\text{Sr}\sim 0.7084$) is occurring.

There is also no $^{87}\text{Sr}/^{86}\text{Sr}$ evidence suggesting that the OG-01 water is from a different aquifer. This is despite OG-01 having a strontium concentration [10.1 mg/L] that is higher than that of seawater (~8 mg/L, Veizer et al., 2003) and double that of any Ogallala waters. OG-01 is an industrial water supply well that is pumped every day into a storage tank (Figure 24). This water is then used to spray down recently constructed roads or for other industrial purposes. The influx of Ca-Mg-Sr into OG-01 may be the result of drawdown in the Ogallala and upwelling of a formation beneath the Ogallala. The Ogallala could be recharged by waters in the underlying Cretaceous aquifer that has higher potentiometric surfaces than the Ogallala in this area (Nativ, 1992). Although OG-01's high TDS, Ca, and Sr concentrations suggests such a scenario, the Sr isotopes indicate that OG-01 has the same source of Sr as other Ogallala groundwaters.



Figure 24. Picture of a well (OG-01) and the storage tank that holds water the well produces.

3.7 CONCLUSIONS

Strontium isotopes can be used as a geochemical monitoring tool at the East Seminole site to verify CO₂ containment once CO₂ flooding begins. The sensitivity of the Triassic Santa Rosa waters and the Ogallala waters to mixing with East Seminole produced waters would be indicative that the seal integrity of the San Andres formation had been compromised. It is extremely unlikely that the produced waters would rise this high, given that produced waters would have to travel over 3500 ft vertically to reach the Santa Rosa. Despite the unlikelihood, ⁸⁷Sr/⁸⁶Sr could act as a monitoring proxy. Considering its depth (1500 ft) and its heightened sensitivity, the Santa Rosa groundwater would be a better indicator of upwelling fluid than

Ogallala aquifer groundwater. The effects would be seen in Santa Rosa formation first and the effects would be more obvious, given the low strontium concentration in Santa Rosa water.

Despite the Sr isotope system's applicability to identifying deep and shallow water mixing, $^{87}\text{Sr}/^{86}\text{Sr}$ is not applicable for studying shallow (<1500 ft) groundwater mixing at the East Seminole site. Similarities in strontium isotope values for the Triassic, Cretaceous, and Tertiary groundwaters mean that $^{87}\text{Sr}/^{86}\text{Sr}$ cannot identify possible mixing of fluids between these units, which is likely to be occurring due to drawdown in the Tertiary Ogallala.

Upper San Andres Formation produced waters from two different sites have distinct general geochemistries and $^{87}\text{Sr}/^{86}\text{Sr}$ isotope ratios. Brine migration from an underlying unit, likely the Wolfcamp, occurred at the Emma oil field. This may have also occurred at the East Seminole oil field, but its produced waters do not reflect it. Instead, East Seminole produced waters have a $^{87}\text{Sr}/^{86}\text{Sr}$ more similar to that of the surrounding lithology. The $^{87}\text{Sr}/^{86}\text{Sr}$ of the East Seminole site produced waters is similar to that of previous work, suggesting historic brine migration occurred at the Emma oil field and not at the East Seminole site. This brine migration altered the geochemistry of the formation fluids.

4.0 A NEODYMIUM AND STRONTIUM ISOTOPE INVESTIGATION OF SEDIMENT SOURCES FOR THE MIDDLE DEVONIAN MARCELLUS SHALE

4.1 INTRODUCTION

The Middle Devonian Marcellus shale in the eastern U.S. is the focus of intense exploration for natural gas. Gas extraction from the Marcellus is expected to continue for the next few decades based on reservoir size (Engelder, 2008) and this extraction is projected to have an important economic impact on the region (Considine, et al., 2009). Determining local and regional sediment sources and depositional environments in the Appalachian Basin during its formation, as well as understanding post-depositional processes, are important for our understanding of the evolution of the basin and subsequent generation of natural gas.

The Marcellus Shale is an informal name given to black, organic-rich shale units within the Marcellus Formation, an unconventional shale gas play located in New York, Pennsylvania, West Virginia, Maryland and Virginia (Figure 25), deposited in the Appalachian foreland basin during the Middle Devonian Period. In this study, we apply Arthur and Sageman's (1994) definition of a black shale as being a black shale or mudrock containing $\geq 1\%$ organic matter. Despite the name, carbonaceous components can shift the color of a black shale from dark black, which is associated with a high organic content, to a medium gray. In order to deposit black, organic-rich shales like the Marcellus, three components are needed: (1) high organic matter

sediments, as well as (2) an anoxic marine environment and (3) low clastic sedimentation rates. The second factor ensures preservation of organics from microbial degradation and the third sustains a high organic to clastic ratio within the deposit.

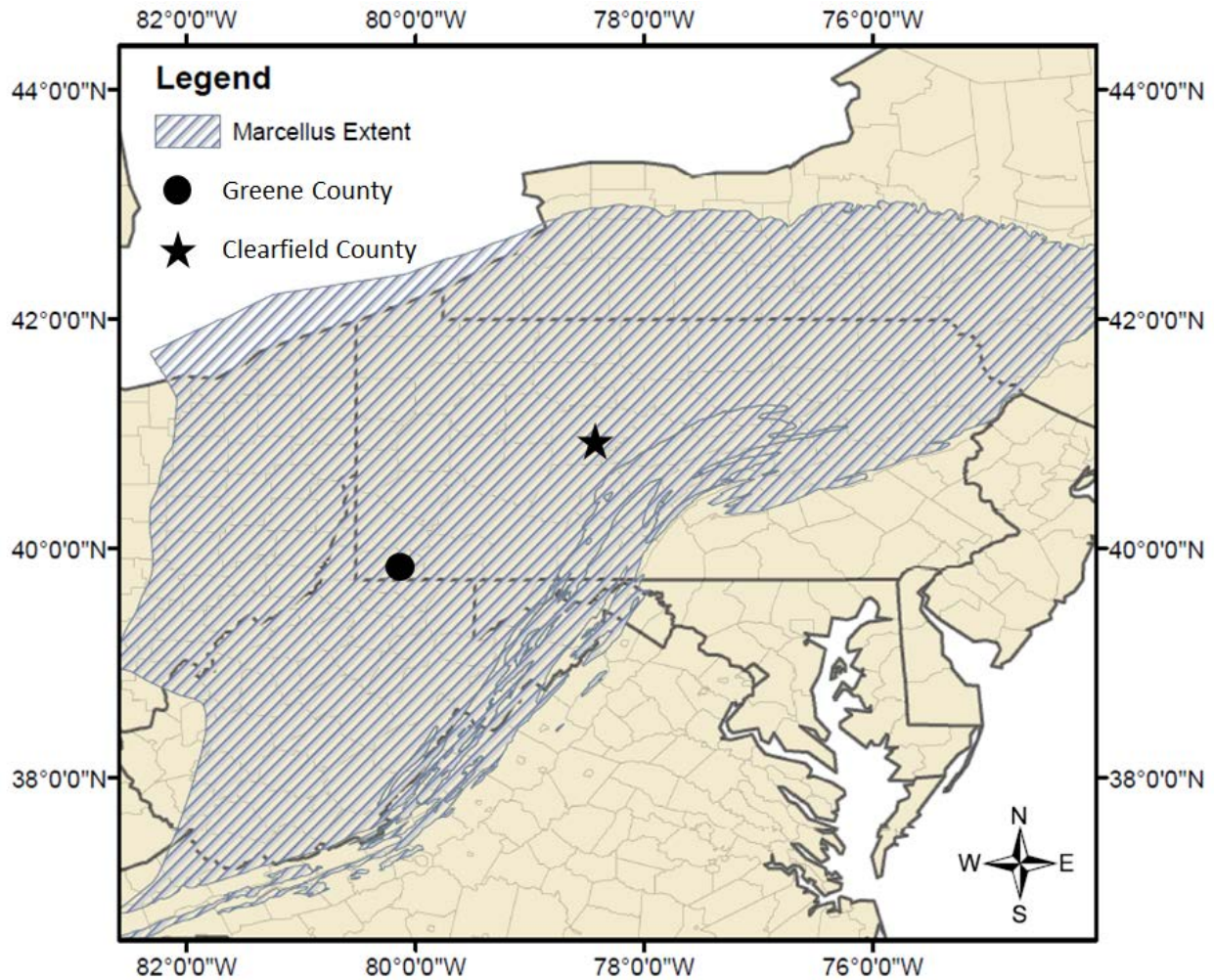


Figure 25. Map showing the geographic extent of the Middle Devonian Marcellus formation. thickness of the organic-rich portion of the Marcellus Shale. GIS data was obtained from the USGS (2002).

These last two factors are connected to the depth and stratification of the water column where deposition is taking place; both of these issues have been acknowledged research areas for black, organic-rich shale deposition for some time (Pettijohn, 1957). A significant amount of active research on black shale deposition focuses on what factors preserved organic material during black shale deposition and lithification; this has resulted in two contrasting models known

as the ‘preservation’ model (Tourtelot, 1979; Demaison and Moore, 1980; Potter et al., 1982; Ettensohn, 1992; Obermajer, 1997) and the ‘productivity’ model (Didyk et al., 1978; Johnson et al., 1989; Pedersen and Calvert, 1990; Murphy et al., 2000; Werne et al., 2002; Sageman et al., 2003).

Basin depth and water column stratification are active and pertinent research areas concerning the deposition of the Marcellus Shale. While basin depth and water column stratification are two of the most relevant issues to depositional models, the source of sediment for the Marcellus could provide valuable insight into the formation of these black shales. Isotopic analysis of these sediments, specifically samarium (Sm)-neodymium (Nd) and rubidium (Rb)-strontium (Sr) analyses, could help identify the formation’s sediment source and also enhance our understanding of the formation’s diagenetic history (O’Nions et al., 1983; Miller and O’Nions, 1984; Nelson and DePaolo, 1988; Lev et al., 2008).

The characteristics of the Marcellus Formation vary across its areal extent. Some of these characteristics have a direct impact on the economic aspect of the Marcellus, as certain parts of the formation produce wet or dry natural gas, while other parts of the formation produce little to no natural gas (Milliken et al., 2013). ‘Dry’ natural gas contains mostly methane while ‘wet’ natural gas has heavier hydrocarbons that include butane and ethane (Dale et al., 2013). Other geologic characteristics of the Marcellus formation are likely reflected in the varying geochemistry of produced waters from Marcellus natural gas wells (Barbot et al., 2013).

One possible explanation for the varying characteristics of the Marcellus is that localized portions of the formation may have different sediment sources and post-depositional histories. Diagenetic processes have been shown to affect reservoir properties such as porosity, permeability, and total organic content as well as the effectiveness of reservoir seals (Laughrey

et al., 2011; Milliken et al., 2013). Post-depositional tectonic activity has also resulted in fluid migration and varying burial depths for Appalachian basin sediments (Evans, 1995; Johnsson, 1986). Sm-Nd and Rb-Sr isotopic analyses can provide insight into whether sediment source and depositional history vary within the formation and across its areal extent. Sm-Nd and Rb-Sr isotopes from the sedimentary core in this study have the potential to enhance our understanding of Marcellus deposition on a localized level.

4.2 RESEARCH GOALS

The characteristics of the shale, including gas and other hydrocarbon productivity, are known to vary both with depth and geographic location within the Appalachian Basin. Important factors controlling these variations could be the source of the organic carbon and clastic sediment, depositional conditions in the basin, diagenetic history, and subsequent tectonic deformation and fluid flow events. Neodymium (Nd) isotopes have long been used to identify and quantify the source(s) of clastic sediments in depositional basins (O’Nions et al., 1983; Nelson and DePaolo, 1988; Linn et al., 1991; McLennan and Hemming, 1992; Gleason et al., 1994; Bock et al., 1998; Patchett et al., 1999; Lev et al., 2008). In this study, we are applying Nd isotopes to the clastic portion of Marcellus shale and related units in order to (1) identify the sediment source terrane; (2) determine the extent to which the sediment source varies temporally (within a single section); (3) determine whether changes in depositional environment (e.g., from organic carbon-rich to carbonate-rich lithologies) are accompanied by changes in primary sediment source; and (4) determine the extent to which diagenesis and subsequent fluid flow events have mobilized and redistributed elements within the Marcellus Formation.

The Appalachian Basin was also subject to periodic deposition of volcanic ash during the middle Devonian. The ash units in this study can provide a geochronological framework, and they also represent a potentially isotopically distinct silicate source to the basin.

4.3 DEPOSITIONAL ENVIRONMENT, SEDIMENT SOURCES AND MINERALOGY OF THE MIDDLE DEVONIAN MARCELLUS SHALE

The Marcellus Formation is often subdivided into the basal Union Springs Member, which contains volcanic ash layers, and the overlying Oatka Creek Member (Lash & Engelder, 2011). Both units thicken along a transect from southwestern to northeastern Pennsylvania (Figure 26). The maximum thickness for the Union Springs Member (160 ft) and the Oatka Creek Member (550 ft) both occur in northeastern Pennsylvania. These two organic-rich black shales are often interbedded with either the Cherry Valley limestone or the Purcell Member. Together, these four units comprise the majority of the lithologies in the Marcellus Formation (Carter et al, 2011), along with localized beds that are discontinuous over the formation's areal extent.

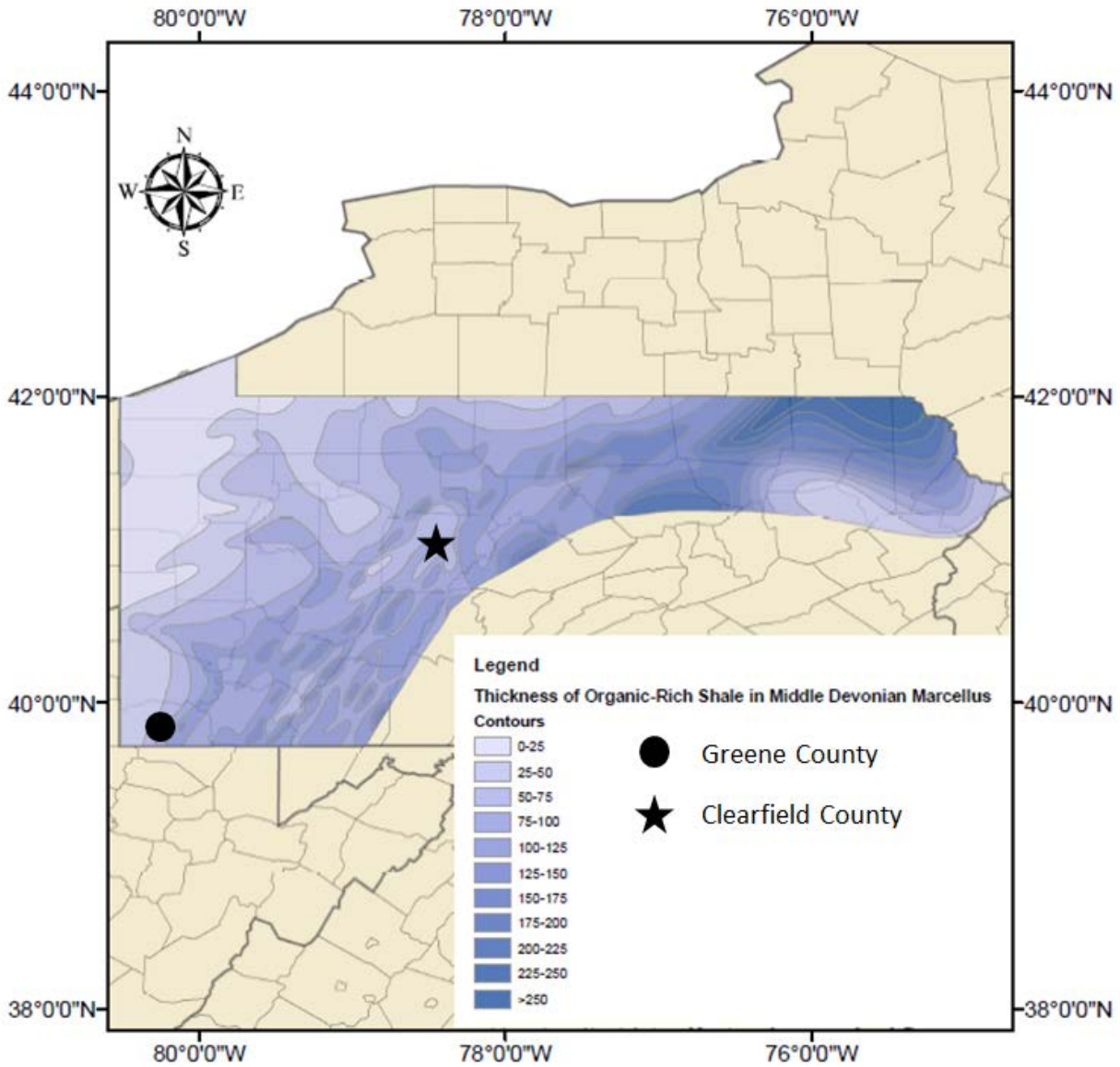


Figure 26. Map showing the thickness of the organic-rich portion of the Marcellus Shale in Pennsylvania. GIS data obtained from Pennsylvania Department of Conservation and Natural Resources.

4.3.1 Depositional environment of the Marcellus Shale

There is not a clear consensus on how organic-rich black shales are deposited. Decades of earlier research presents two models that depict contrasting depositional environments. The preservation model presents an environment where the deepest portion of the water column, also known as the

benthic zone, preserves organic material due to anoxic conditions that persist arising from a near permanent pycnocline and low clastic input from sediment sources (Tourtelot, 1979; Demaison and Moore, 1980; Potter et al., 1982, Ettensohn, 1992; Obermajer, 1997). The production model places emphasis on seasonal thermoclines and primary producers that can elevate the organic content of basal waters so much that the waters become anoxic (Didyk et al., 1978; Johnson et al., 1989; Pedersen and Calvert, 1990; Murphy et al., 2000; Werne et al., 2002; Sageman et al., 2003). It is likely that the deposition of organic-rich black shales is more complicated than these two proposed models and the Middle Devonian Marcellus shale, with its varying geologic and hydrocarbon characteristics, presents an opportunity to improve upon previous and current models.

In order to deposit organic-rich black shales, anoxic water conditions are necessary (Arthur and Sageman, 1994). Anoxic conditions ensure that microbial degradation of organic matter is slowed so that most of the deposited organic matter persists till it is compacted and lithified. In these conditions, organic matter falls to the floor of a water body and the organisms that typically metabolize this organic matter cannot because of the lack of oxygen in the water. The organic matter accumulates as a black mud, and if anoxic conditions continue until lithification and burial to the approximate depths of the natural gas window, this rock unit will become a potential source rock for hydrocarbon production (Philippi, 1974; Ishiwatari et al., 1977).

Middle Devonian Appalachian shales, including the Marcellus Shale, were deposited within the foreland of the Appalachian Basin as a result of the Acadian orogeny. The Acadian orogeny was a series of collisions that involved the Avalonia terrane or possibly a series of terranes colliding with the eastern North American plate during a time period that extended from

the Late Silurian to Devonian (~420-360 Ma; Rast and Skehan, 1993). Although the Taconian (Mid-Late Ordovician, ~470-445 Ma) and the Allegheny (Pennsylvanian-Permian, ~323-250 Ma) orogenies also affected the Appalachian foreland basin, previous work suggests that the Acadian orogeny established the foreland basin where the Marcellus was deposited (Ettensohn and Barry 1981; Ver Straeten and Brett, 2000).

The Marcellus Shale represents a distal facies of the Catskill delta complex that was deposited in the Appalachian foreland basin, a marine basin that may have been occasionally closed off from the ocean (Ettensohn and Barry, 1981). The collision of North America with the Avalonia terrane resulted in the formation of orogenic highlands at near-equatorial latitudes, as well as the subsidence of areas immediately westward of the mountain range. This subsidence resulted in the creation of numerous basins, including the Appalachian foreland basin, which received little precipitation due to the rain shadow created by the orogenic highlands to the east (Ettensohn and Barron, 1981). The Marcellus shale was deposited in this foreland basin and the conditions that mountain range that was to the east of the basin may have been a source of sediment for the Marcellus.

Long-term subsidence in the Appalachian basin allowed a voluminous wedge of sediment, as much as 9,000 ft in thickness, to accumulate (Kepferle, 1993). The Marcellus formation lies within the westward-prograding Catskill delta complex, which features several cycles of organic-rich shale deposition, followed by interbedding of lighter colored shales and siltstones, and then capped by a limestone or carbonate-rich shale. Kepferle (1993) documented eight of these cycles with the Marcellus cycle having the highest carbonate content and hypothesized that the organic rich black shales were deposited in an anaerobic zone similar to

other Devonian shales in the Appalachian, but the large amount of limestone and high organic carbon content within the Marcellus suggest this cycle may have been unique.

There is some evidence in the sedimentology that the more distal reaches of the basin, where the water depth was lower, had experienced bioturbation and reworking by storm currents, suggesting that oxygenation took place as the sea level declined (Griffing and Ver Straeten, 1991). As the Appalachian foreland basin prograded, sediment began to fill the basin, but as this happened there was a regression and an influx of sediment. This caused the basin to grow shallower over time and mixing of the water column became more common, resulting in the eventual deposition of more gray shales and carbonates (Ver Straeten and Brett, 2000; Sageman et. al. 2003). The only input of oxygen to the black-muds would be through turbidite deposits and regressing sea levels (Kepferle, 1993).

The interbedded gray shales in the formation were likely deposited when the water level of the basin lowered due to basin wide uplift (Ettensohn, 2004). Eventually, erosion of the orogenic highlands to the east of the basin increased precipitation in the Appalachian foreland basin. The previously subsiding basin then rebounded as it filled with an influx of sediment from the orogenic-highlands, creating a much shallower basin. The new basin depth, as well as an increase in the occurrence of sea level regressions, caused a transition from black shale deposition to the deposition of carbonates and carbonaceous shales (Ettensohn and Barry, 1981).

4.3.2 Sediment sources of the Marcellus Shale

The collision of the eastern North American plate with the Avalonia terrane resulted in the coeval subsidence of the Appalachian basin and the uplift of the orogenic highlands immediately

to the east of the basin (Ver Straeten, 2009). These orogenic highlands are estimated to have been sizeable mountains with an approximate height of 4 km (Bradley, 1982).

When the Marcellus shale was deposited, the location of the Appalachian Foreland basin sat south of the equator. The foreland basin was located between latitudes 30-35°, which would place the basin in an arid to semi-arid climate (Sageman et al., 2013). Fluvial inputs to the Appalachian foreland basin are likely, but they may have been confined to depositional environments more proximal to the orogenic highlands than the Marcellus. Based on the Marcellus being categorized as a distal mudstone and its abundance of eolian sediments, wind erosion of the orogenic highlands to the east was likely a primary source of sediment to the Marcellus (Sageman et al., 2003). Although it is possible these eolian sediments have another source, the size and proximity of these orogenic highlands makes them the most likely sediment source for the Marcellus.

4.3.3 Volcanic ashes

The Tioga ash beds are interbedded with the basal part of the Marcellus and the upper Onondaga limestone. Originally thought to be one single ash fall, these ash beds are now thought to represent several different volcanic events (de Witt et al., 1993; Ver Straeten, 2009). The presence of these ash beds throughout the Northern Appalachian basin suggests the possibility of widespread volcanic activity during the Middle Devonian.

Despite their ubiquity in Middle Devonian formations, the ash layers have an average thickness of 15-20 mm (Hosterman, 1993). There is the possibility that the small sedimentation flux into the basin actually caused settling volcanic ash to become amalgamated with other sediments at the bottom of the basin (Hosterman, 1993). Depositional environments with a

negligible sediment budget and a high sea level may accommodate volcanic sediment deposition; however it is possible that this environment might allow volcanic sediments to settle into and interbed with organic rich sediment sitting at the bottom of a basin, resulting in mixing of volcanic sediments with clastics derived from a sedimentary source (Ver Straeten, 2008). The presence of biotite in the Marcellus and other middle and Upper Devonian shales may be the result of volcanic ash mixing with unlithified black mud (Hosterman, 1993).

4.3.4 Mineralogy of the Marcellus Shale

Hosterman (1993) analyzed the mineralogy of 189 Marcellus shale samples from 48 drill holes. The shale contains quartz (20%), calcite (25%), and pyrite (5%), but is dominated by clay minerals (50%). Of these clay minerals, illite (70%) constituted the greatest percentage, while the remainder was chlorite (15%) and illite-smectite (15%), with trace amount of illite-chlorite and no evidence of kaolinite in the clay minerals.

Collectively for Middle and Upper Devonian shales, Hosterman (1993) noted that the presence of pyrite often coincided with high total organic content (TOC) levels. Previous work for black shales has shown that highly reducing, anaerobic environments result in pyrite deposition, which would also favor the preservation of organic material (Drobner et al, 1990). When carbon deposition takes place in an anaerobic environment, the breakdown of the organic material will result in reducing chemical compounds like hydrogen-sulfide and Fe(II). These compounds lower the Eh and foster reducing conditions. Pyrite content and total organic content do not always correlate, but peaks in pyrite and total organic content (TOC) have been shown to correlate with maximum flooding surfaces, which mark the transition from a transgression to a regression (Lash and Engelder, 2011).

Other Devonian-aged shales that lie above the Marcellus tend to have kaolinite in trace amounts. Kaolinite is a coarser grained clay mineral and tends to be deposited closer to its source than other smaller grained clays, like smectite. The presence of kaolinite in the younger shales may signify that they were closer to the sediment source than the Marcellus (Hosterman, 1993). This previous work suggests that the area of the depositional basin was at a peak during the Marcellus deposition, and that it grew smaller during the deposition of the overlying shales.

4.4 APPROACH AND METHODS

This study involves characterization of the Sm-Nd and Rb-Sr systematics of Marcellus shale and stratigraphically adjacent units (capping limestone, underlying Onondaga Limestone and Tioga bentonite volcanic ashes) from core samples and core cuttings. Most previous research has involved analysis of outcrop samples; however it has been suggested that subaerial weathering can potentially alter geochemical signatures (Ehrenberg and Nadeau, 2002). We are attempting to minimize these effects by using only core and cutting samples that are exposed to a carefully controlled sequential extraction process.

4.4.1 Sampling

Most of the samples for this study were obtained from a core extracted from a well drilled in Greene County, Pennsylvania (Figure 25, Figure 27). One volcanic ash was obtained from a core extracted from Clearfield County, PA. The lithologies, ranging from primarily carbonate to black shale, were chosen in collaboration with colleagues from West Virginia University, and span a

depth range of ~120 ft. After cutting a piece of core weighing several grams, the sample was crushed with a mortar and pestle, sieved to <2 mm, and split for different experiments.

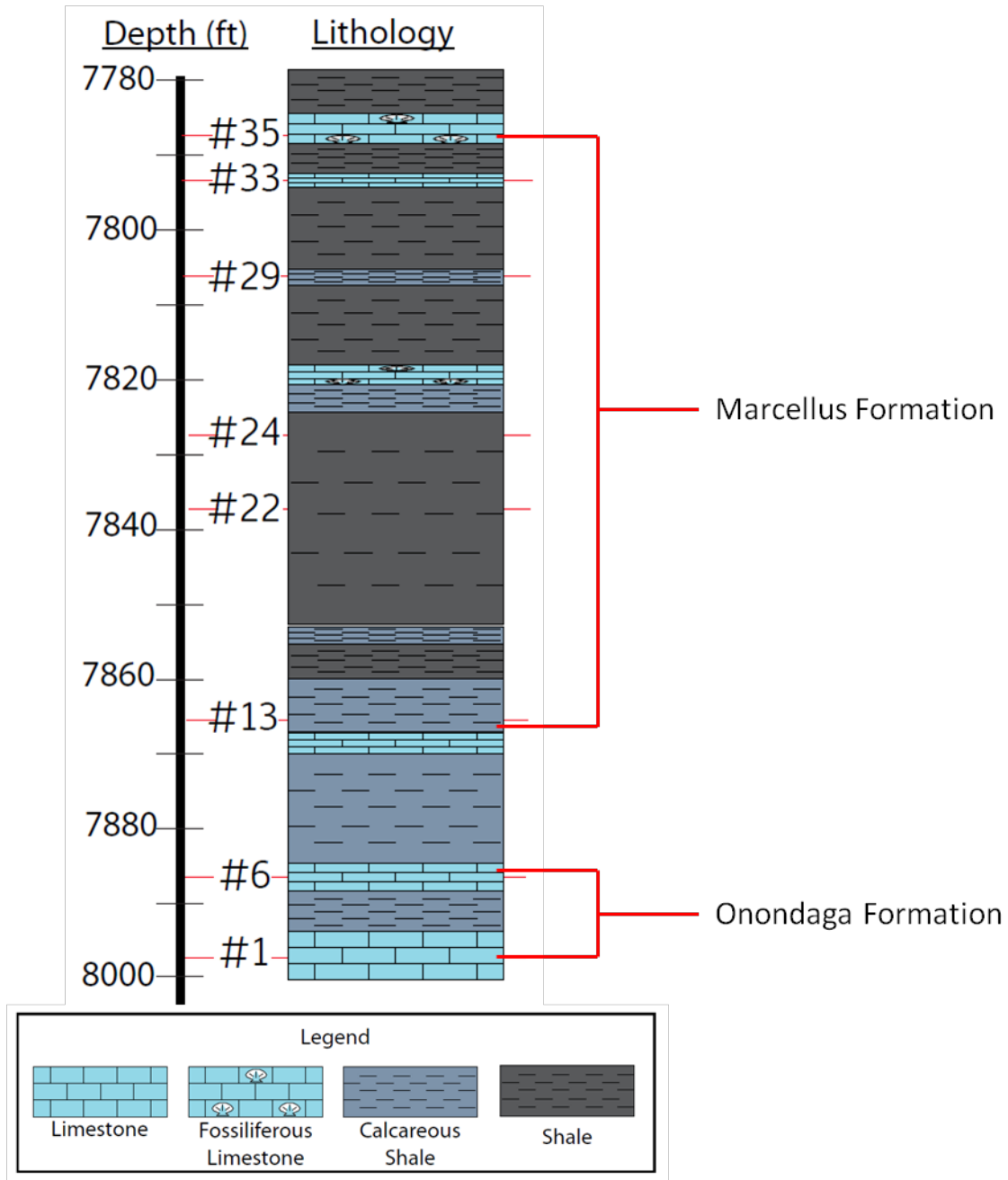


Figure 27. Simplified stratigraphy of core and sedimentary sample depths from this study; lithology based on gamma ray log.

4.4.2 Sequential extraction

Ultrapure water, ammonium acetate, and acetic acid extractions were carried out on crushed sedimentary core samples to characterize the soluble salt, exchangeable/sorbed and carbonate mineral phases respectively (Figure 28). Approximately 0.1 g of sample was weighed and then subjected to a sequential extraction process. First, ~10 mL of ultrapure water (18.2 MΩ) was added to each sample and shaken for ~8 hours. The samples were then centrifuged for 30 minutes at 4000 RPM and the water leachate was removed with a pipette into an acid-washed 30 mL poly bottle. The water leachate was acidified to 2% nitric acid (HNO₃) using Optima™ ultrapure HNO₃. This water leaching step was then repeated except that on the second addition of ultrapure water, the sample was only agitated for 30 minutes before being centrifuged and the leachate removed.

Next, 1 N ammonium acetate (NH₄OAc), buffered to pH ~8.14, was added to the samples to extract exchangeable cations. This step followed a similar process to that of the ultrapure water leaching procedure and was conducted in two separate steps, both times adding ~10 mL of ammonium acetate. The leachates were pipetted into an acid cleaned PMP beaker, dried down, and dissolved in 2% HNO₃.

Following the removal of the second ammonium acetate leachate, 8% acetic acid was added to the sample to extract carbonate minerals. The acetic acid was also added in two 10 mL increments, with the sample being shaken for 8 hours after the first addition of acetic acid and only for 30 minutes after the second addition of acetic acid. The acetic acid leachate was also pipetted out into a separate acid cleaned PMP beaker, dried down, and taken up in 2% HNO₃.

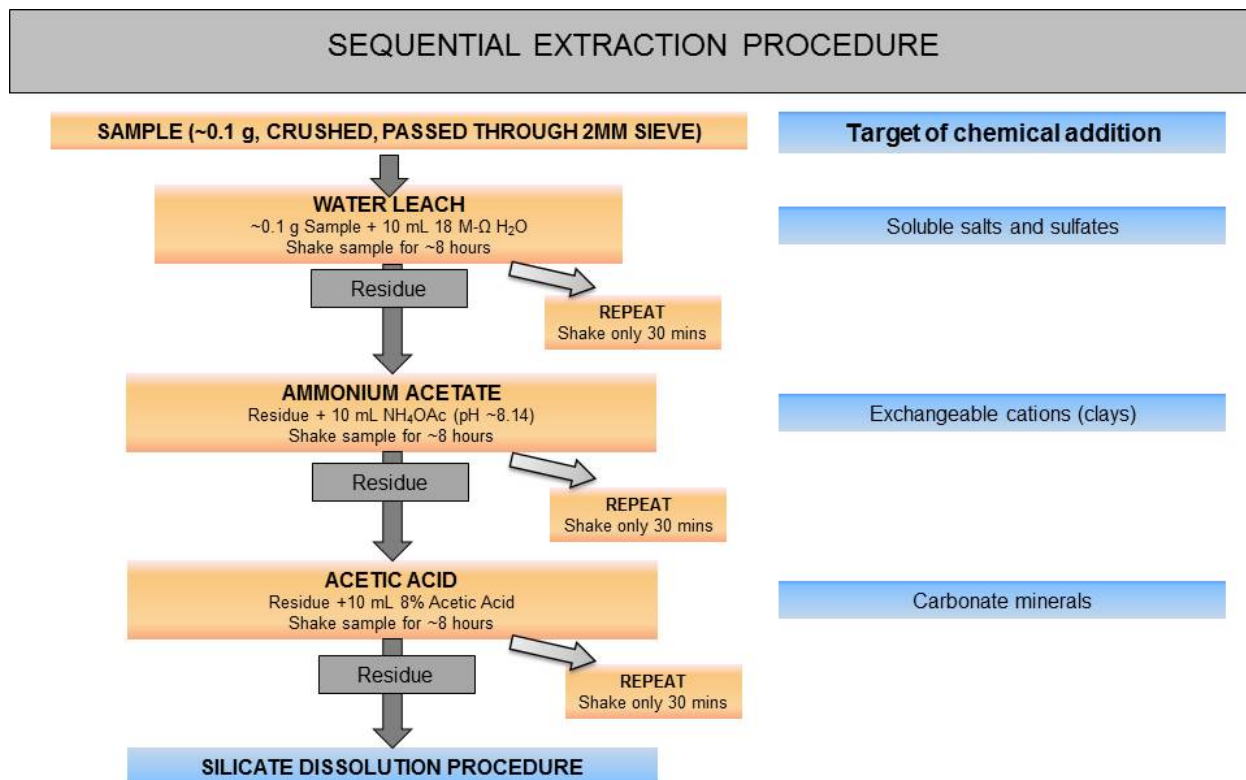


Figure 28. Flow chart of sequential extraction procedure for sedimentary samples.

4.4.3 Sample dissolution

The extraction residues and volcanic ashes were dissolved using a multi-step HF-HClO₄-nitric acid dissolution method modified after Yokoyama et al. (1999). This procedure involved the addition of numerous acids to the extraction residues as depicted in Figure 29. The resultant solution was then fluxed in capped Teflon vials to 100°C and then dried down before the addition of the next acid. The chemicals added in this procedure included nitric, hydrofluoric, and perchloric acid as well as hydrogen peroxide. If normality is not specified, this means that the chemical added was an undiluted, Optima™ ultrapure solution.

Nitric acid (1 mL) was first added in this manner to the samples to evolve gas from oxidized materials. Next, 2 mL of hydrofluoric acid and 2 mL of perchloric acid were added sequentially to the sample to promote silicate dissolution. After fluxing and dry down, 1 mL of perchloric acid was added to break down fluorides. 6 N hydrochloric acid (0.5 mL) was then added to dissolve any remaining refractory minerals. The final step was sequential addition of nitric acid (3 mL) and hydrogen peroxide (3 mL) to oxidize the sample and dissolve any remaining organic material.

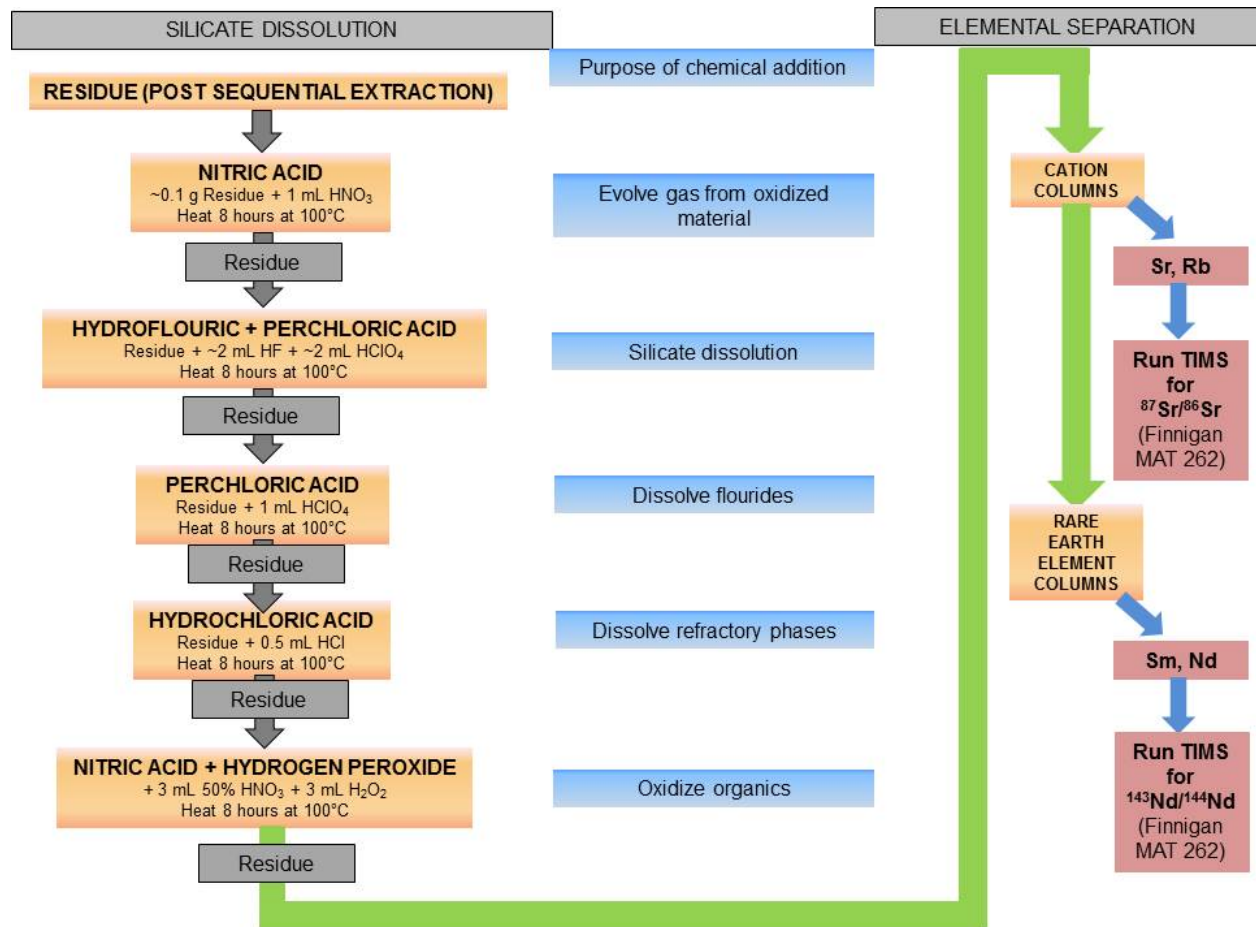


Figure 29. Flow chart of silicate dissolution procedure before isotopic analysis of silicate-organic residue.

4.4.4 Isotopic Analysis

The silicate-organic residue that remained after the dissolution procedure was then put through a two part, ion exchange column procedure similar to the one used by Eugster et al., 1970. This procedure first separated the rare earth elements (REE) from the residue using LNSpec® resin (Eichrom) cation exchange columns. Strontium (Sr), rubidium (Rb), and REE fractions were collected individually during separate elution steps in this exchange chromatography. The second ion exchange column experiment also used LNSpec® resin (Eichrom) to isolate neodymium (Nd) and samarium (Sm) from the REE fraction.

Sr isotopic analysis was carried out by multi-collector ICP-MS at the University of Pittsburgh. Approximately 2 µg of Sr were aliquoted from the Sr separate, dried down, and redissolved in 2% HNO₃ for multi-collector ICP-MS analysis. The NIST strontium standard SRM 987 was measured during the same analytical run as the other samples and the multi-collector reported a ⁸⁷Sr/⁸⁶Sr of 0.710302 ±0.000008.

Approximately 150 ng of Nd were loaded onto a rhenium filament and analyzed using a Finnigan MAT 262 thermal ionization mass spectrometer at the University of Pittsburgh. The La Jolla Nd oxide standard was also run concurrently with the samples and was measured at an average value of 0.511026±0.000007.

4.5 RESULTS

4.5.1 Neodymium isotope geochemistry

Neodymium (Nd) isotope data were obtained on a subset of samples from the Greene County core. None of the leachates had enough Sm-Nd to analyze isotopically, so all of the results here are from the silicate organic residues obtained from the procedure depicted in Figure 29. The samples range from marly limestone to calcareous shale to organic-rich black shale. Shales within the Marcellus Formation can have high calcium carbonate contents that can reflect post-depositional/diagenetic precipitation. To understand the provenance of the silicate and organic portions of the shale, the residues remaining after the acetic acid leaches were used. The acetic acid-soluble portions of shales in this section of the core ranged from 0.2 to 4.4% (Phan et al, 2012); the residue of one limestone (#35) was analyzed as well. Two volcanic ash samples were also analyzed; one was from the same Greene County core that produced the shale and limestone samples, while the other volcanic ash sample was from a core in Clearfield County, Pennsylvania.

Neodymium isotope data are reported using epsilon (ϵ) notation as described by DePaolo and Wasserburg (1976):

$$\epsilon_{Nd}(0) = \left[\frac{{}^{143}\text{Nd}/{}^{144}\text{Nd}_{\text{sample}}(T)}{{}^{143}\text{Nd}/{}^{144}\text{Nd}_{\text{CHUR}}(T)} - 1 \right] 10^4$$

This expression describes a sample's deviation from the chondritic uniform reservoir (CHUR), thought to represent bulk Earth values. Applying DePaolo's depleted mantle model (1981) to the

$\epsilon_{Nd(0)}$ and $\epsilon_{Nd(T)}$, a mantle derivation age (T_{DM}) can be determined. This is also known as the crust formation age (Nelson and DePaolo, 1988) and indicates when a portion of the crust was extracted from the upper mantle.

Nd isotope data were produced for seven samples (Table 10). Five of these residues are from sedimentary rocks, including shales and the carbonate-rich lithology, which consist primarily of clastic silicate minerals and organic matter. These sedimentary residues yielded $^{147}\text{Sm}/^{144}\text{Nd}$ ratios between 0.1003-0.1227. The $\epsilon_{Nd(T)}$ values fell within a tight range of -7.0 to -7.7 (Table 10) when corrected to 390 Ma (Middle Devonian; based on U-Pb dating of ashes). Depleted mantle model ages (T_{DM}) are between 1.38-1.59 Ga for these sedimentary samples. The three sedimentary samples not represented in Table 10 did not have enough Nd for isotopic analysis.

Two volcanic ash samples had results that produced a wider range. The $^{147}\text{Sm}/^{144}\text{Nd}$ for the Greene County ash (0.1630) was higher than that of the Clearfield County ash (0.1177). The $^{147}\text{Sm}/^{144}\text{Nd}$ for the Greene County ash also was higher than that of any sedimentary sample. The $\epsilon_{Nd(T)}$ values for both the Greene and Clearfield County ashes (-6.2 and -3.5) fell outside of the sedimentary sample range.

Table 10. Sm-Nd concentration isotope data for Marcellus core and volcanic ash organic-silicate residues.

Depth (ft)	#	$^{147}\text{Sm}/^{144}\text{Nd}$	$^{143}\text{Nd}/^{144}\text{Nd}$	$e_{\text{Nd}}(0)^a$	$e_{\text{Nd}}(T)$ 390	T_{DM} Ga
<i>Marcellus Residues</i>						
7788	35	0.1227	0.511302 ± 0.000007	-10.65 ± 0.14	-7.0	1.59
7807	29	0.1163	0.511257 ± 0.000010	-11.53 ± 0.20	-7.5	1.55
7828	24	0.1003	0.511221 ± 0.000007	-12.23 ± 0.14	-7.4	1.38
7838	22	0.1114	0.511233 ± 0.000008	-12.00 ± 0.16	-7.7	1.52
7866	13	0.1127	0.511264 ± 0.000006	-11.39 ± 0.12	-7.2	1.49
<i>Core Volcanic Ashes</i>						
7894	Greene	0.1630	0.511446 ± 0.000006	-7.83 ± 0.12	-6.2	2.44
7910	Clearfield	0.1177	0.511466 ± 0.000011	-7.44 ± 0.21	-3.5	1.25

^aNormalized to $^{143}\text{Nd}/^{144}\text{Nd}_{\text{CHUR}} = 0.511847$.

4.5.2 Strontium isotope geochemistry

Strontium isotope data were obtained from the residues of all eight of the shale and limestone samples from the Greene county core and for both of the volcanic ashes. The $^{87}\text{Sr}/^{86}\text{Sr}$ values are reported as their present-day values and their corrected values [$^{87}\text{Sr}/^{86}\text{Sr}(T)$] for the estimated time of deposition (~390 Ma) (Table 11). There is a large range of measured $^{87}\text{Sr}/^{86}\text{Sr}$ values for these samples. The results for the shale samples (0.7435-0.7782) have a tighter range than from those of the limestone samples (0.7085-0.764286). The volcanic ash samples have similar measured $^{87}\text{Sr}/^{86}\text{Sr}$ values (0.7181-0.7197).

When corrected for age using the current Sr and Rb concentrations, most of the sedimentary samples had a smaller range (0.7081-0.723503) than their initial values. This smaller range excludes one outlier, the fossiliferous limestone (0.7444) that is stratigraphically above the other samples (Figure 27) and has a corrected value that is more radiogenic than other samples.

The corrected $^{87}\text{Sr}/^{86}\text{Sr}$ values for the volcanic ash samples (0.7080-0.7150) are close to the values reported for the majority of the sedimentary samples. Ash sample COLD5, from the Clearfield County core, yielded the lowest corrected value of any of the samples.

Table 11. Sr isotope ratios of Marcellus and volcanic ash organic-silicate residue reflecting modern day values and original Sr(T) isotope ratio at time of deposition.

Depth (ft)	#	Lithology	$^{87}\text{Sr}/^{86}\text{Sr}$	$^{87}\text{Sr}/^{86}\text{Sr(T)}$
<i>Marcellus Residues</i>				
7788	35	fossiliferous limestone	0.764286 ± 0.000008	0.744420
7794	33	limestone	0.722740 ± 0.000008	0.710423
7807	29	calcareous shale	0.774025 ± 0.000008	0.713956
7828	24	black to dark gray shale	0.778183 ± 0.000008	0.723503
7838	22	black shale	0.743520 ± 0.000008	0.711002
7866	13	shale	0.756633 ± 0.000008	0.716584
7887	6	black marly limestone	0.726464 ± 0.000008	0.711677
7898	1	marl; fine black laminae	0.708530 ± 0.000008	0.708145
<i>Core Volcanic Ashes</i>				
7894	Greene	volcanic ash	0.719724 ± 0.000008	0.715046
7910	Clearfield	volcanic ash	0.718142 ± 0.000008	0.707951

4.6 DISCUSSION

4.6.1 Sm-Nd systematics: Implications for post-depositional disturbances

Before Nd isotopic data can be used for provenance information, the data must be analyzed for evidence of post-depositional resetting of the REE elements. While trace elements are typically immobile in surface water reactions, the redox conditions and post-depositional disturbances associated with organic-rich black shales can disturb and redistribute rare earth elements (Milliken et al., 1981; Milodowski and Zalaisiewicz, 1991; Lev et al., 1998). The redistribution or resetting of REE elements of a sample is often evident in decreased or increased $^{147}\text{Sm}/^{144}\text{Nd}$ and

T_{DM} values. If these values suggest a resetting of the REE elements, provenance information from the Sm-Nd isotopic data may not be accurate.

To investigate whether the Sm-Nd isotopic system was disturbed, we compared our results with those from previous work by Lev et al. (2008). All of our shale samples exhibit $^{147}\text{Sm}/^{144}\text{Nd}$ between 0.10-0.12, which is the expected range for unaltered Devonian organic-rich, black shales (Lev et al., 2008). When $^{147}\text{Sm}/^{144}\text{Nd}$ is plotted against T_{DM} , the values for the Marcellus Shale samples fall within the expected range for Devonian-age Appalachian basin shales (Figure 30). This indicates that the $^{147}\text{Sm}/^{144}\text{Nd}$ values for the shales are likely representative of the rare earth element composition during the time of deposition and that post or syn-depositional events do not appear to have redistributed the rare earth elements.

Although we only have Sm-Nd data for one limestone sample (#35), it plots outside of the expected range for shales (Figure 30). This sample appears to fall on the pathway for diagenetic disturbance of REEs and it appears to have been affected by a minimal amount of disturbance. Despite this, post-depositional processes do not appear to have disturbed the shale samples and their Sm-Nd data could provide reliable provenance information (McLennan, 1989).

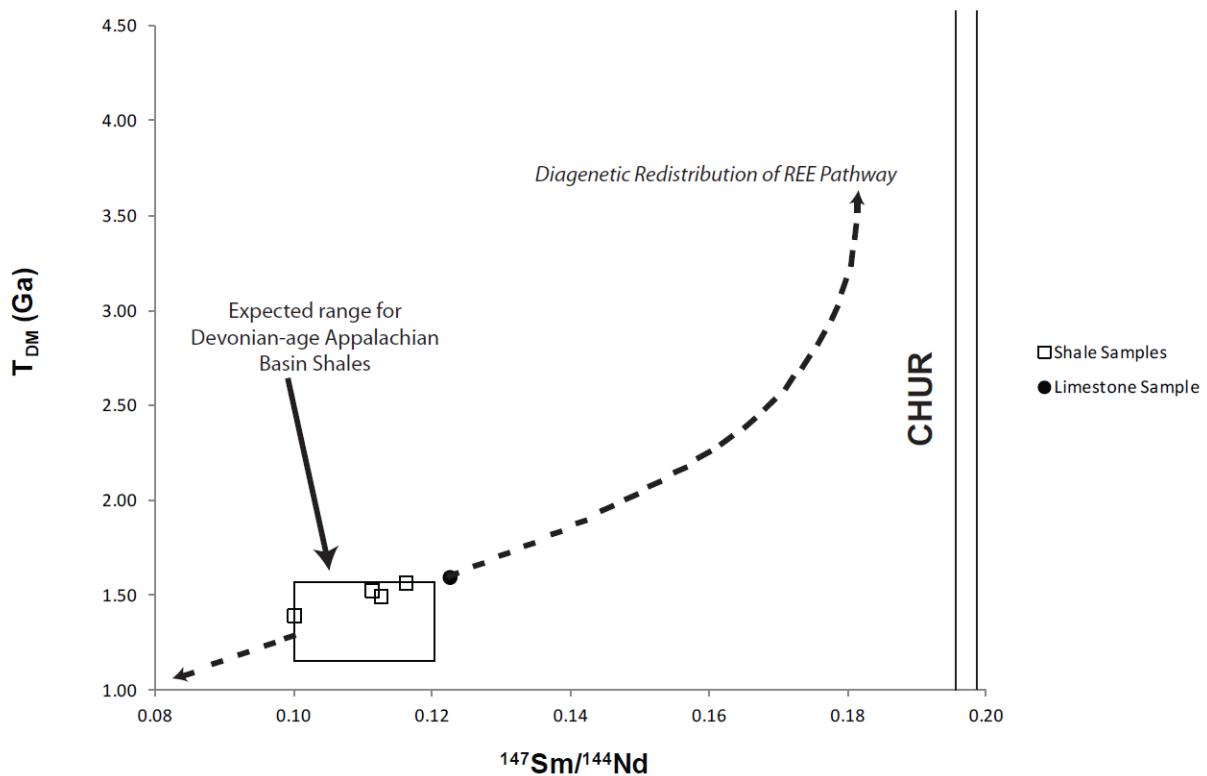


Figure 30. Mantle model ages [T_{DM} (Ga)] vs. $^{147}\text{Sm}/^{144}\text{Nd}$. The shale samples from this study plot clearly in the expected range for Devonian-age Appalachian Basin shales. The one limestone sample lies just outside of this range and on the projected pathway of sediments that had rare earth element redistribution. This image is modified from Lev et al., 2008.

4.6.2 Rb-Sr systematics: Implications for post-depositional disturbances

Rb-Sr isotopes are more susceptible to disturbances than Sm-Nd isotopes. Both Rb and Sr are vulnerable to weathering, as both can be easily mobilized in aqueous solutions (Dasch, 1969). This preferential leaching can alter the Rb-Sr ratio in a rock, making it difficult to correct back for its depositional age.

Despite the mobility of Sr in sedimentary systems, most of the $^{87}\text{Sr}/^{86}\text{Sr}$ values of the sedimentary organic-silicate residues converge around a common age of ~400 Ma when corrected back for ^{87}Rb decay (Figure 31) with the exception of limestone sample #35, which

also showed evidence of disturbance in the Sm-Nd system (Section 4.6.1). This matches the approximate Middle Devonian time frame when these rock units were deposited suggesting that post-depositional processes, such as fluid migration or metamorphism, did not strongly disturb the Rb-Sr systematics for most of these Marcellus formation samples. This indicates that Sm-Nd isotope data are likely to provide accurate sediment provenance information.

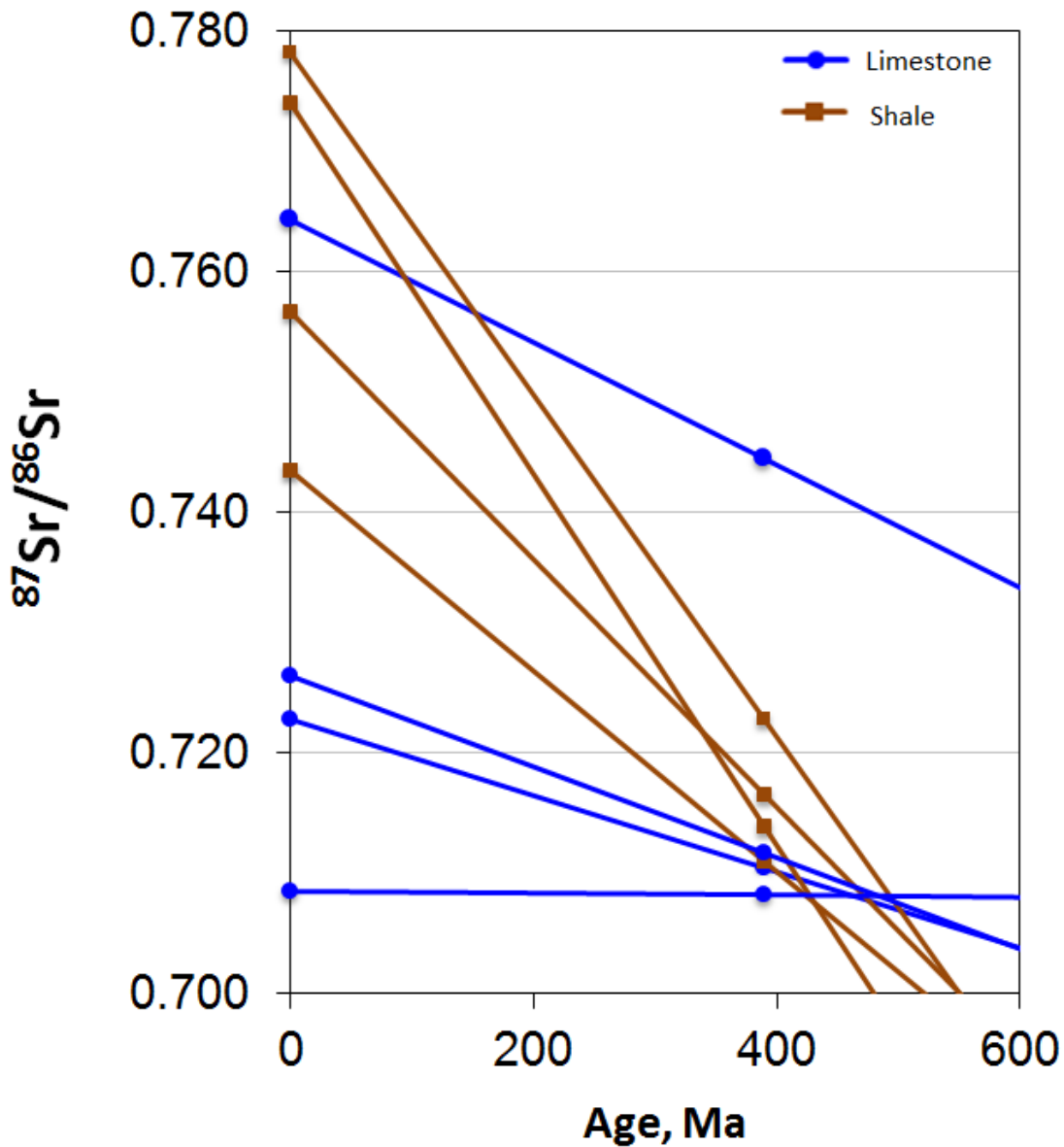


Figure 31. Strontium isotopic evolution of limestone residues (blue lines, circles) and shale residues (brown lines, squares).

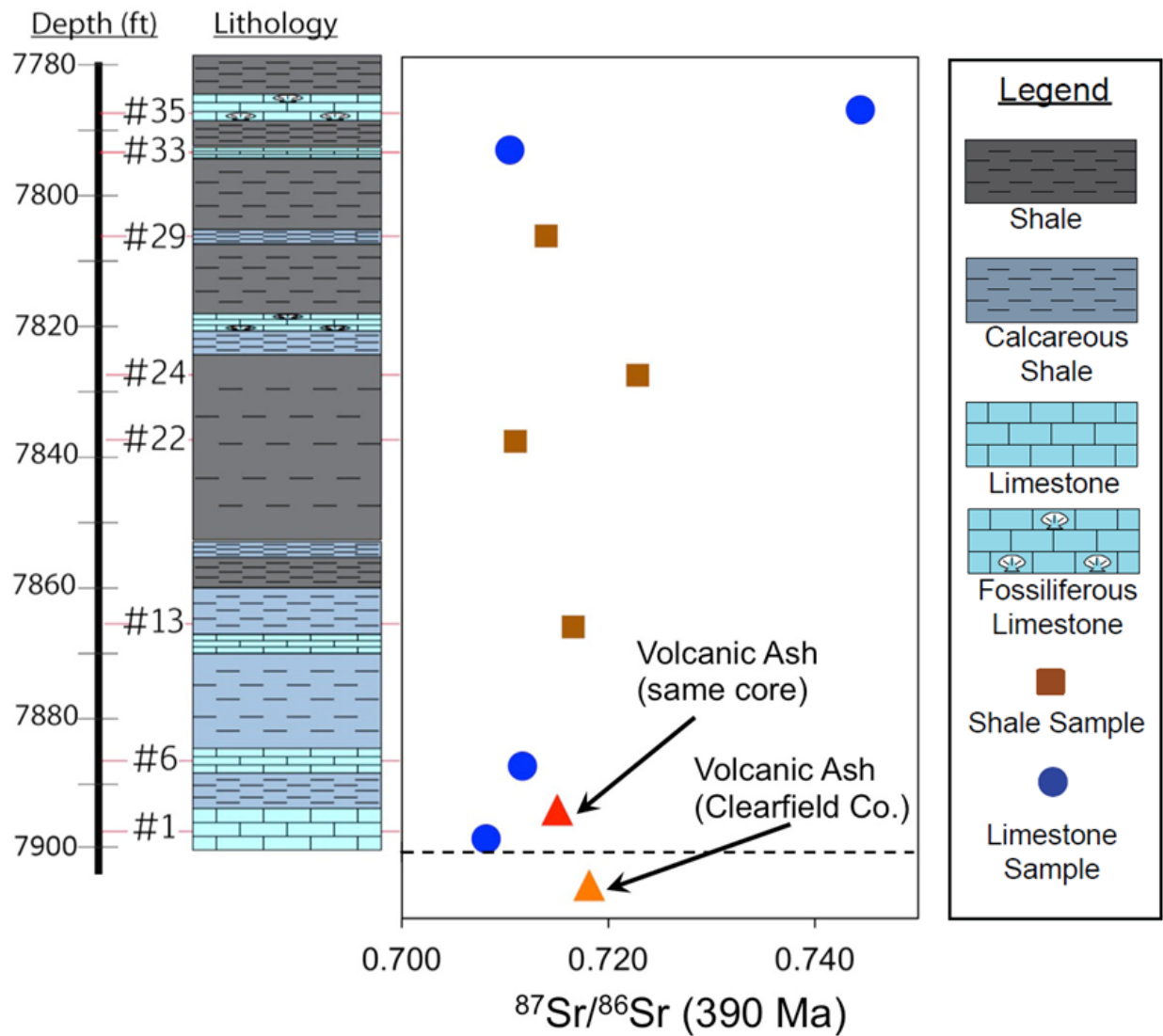


Figure 32. Strontium isotope variations from the Greene and the Clearfield County cores.

4.6.3 Identifying the sediment source terrane

Once adjusted for the approximate age of deposition, ϵ_{Nd} and depleted mantle model ages [T_{DM}] are good indicators of sediment source terrain. For the sedimentary samples in this study, at the time of deposition, $\epsilon_{\text{Nd}}(390 \text{ Ma}) = -7.35 \pm 0.30$ (1σ), corresponding to mantle model depletion

ages between 1.4-1.6 Ga (Table 10, Figure 33). Different terrane sources have unique ϵ_{Nd} values and they tend to be more negative with age. For example, Archean basement rock have ϵ_{Nd} between -17 and -26, while recent volcanic rocks have positive values >2 ; in the eastern United States pre-Appalachian sediments (-12 to -17) and post-Ordovician (-5 to -13) sediments fall into different ranges (Patchett and Ruiz, 1989; Gleason et al., 1994; Patchett et al., 1999). These post-Ordovician sediments are believed to have originated from the Grenville orogenic belt.

The results from this study, with $\epsilon_{Nd}(390 \text{ Ma}) = -7.35 \pm 0.30$ and $T_{DM} = 1.4-1.6 \text{ Ga}$, fall into the range of other samples from the Grenville orogenic belt (Patchett et al., 1999). During the estimated time when these sediments were deposited, $\sim 390 \text{ Ma}$, the study area was in a foreland basin setting with orogenic highlands to the east. These highlands would have provided a source of fluvial and eolian input, as wind at that time went primarily from east to west (Parrish and Lavin, 1982).

The suggestion that the Grenville orogenic belt is the source terrane for these Marcellus Formation sedimentary samples is not surprising; it is believed to be the primary sediment source of many rocks in the Appalachian basin and outside of it. Aside from indicating a source terrane, the limited range of ϵ_{Nd} suggests that the sediment source was consistent during the deposition of these sediments.. This limited range of ϵ_{Nd} suggests a sustained period of sediment input from the Grenville orogenic belt with minimal variation. The mantle model ages (1.4 to 1.6 Ga) also indicate a more evolved terrane source; both isotopic homogenization and an evolved terrane source have been interpreted to indicate an association with Grenville aged Appalachian fold-thrust belt rocks (Gleason et al., 1994).

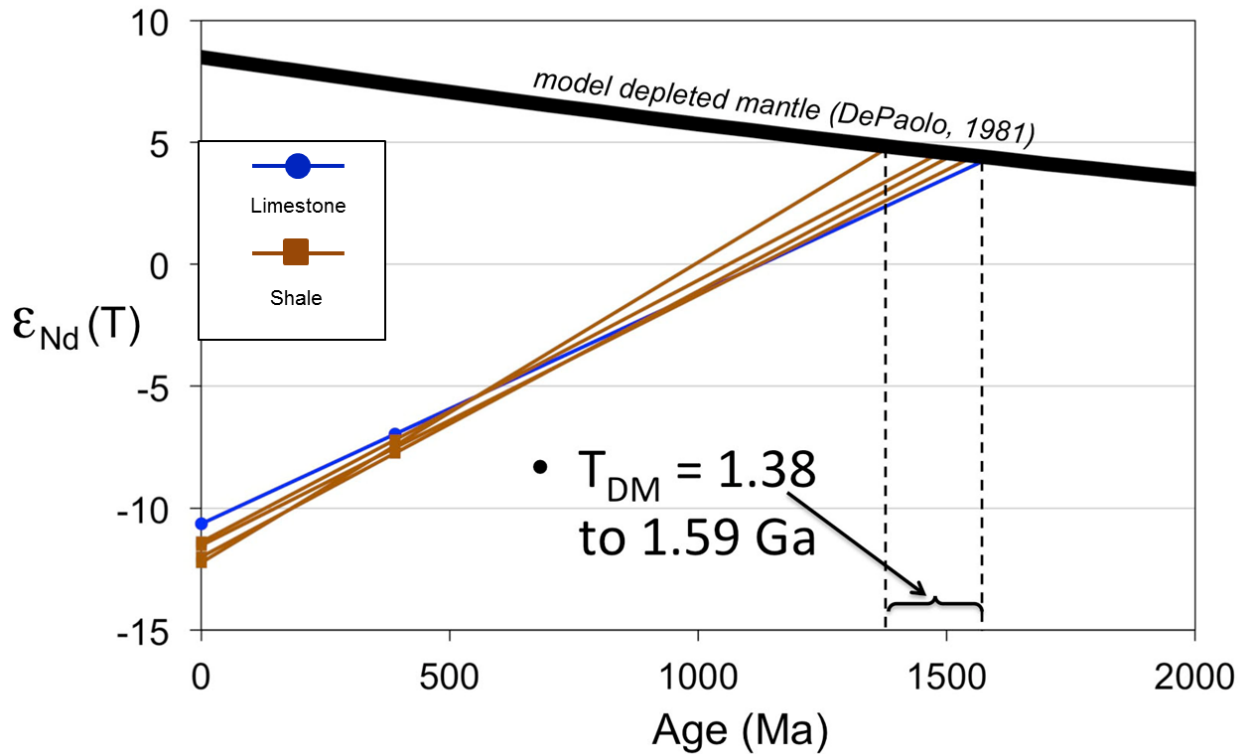


Figure 33. Depleted mantle model ages for shale and carbonate residues from the Greene County core.

4.6.4 Sediment source variation within the cores: volcanic ashes

The $\epsilon_{Nd}(T)$ results for the volcanic ash samples (-3.5 and -6.2, Table 10) are offset and distinct from those of the Middle Devonian aged sedimentary rocks (Figure 34). These $\epsilon_{Nd}(T)$ values are more positive and are associated with crystallization ages younger than Grenville aged sediments.

The volcanic ash from Clearfield County has a more positive $\epsilon_{Nd}(T)$ (-3.5) than the sedimentary samples, consistent with derivation from Grenville aged crust mixed with juvenile mantle material. Previous work has shown that isotopic signatures of mature crust are visible in foreland basin Ordovician bentonite ashes (Samson et al., 1989).

The Greene County volcanic ash sample is from the same core as the sedimentary samples in this study. This Greene County volcanic ash appears to also have a stronger component of older crust material that amalgamated with a juvenile melt, resulting in a lower ϵ_{Nd} (T).

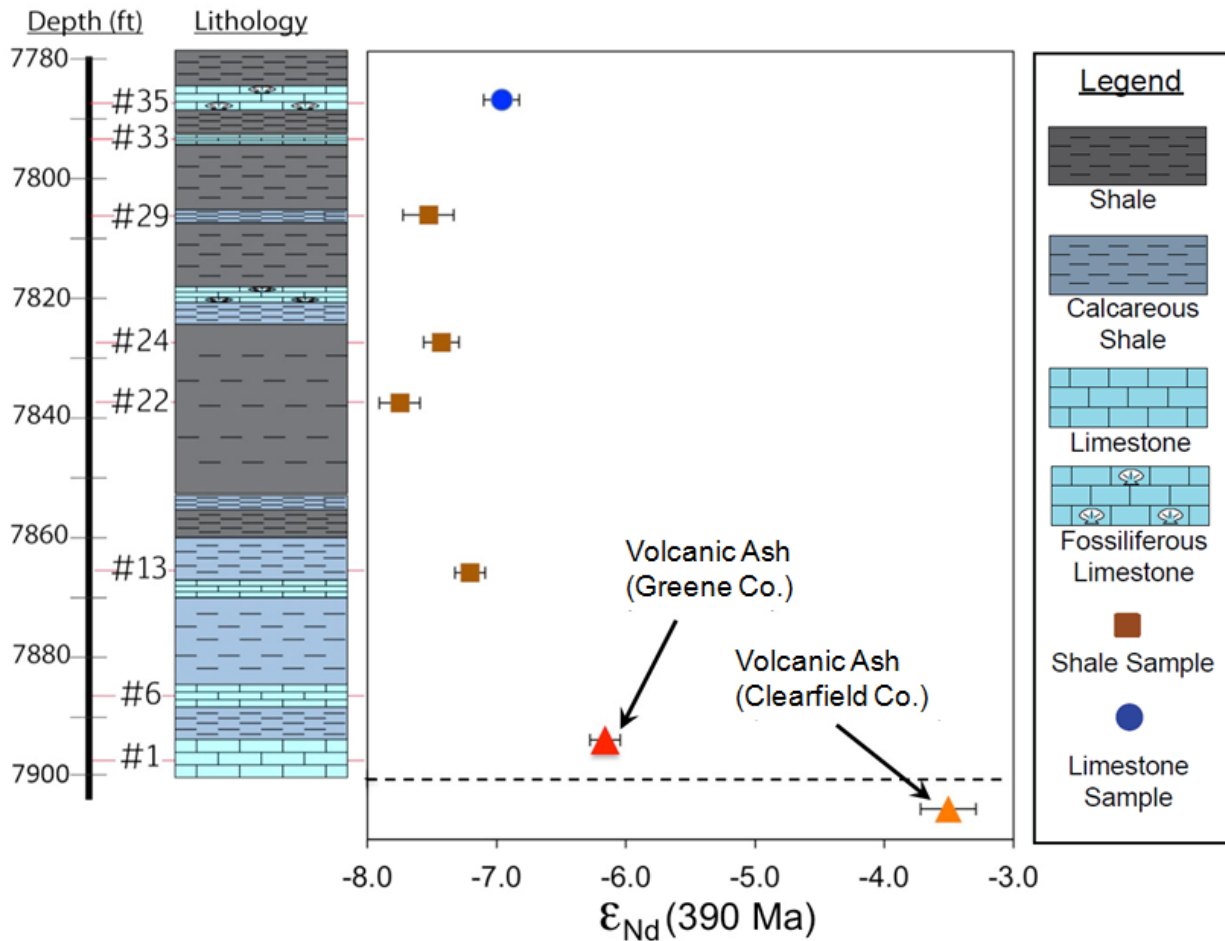


Figure 34. Neodymium isotope results for Marcellus shale (squares), carbonate (circle) and volcanic ashes (triangles) from this study.

4.6.5 Depositional environment and source terrane

The $\epsilon_{Nd}(T)$ value and the mantle model age for the one limestone sample (#35) is similar to that of the four shale samples (Figure 33, Figure 34). The shales had varying carbonate contents

(Phan et al., 2012), indicating shifting depositional environments within this core. The model ages suggest that the clastic portion of these rocks was derived from a common source despite their varying depositional environments. The $^{147}\text{Sm}/^{144}\text{Nd}$ values of every sample (Table 10) fall within the expected range (0.10-0.12) for Devonian-age Appalachian basin shales (Lev et al., 2008). This is a limited sample size, but it appears that depositional environment did not have an effect on source terrane in these samples.

4.6.6 Organic-silicate residues primary holders of Nd-Sm

Previous work (Bros et al., 1992) has shown that in some cases, clays can hold rare earth elements and that the Sm-Nd of clay leaches can date illitization during diagenesis. Unfortunately, none of the leaches had a high enough Nd or Sm concentration to analyze isotopically. While these data would have been welcome, the scarcity of Nd or Sm in the water, ammonium acetate, or acetic leaches does indicate that soluble salts and sulfates, exchangeable cations, and carbonate minerals are not the primary holders of rare earth elements in these samples. Organics and silicates appear to hold the majority of rare earth elements for these sedimentary samples from the Marcellus formation.

4.7 CONCLUSIONS

Nd and Sr isotopic analysis of Marcellus Formation sedimentary samples suggests that post-depositional disturbance was minimal to the samples in this study. The Sm/Nd ratios and the mantle model ages for this study were not decreased or elevated above the typical range for

Devonian-aged Appalachian shales (Lev et al., 2008). The Sr isotope data also shows no evidence of any major disturbance to the silicate portion of our samples subsequent to the Devonian.

Diagenesis and post-depositional fluid flow events did not mobilize or redistribute REEs within our shale samples in this study. These results are in contrast to previous work (Lev et al., 2008) that reported diagenetic redistribution of REEs in Devonian-age Appalachian Basin shales from southwestern Virginia. These samples were from outcrop samples, so the redistribution might be due to subaerial weathering. In either case, our results indicate that diagenetic processes did not affect or did not have as significant effect on our samples. Based on this, if the redistribution of REE in the southwestern Virginia sample were not due to subaerial weathering, it is possible that these two sets of samples were exposed to regionally varying post-depositional diagenetic or fluid flow events.

Based on the Sm-Nd isotopic data, the sediment source was likely Greenville-aged crust. The Acadian orogeny resulted in uplift and subsequent erosion of the Greenville aged crust to the east of the current sample location. The Nd isotopic data suggests that these eastern orogenic highlands were the well mixed sediment source for the Marcellus formation. In order to deposit these organic-rich black shales, clastic input had to be low to maintain the high organic content in the not-yet lithified black mud. The sediment input from Greenville-aged crustal orogenic highlands was therefore likely quite low, because the ratio of organic matter to clastics in this accumulating black mud had to remain high in order for it to produce the natural gas that it does today. Taking this low overall sedimentation rate into account, if there was another sediment input, its contribution would likely be noticeable. Homogenized isotopic values for ϵ_{Nd} and T_{DM} suggest that this sediment input from Greenville aged crust was consistent over time and

considering the low overall sedimentation rate necessary to produce these black shales, it was the dominant source in the samples.

The differing $\epsilon_{Nd}(390 \text{ Ma})$ and mantle model ages for the volcanic ashes suggest that disparate source terranes mixed with upwelling juvenile mantle to produce these values. Since these samples are from similar depths from different cores, it is likely that terrane availability shifted for different volcanic events.

One limestone sample in this study did have a slightly elevated $^{147}\text{Sm}/^{144}\text{Nd}$ indicating a small amount of REE redistribution. This suggests that the small amount of clastic material in this carbonate was either fractionated during deposition or was potentially more vulnerable to post-depositional or syndepositional processes. The depositional environment did differ from that of the shale samples, perhaps making it more susceptible to syndepositional processes. These results suggest that carbonate material is more sensitive to post-depositional redistribution of REE.

Despite the indicated redistribution of REEs in the limestone sample (#35), all of the sedimentary samples had ϵ_{Nd} and T_{DM} that suggested the same Greenville orogenic belt sediment source. This sediment source does not vary temporally over a single section regardless of changes in depositional environment or carbonate content of the shales. This isotopic homogenization suggests that the Greenville orogenic belt was a consistent provenance and that there was no noticeable input from far-traveled Archean or volcanic sources during sedimentary deposition.

5.0 CONCLUDING REMARKS

5.1 CONCLUSIONS

This dissertation contains three studies that use isotopic data in conjunction with geology and geochemistry to identify subsurface rock and fluid interactions. This work illustrates that isotopic systems are sensitive to short term geologic processes, like groundwater mixing, and long term geologic processes, like diagenesis. Isotopic analyses were done on water and rock samples across varying geologic settings. The implications of the results have broad applications to future studies involving carbon capture and storage, brine migration, and post-depositional processes.

The first study demonstrated that Sr isotopes are sensitive tracers to the intrusion of CO₂-related brines at a natural analog site. Sr isotopes are extremely sensitive to intrusion of deep-sourced saline waters in this case, and may in general be a very sensitive means of monitoring brines displaced by CO₂ injection. Pairing Sr isotopes with C isotopes also allowed us to distinguish between two different CO₂ migration pathways that had similar geochemical effects on groundwaters, but distinct effects on the isotopic data. Combining this isotopic data with geochemical data indicated that diffuse CO₂ migration has a negative impact on the site's groundwater. The Sr data from the area also indicates that faults can act as both conduits and barriers at this location. Sr and C isotopes enhanced the interpretation and understanding of

complex water-rock reactions that were occurring at this site. Together, these systems are an appropriate addition to current monitoring and verification strategies.

The second study demonstrated that two oil fields producing from the same formation can be geochemically and isotopically distinct. Brine migration from an underlying unit likely affected only one of the sites, resulting in the distinct geochemistries. The groundwater formations above the oil field at this site have Sr signatures that would be sensitive to fluid migration from the underlying formation. Monitoring these signatures could be a technique for ensuring the seal integrity above the producing formation. The Sr isotope system is not applicable to studying the effects of drawdown in the Ogallala at this site as the underlying upper aquifer waters have either identical Sr signatures or strontium concentrations much lower than the Ogallala.

In the third study, Nd and Sr isotopic analysis of Marcellus Formation sedimentary samples were used to identify source terrane and post-depositional history. Based on the Sm-Nd isotopic data, the sediment source was likely eastern orogenic highlands with Greenville-aged crust. Homogenized isotopic values for ϵ_{Nd} and T_{DM} suggest that this sediment input from Greenville aged crust was consistent over time. Nd and Sr isotope data indicated that post-depositional disturbance was minimal, so the Nd isotope values likely reflect terrane source. These Nd isotopic values produced a narrow range that indicated that the Greenville orogenic belt was a sediment source and that there was no noticeable input from Archean or volcanic sources during sedimentary deposition. The Sm/Nd ratios and the mantle model ages for this study were within the expected range not for Devonian-aged Appalachian shales. The Sr isotope data also shows no evidence of any major disturbance to the silicate portion of our samples subsequent to the Devonian.

5.2 RECOMMENDATIONS FOR FUTURE WORK

Based on the research in this study, the author recommends the following research avenues to address existing geologic, geochemical, and isotopic knowledge gaps:

- Apply Sr and C isotopes to other natural analog sites to investigate the pair's ability to identify CO₂ migration pathways.
- Extend Nd and Sr isotopic research to other Marcellus Formation sediments from areas of varying production; investigate to see if sediment source and post-depositional history vary by locality.
- Analyze other organic-rich, black shales for Nd isotopes and see if sediment sources for these shales were also consistent and show little evidence of post-depositional disturbance.
- Sample East Seminole oil field post CO₂ injection and monitor any changes in geochemical or Sr isotopic results; model reactions taking into account presence of CO₂ and high ionic content of solutions.
- Obtain formation water samples and core samples from units that underlie the Upper San Andres; analyze geochemically and isotopically to help identify source of brine migration at Emma oil field.
- Compile a comparative list of Sr isotopic ratios for Permian Basin deep brines and deep brines from formations that are close to the Marcellus; Investigate to see how brines from similar geologic ages compare.

BIBLIOGRAPHY

- Arthur, M. A., and Sageman, B. B., 1994. Marine shales: depositional mechanisms and environments of ancient deposits. *Annual Review of Earth and Planetary Sciences*, 22, 499-551.
- Banner, J.L., 2004. Radiogenic isotopes: systematic and applications to earth surface processes and chemical stratigraphy. *Earth-Science Reviews* 65, 141-194.
- Barbot, E., Vidic, N. S., Gregory, K. B., & Vidic, R. D., 2013. Spatial and Temporal Correlation of Water Quality Parameters of Produced Waters from Devonian-Age Shale following Hydraulic Fracturing. *Environmental science & technology*, 47(6), 2562-2569.
- Bassett, R. L., & Bentley, M. E., 1982. Geochemistry and hydrodynamics of deep formation brines in the Palo Duro and Dalhart Basins, Texas, USA. *Journal of Hydrology*, 59(3), 331-372.
- Bein, A., & Dutton, A. R., 1993. Origin, distribution, and movement of brine in the Permian Basin (USA): A model for displacement of connate brine. *Geological Society of America Bulletin*, 105(6), 695-707.
- Bentley, M. E., 1981. Regional hydraulics of brine aquifers, Palo Duro and Dalhart Basins, Texas: in. *Geology and Geohydrology of the Palo Duro Basin, Texas Panhandle: A Report on the Progress of Nuclear Waste Isolation Feasibility Studies*, prepared by Bureau of Economic Geology, University of Texas at Austin for US Department of Energy, Geological Circular, 81-3.
- Bock, B., McLennan, S.M., Hanson, G.N., 1998. Geochemistry and provenance of the Middle Ordovician Austin Glen Member (Normanskill Formation) and the Taconian Orogeny in New England. *Sedimentology* 45, 635-655.
- Bradley, D. C., 1982. Subsidence in late Paleozoic basins in the northern Appalachians. *Tectonics*, 1(1), 107-123.
- Bradley, R. G., & Kalaswad, S., 2003. *Groundwater Resources of the Dockum Aquifer in Texas*. Texas Water Development Board.
- Bros, R., Stille, P., Gauthier-Lafaye, F., Weber, F., & Clauer, N., 1992. Sm-Nd isotopic dating of Proterozoic clay material: an example from the Francevillian sedimentary series, Gabon. *Earth and Planetary Science Letters*, 113(1), 207-218.

- Bureau of Economic Geology [computer file], 2005. Integrated synthesis of the Permian Basin: Project GIS data. Available FTP: <http://www.beg.utexas.edu/resprog/permianbasin/gis.htm> [October 24, 2013].
- Bureau of Economic Geology [computer file], 2008. Permian Basin geologic synthesis project: Project GIS Data. Available FTP: <http://www.beg.utexas.edu/resprog/permianbasin/gis.htm> [July 6, 2013].
- Burke, W. H., Denison, R. E., Hetherington, E. A., Koepnick, R. B., Nelson, H. F., & Otto, J. B., 1982. Variation of seawater $^{87}\text{Sr}/^{86}\text{Sr}$ throughout Phanerozoic time. *Geology*, 10(10), 516-519.
- Cai, C., Worden, R. H., Wang, Q., Xiang, T., Zhu, J., & Chu, X., 2002. Chemical and isotopic evidence for secondary alteration of natural gases in the Hetianhe Field, Bachu Uplift of the Tarim Basin. *Organic geochemistry*, 33(12), 1415-1427.
- Carter, K. M., Harper, J. A., Schmid, K. W., & Kostelnik, J., 2011. Unconventional natural gas resources in Pennsylvania: The backstory of the modern Marcellus Shale play. *Environmental Geosciences*, 18(4), 217-257.
- Cavazza, W. 1986. Miocene Sediment Dispersal in the Central Española Basin, Rio Grande Rift, New Mexico, U.S.A. *Sedimentary Geology* 51, 119-135.
- Cirrus Associates, LLC. 2011. Geology Report, Dockum Well SR-1, City of Seminole, Gaines County, Texas.
- Clayton, M., Kjellsoon, J., Webber, M.E., Rainwater, K., Schroeder, J., Clark, J., and Harral, M. 2013. On the integration of renewable power and brackish groundwater desalination in Texas (White Paper).
- Considine, T., Watson, R., Entler, R., & Sparks, J., 2009. An emerging giant: Prospects and economic impacts of developing the Marcellus shale natural gas play. The Pennsylvania State University.
- Cowan, P. E., & Harris, P. M., 1986. Porosity distribution in San Andres Formation (Permian), Cochran and Hockley counties, Texas. *American Association of Petroleum Geologists Bulletin*, 70(6), 888-897.
- Cumming, K. A. C., 1997. Hydrogeochemistry of Ground Water in Chimayó, New Mexico. Masters Thesis, Northern Arizona University, 117.
- de Witt Jr, W., Roen, J. B., & Wallace, L. G., 1993. Stratigraphy of Devonian black shales and associated rocks in the Appalachian basin. *Petroleum geology of the Devonian and Mississippian black shale of eastern North America: US Geological Survey Bulletin* 1909, B1-B57.

- Dale, A. T., Khanna, V., Vidic, R. D., & Bilec, M. M., 2013. Process Based Life-Cycle Assessment of Natural Gas from the Marcellus Shale. *Environmental Science & Technology* 47, 5459-5466.
- Dasch, E. J., 1969. Strontium isotopes in weathering profiles, deep-sea sediments, and sedimentary rocks. *Geochimica et Cosmochimica Acta* 33(12), 1521-1552.
- DePaolo, D.J., 1981. Neodymium isotopes in the Colorado Front Range and crust-mantle evolution in the Proterozoic. *Nature* 291, 193-196.
- DePaolo, D. J., & Wasserburg, G. J., 1976. Nd isotopic variations and petrogenetic models. *Geophysical Research Letters*, 3(5), 249-252.
- Demaison, G. J., & Moore, G. T., 1980. Anoxic environments and oil source bed genesis. *Organic Geochemistry*, 2(1), 9-31.
- Didyk, B. M., Simoneit, B. R. T., Brassell, S. T., & Eglinton, G., 1978. Organic geochemical indicators of palaeoenvironmental conditions of sedimentation. *Nature*, 272(5650), 216-222.
- Department of Energy (DOE), National Energy Technology Laboratory, 2008. Carbon sequestration through enhanced oil recovery. U.S. Department of Energy publication, 1-4.
- Department of Energy (DOE), National Energy Technology Laboratory, 2010. Carbon dioxide enhanced oil recovery: Untapped domestic energy supply and long term carbon storage solution. U.S. Department of Energy publication, 1-32.
- Department of Energy (DOE), National Energy Technology Laboratory, 2012. Carbon utilization and storage atlas (4th Edition). U.S. Department of Energy publication, 1-130.
- Drobner, E., Huber, H., Wächtershäuser, G., Rose, D., & Stetter, K. O., 1990. Pyrite formation linked with hydrogen evolution under anaerobic conditions. *Nature*, 346, 742-744.
- Dutton, A. R. 1987. Origin of brine in the San Andres Formation, evaporite confining system, Texas Panhandle and eastern New Mexico. *Geological Society of America Bulletin*, 99(1), 103-112.
- Dutton, A. R., 1989. Hydrogeochemical processes involved in salt-dissolution zones, Texas panhandle, USA. *Hydrological processes*, 3(1), 75-89.
- Dutton, A. R., Reedy, R. C., & Mace, R. E., 2001. Saturated Thickness in the Ogallala Aquifer in the Panhandle Water Planning Area: Simulation of 2000 Through 2050 Withdrawal Projections. Bureau of Economic Geology, University of Texas at Austin.
- Dutton, S. P., Kim, E. M., Broadhead, R. F., Raatz, W. D., Breton, C. L., Ruppel, S. C., & Kerans, C., 2005. Play analysis and leading-edge oil-reservoir development methods in the Permian basin: Increased recovery through advanced technologies. *AAPG bulletin*, 89(5), 553-576.

- Ehrenberg, S.N., Nadeau, P.H., 2002. Post-depositional Sm/Nd fractionation in sandstones: Implications for neodymium-isotope stratigraphy. *J. Sed. Res.* 72, 304-315.
- Engelder, T., 2009. Marcellus 2008: Report card on the breakout year for gas production in the Appalachian Basin. *Fort Worth Basin Oil and Gas Magazine*, 20.
- Ettensohn, F. R., & Barron, L. S., 1981. Depositional model for the Devonian-Mississippian black-shale sequence of North America: a tectono-climatic approach (No. DOE/ET/12040-2). Kentucky Univ., Lexington (USA). Dept. of Geology.
- Ettensohn, F.R. 1992. Controls on the origin of the Devonian-Mississippian oil and gas shales, east-central United States. *Fuel*, 71, 1487-1492.
- Ettensohn, F. R. 2004. Modeling the nature and development of major Paleozoic clastic wedges in the Appalachian Basin, USA. *Journal of Geodynamics*, 37(3), 657-681.
- Eugster, O., Tera, F., Burnett, D. S., & Wasserburg, G. J., 1970. Isotopic composition of gadolinium and neutron-capture effects in some meteorites. *Journal of Geophysical Research*, 75(14), 2753-2768.
- Evans, M. A., 1995. Fluid inclusions in veins from the Middle Devonian shales: A record of deformation conditions and fluid evolution in the Appalachian Plateau. *Geological Society of America Bulletin*, 107(3), 327-339.
- Fisher, R.S., & Kreitler, C. W., 1987. Geochemistry and hydrodynamics of deep-basin brines, Palo Duro Basin, Texas, USA. *Applied Geochemistry*, 2(5), 459-476.
- Frenzel, P. F., 1995. Geohydrology and simulation of ground-water flow near Los Alamos, north-central New Mexico. USGS water-resources investigation, 99-1049.
- Galusha, T., and Blick, J. C., 1971. Stratigraphy of the Santa Fe Group, New Mexico. New York: American Museum of Natural History, 127.
- Gardiner, J.B., Stewart, B.W., Capo, R.C., and Hakala, J.A., 2009. Strontium isotope tracking of groundwater-CO₂ interactions in Chimayó, New Mexico, and implications for carbon storage in geologic formations. Poster presentation at AGU December Meeting.
- Gardiner, J.B., Stewart, B.W., Capo, R.C., Hakala, J.A., and Keating E.H., 2010. Tracking CO₂ migration through a sandstone aquifer using Sr isotopes: Chimayó, New Mexico, USA. Oral presentation at International Goldschmidt Conference.
- Gardiner, J.B., Stewart, B.W., Capo, R.C., Phan, T.T., Sharma, S., and Toro, J., 2012. A neodymium isotope investigation of sediment sources of the Middle Devonian Marcellus Formation, Pennsylvania, USA. Oral presentation at Geological Society of America Annual Meeting.

- Gilfillan, S., Wilkinson, M., Haszeldine, R. S., Shipton, Z. K., Nelson, S. T., and Poreda, R. J., 2011. He and Ne as tracers of natural CO₂ migration up a fault from a deep reservoir. *International Journal of Greenhouse Gas Control* 5, 1507-1516.
- Goldhaber, M.D, 2005. Sulfur-rich sediments. Mackenzie, F. T., Editor. *Sediments, diagenesis, and sedimentary rocks: Treatise on Geochemistry, Volume 7*. Elsevier.
- Gray, T.J., 1989. Development Study: East Seminole San Andres Field, Gaines County, Texas. Mobil Exploration: Internal paper.
- Gleason, J.D., Patchett, P.J., Dickinson, W.R., Ruiz, J., 1994. Nd isotopes link Ouachita turbidites to Appalachian sources. *Geology* 22, 347-350.
- Gómez, P., Garralón, A., Buil, B., Turrero, M. J., Sánchez, L., & de la Cruz, B., 2006. Modeling of geochemical processes related to uranium mobilization in the groundwater of a uranium mine. *Science of the Total Environment*, 366(1), 295-309.
- Grauch, V.J.S., Philips, J.D., Koning, D.J., Johnson, P.S., and Bankey, Viki., 2009. Geophysical interpretations of southern Española Basin, New Mexico, that contribute to understanding its hydrogeologic framework. U.S. Geological Survey Professional paper 1761, 88 p.
- Griffing, D. H., & Ver Straeten, C. A., 1991. Stratigraphy and depositional environments of the lower part of the Marcellus Formation (Middle Devonian) in eastern New York State. In New York State Geological Association 63rd Annual Meeting, SUNY Oneonta (pp. 205-234).
- Heim, R., 2013. U.S. Drought Monitor, weekly publication, released July 16, 2013. Accessed via droughtmonitor.unl.edu. National Climatic Data Center and NOAA.
- Hinkle, S. R., and Snyder, D. T., 1997. Comparison of chlorofluorocarbon-age dating with particle-tracking results of a regional ground-water flow model of the Portland Basin, Oregon and Washington. US Geological Survey water-supply paper 2483, 1-47.
- Hosterman, J. W. 1993. Illite crystallinity as an indicator of the thermal maturity of Devonian black shales in the Appalachian Basin. Roen, JB, and Kepferle, RC, Petroleum geology of the Devonian and Mississippian black shale of eastern North America, US Geological Survey Bulletin, G1-G9.
- Ishiwatari, R., Ishiwatari, M., Rohrback, B. G., & Kaplan, I. R., 1977. Thermal alteration experiments on organic matter from recent marine sediments in relation to petroleum genesis. *Geochimica et Cosmochimica Acta*, 41(6), 815-828.
- Jobson, A. M., Cook, F. D., & Westlake, D. W. S., 1979. Interaction of aerobic and anaerobic bacteria in petroleum biodegradation. *Chemical Geology*, 24(3), 355-365.
- Johnsson, M.J., 1986. Distribution of maximum burial temperatures across northern Appalachian Basin and implications for Carboniferous sedimentation patterns, *Geology*, 14(5), 384-387.

- Johnson, C. M., Beard, B. L., & Roden, E. E., 2008. The iron isotope fingerprints of redox and biogeochemical cycling in modern and ancient Earth. *Annual Reviews of Earth and Planetary Sciences*, 36, 457-493.
- Johnson, J., Johnson, P. N., Segarra, E., & Willis, D., 2009. Water conservation policy alternatives for the Ogallala Aquifer in Texas. *Water Policy*, 11(5), 537-552.
- Kaszuba, J. P., Janecky, D.R., Snow, M.G., 2003. Carbon dioxide reaction processes in a model brine aquifer at 200°C and 200 bars: implications for geologic sequestration of carbon. *Applied Geochemistry* 18, 1065-1080.
- Kaszuba, J.P., Janecky, D.R., Snow, M.G., 2005. Experimental evaluation of mixed fluid reactions between supercritical carbon dioxide and NaCl brine: Relevance to the integrity of a geologic carbon repository. *Chemical Geology* 217, 277-293.
- Keating, E. H., Fessenden, J.; Kanjorski, N.; Koning, D.J.; and Pawar, R., 2010. The impact of CO₂ on shallow groundwater chemistry: observations at a natural analog site and implications for carbon sequestration. *Environmental Earth Sciences* 60, 521-536.
- Keating, E.H., Hakala, J.A., Viswanathan, H., Capo, R., Stewart, B., Gardiner, J., Guthrie, G., Carey, William J., and Fessenden, J., 2011. The challenge of predicting groundwater quality impacts in a CO₂ leakage scenario: Results from field, laboratory, and modeling studies at a natural analog site in New Mexico, USA. *Energy Procedia* 4, 3239-3245.
- Keating, E.H., Newell, D., Viswanathan, H., Carey, J.W., Zyvoloski, G., and Pawar, R., 2013. CO₂/Brine Transport into Shallow Aquifers along Fault Zones. *Environmental Science and Technology*, 47, 290-297.
- Keller, G. R., and Baldrige, W. S., 1999. The Rio Grande rift: A geological and geophysical overview. *Rocky Mountain Geology*, 34, 121-130.
- Kelley, S., 2012. Conceptual models of the Rio Grande Rift. *New Mexico Bureau of Geology & Mineral Resources: Lite Geology*, Spring 2012, 2-4.
- Kepferle, R. C. 1993. A depositional model and basin analysis for the gas-bearing black shale (Devonian and Mississippian) in the Appalachian basin. *Petroleum geology of the Devonian and Mississippian black shale of eastern North America: US Geological Survey Bulletin*, F1-F23.
- Kharaka, Y.K., Cole, D.R., Hovorka, S.D., Gunter, W.D., Knauss, K.G., Freifeld, B.M., 2006a. Gas-water-rock interactions in Frio Formation following CO₂ injection: Implications for the storage of greenhouse gases in sedimentary basins. *Geology* 34, 577-580.
- Kharaka, Y. K., Cole, D. R., Thordsen, J. J., Kakouros, E., & Nance, H. S., 2006b. Gas–water–rock interactions in sedimentary basins: CO₂ sequestration in the Frio Formation, Texas, USA. *Journal of Geochemical Exploration*, 89, 183-186.

- Kharaka, Y. K., Thordsen, J. J., Hovorka, S. D., Seay Nance, H., Cole, D. R., Phelps, T. J., & Knauss, K. G., 2009. Potential environmental issues of CO₂ storage in deep saline aquifers: Geochemical results from the Frio-I Brine Pilot test, Texas, USA. *Applied Geochemistry*, 24(6), 1106-1112.
- Kharaka, Y.K., Thordsen, James J., Kakouros, E., Ambats, G., Herkelrath, W.N., Beers, S.R., Birkholzer, J.T., Apps, J.A., Spycher, N.F. Zheng, L., Trautz, R.C., Rauch, H.W., Gullickson, K.S., 2010. Changes in the chemistry of shallow groundwater related to the 2008 injection of CO₂ at the ZERT field site, Bozeman, Montana. *Environmental Earth Science* 60, 273-284
- Knauth, L. P., & Beeunas, M. A., 1986. Isotope geochemistry of fluid inclusions in Permian halite with implications for the isotopic history of ocean water and the origin of saline formation waters. *Geochimica et Cosmochimica Acta*, 50(3), 419-433.
- Koning, D. J., Nyman, M., Horning, R., Eppes, M., & Rogers, S., 2002. Geologic map of the Cundiyo 7.5-minute quadrangle. Santa Fe County, New Mexico: New Mexico Bureau of Geology and Mineral Resources Open-File Geologic Map OF-GM-56, scale 1:24,000.
- Koning, D. J., 2003. Geologic map of the Chimayo 7.5-minute quadrangle. Rio Arriba and Santa Fe counties, New Mexico: New Mexico Bureau of Geology and Mineral Resources, Open-file Geologic Map OF-GM-71, scale 1:24,000.
- Langmuir, D., 1978. Uranium solution-mineral equilibria at low temperatures with applications to sedimentary ore deposits. *Geochimica et Cosmochimica Acta*, 42(6), 547-569.
- Langmuir, D., & Melchior, D., 1985. The geochemistry of Ca, Sr, Ba and Ra sulfates in some deep brines from the Palo Duro Basin, Texas. *Geochimica et Cosmochimica Acta*, 49(11), 2423-2432.
- Lash, G. G., & Engelder, T., 2011. Thickness trends and sequence stratigraphy of the Middle Devonian Marcellus Formation, Appalachian Basin: Implications for Acadian foreland basin evolution. *AAPG Bulletin*, 95(1), 61-103.
- Laughrey, C. D., Ruble, T. E., Lemmens, H., Kostelnik, J., Butcher, A. R., Walker, G., & Knowles, W., 2011. Black Shale Diagenesis: Insights from Integrated High-Definition Analyses of Post-Mature Marcellus Formation Rocks, Northeastern Pennsylvania. *AAPG Search and Discovery*, Article #110150.
- Lehman, T., & Chatterjee, S., 2005. Depositional setting and vertebrate biostratigraphy of the Triassic Dockum Group of Texas. *Journal of Earth System Science*, 114(3), 325-351.
- Lev, S. M., McLennan, S. M., Meyers, W. J., & Hanson, G. N., 1998. A petrographic approach for evaluating trace-element mobility in a black shale. *Journal of Sedimentary Research*, 68(5), 970-980.
- Lev, S.M., Filer, J.K., Tomascak, P.B., 2008. Orogenesis vs. diagenesis: Can we use organic-rich shales to interpret the tectonic evolution of a depositional basin? *Earth-Sci. Rev.* 86, 1-14.

- Lewicki, J.L., Hilley, G.E., Dobeck, L., McLing, T.L., Kennedy, B.M., Bill, M., & Marino, B.D.V., 2013. Geologic CO₂ input into groundwater and the atmosphere, Soda Springs, ID, USA. *Chemical Geology*, 339, 61-70.
- Linn, A.M., DePaolo, D.J., Ingersoll, R.V., 1991. Nd-Sr isotopic provenance analysis of Upper Cretaceous Great Valley fore-arc sandstones. *Geology* 19, 803-806.
- Little, M.G. and Jackson, R.B., 2010. Potential impacts of leakage from deep CO₂ geosequestration on overlying freshwater aquifers. *Environmental Science & Technology*, 44(23), 9225-9232.
- Lollar, B. S., and Ballentine, C. J., 2009. Insights into deep carbon derived from noble gases. *Nature Geoscience*, 2(8), 543-547.
- Lueth, V. W., Rye, R. O., & Peters, L., 2005. "Sour gas" hydrothermal jarosite: ancient to modern acid-sulfate mineralization in the southern Rio Grande Rift. *Chemical Geology*, 215(1), 339-360.
- McLennan, S. M., 1989. Rare earth elements in sedimentary rocks; influence of provenance and sedimentary processes. *Reviews in Mineralogy and Geochemistry*, 21(1), 169-200.
- McLennan, S.M., Hemming, S., 1992. Samarium/neodymium elemental and isotopic systematics in sedimentary rocks. *Geochimica et Cosmochimica Acta* 56, 887-898.
- Mehta, S., Fryar, A. E., & Banner, J. L., 2000. Controls on the regional-scale salinization of the Ogallala aquifer, Southern High Plains, Texas, USA. *Applied Geochemistry*, 15(6), 849-864.
- Milici, Robert C., and Swezey, Christopher S., 2006. Assessment of Appalachian Basin Oil and Gas Resources: Devonian Shale-Middle and Upper Paleozoic Total Petroleum System. USGS Open-File Report 2006-1237.
- Miller, R. G., & O'Nions, R. K., 1984. The provenance and crustal residence ages of British sediments in relation to palaeogeographic reconstructions. *Earth and Planetary Science Letters*, 68(3), 459-470.
- Milliken, K. L., Land, L. S., & Loucks, R. G., 1981. History of burial diagenesis determined from isotopic geochemistry, Frio Formation, Brazoria County, Texas. *American Association of Petroleum Geologists, Bulletin*, 65, 1397-1413.
- Milliken, K. L., Rudnicki, M., Awwiller, D. N., & Zhang, T., 2013. Organic matter-hosted pore system, Marcellus Formation (Devonian), Pennsylvania. *AAPG bulletin*, 97(2), 177-200.
- Milodowski, A. E., & Zalasiewicz, J. A., 1991. Redistribution of rare earth elements during diagenesis of turbidite/hemipelagite mudrock sequences of Llandovery age from central Wales. *Geological Society, London, Special Publications*, 57, 101-124.
- Moody, J. R., 1982. The NBS clean laboratories for trace element analysis. *Analytical Chemistry*, 54(13), 1358A-1376A.

- Mozley, P. S., and Goodwin, L. B., 1995. Patterns of cementation along a Cenozoic normal fault: A record of paleoflow orientations. *Geology*, 23(6), 539-542.
- Muller, F. L., & Bleie, B., 2008. Estimating the organic acid contribution to coastal seawater alkalinity by potentiometric titrations in a closed cell. *Analytica chimica acta*, 619(2), 183-191.
- Nativ, R., 1992. Recharge into Southern High Plains aquifer—possible mechanisms, unresolved questions. *Environmental Geology and Water Sciences*, 19(1), 21-32.
- Nelson, B.K., and DePaolo, D.J., 1988. Comparison of isotopic and petrographic provenance indicators in sediments from Tertiary continental basins of New Mexico. *J. Sed. Petrol.* 58, 348-357.
- O’Nions, R.K., Hamilton, P.J., Hooker, P.J., 1983. A Nd isotope investigation of sediments related to crustal development in the British Isles. *Earth Planetary Science Letters* 63, 229-240.
- Obermajer, M., Fowler, M. G., Goodarzi, F., & Snowdon, L. R. (1997). Organic petrology and organic geochemistry of Devonian black shales in southwestern Ontario, Canada. *Organic Geochemistry*, 26(3), 229-246.
- Parrish, J. B., and Lavin, P. M., 1982. Tectonic model for kimberlite emplacement in the Appalachian Plateau of Pennsylvania. *Geology*, 10(7), 344-347.
- Patchett, P.J., Ross, G.M., Gleason, J.D., 1999. Continental drainage in North America during the Phanerozoic from Nd isotopes. *Science* 283, 671-673.
- Pearce, J. M., Holloway, S., Wacker, H., Nelis, M. K., Rochelle, C., & Bateman, K., 1996. Natural occurrences as analogues for the geological disposal of carbon dioxide. *Energy Conversion and Management*, 37(6), 1123-1128.
- Pedersen, T. F., & Calvert, S. E., 1990. Anoxia vs. Productivity: What Controls the Formation of Organic-Carbon-Rich Sediments and Sedimentary Rocks? *AAPG Bulletin*, 74(4), 454-466.
- Pettijohn, F. J., 1957. *Sedimentary Rocks*. Harper & Row.
- Philippi, G. T., 1974. The influence of marine and terrestrial source material on the composition of petroleum. *Geochimica et Cosmochimica Acta*, 38(6), 947-966.
- Plasynski, S.I., Litynski, J.T., McIlvried, H.G., and Srivastava, R.D., 2009. Progress and New Developments in Carbon Capture and Storage. *Plant Science* 28; 123-138.
- Potter, P. E., Maynard, J. B., & Pryor, W. A., 1982. Appalachian gas bearing Devonian shales: Statements and discussions. *Oil and Gas Journal*, 80(4), 290-318.
- Quattrocchi, F., Barbieri, M., Bencini, R., Cinti, D., Durocher, K., Galli, G., Pizzino, L., Shevalier, M., and Voltattorni, N., 2006. Strontium isotope ($^{87}\text{Sr}/^{86}\text{Sr}$) chemistry in

- produced oil field waters: The IEA CO₂ monitoring and storage project. In *Advances in the Geological Storage of Carbon Dioxide* (pp. 243-259). Springer Netherlands.
- Spivak-Birndorf, L. J., Stewart, B. W., Capo, R. C., Chapman, E. C., Schroeder, K. T., & Brubaker, T. M., 2012. Strontium isotope study of coal utilization by-products interacting with environmental waters. *Journal of Environmental Quality* 41(1), 144-154.
- Stevens, S. H., Pearce, J. M., & Rigg, A. A. J., 2001a, May. Natural analogs for geologic storage of CO₂: An integrated global research program. In *Proceedings of the First National Conference of Carbon Sequestration*, National Energy Technology Laboratory, Washington, DC, USA.
- Stevens, S. H., Kuuskraa, V. A., Gale, J., & Beecy, D., 2001b. CO₂ injection and sequestration in depleted oil and gas fields and deep coal seams: worldwide potential and costs. *Environmental Geosciences*, 8(3), 200-209.
- Rajagopalan, S., Anderson, T. A., Fahlquist, L., Rainwater, K. A., Ridley, M., & Jackson, W. A., 2006. Widespread presence of naturally occurring perchlorate in high plains of Texas and New Mexico. *Environmental Science and Technology*, 40(10), 3156-3162.
- Ramondetta, P. J., 1982a. Facies and Stratigraphy of the San Andres Formation, Northern and Northwestern Shelves of the Midland Basin, Texas and New Mexico, Texas Bureau of Economic Geology, UT Austin, Texas. Report of Investigations No. 128, p. 56.
- Ramondetta, P. J., 1982b. Genesis and emplacement of oil in the San Andres Formation, northern shelf of the Midland Basin, Texas. Bureau of Economic Geology, University of Texas at Austin, Report of Investigation No. 166, p. 39.
- Rast, N., & Skehan, J. W., 1993. Mid-Paleozoic orogenesis in the North Atlantic: the Acadian orogeny. *The Acadian Orogeny: Recent studies in New England, Maritime Canada, and the autochthonous foreland*. Geological Society of America Special Paper, 275.
- Ruppel, S. C., & Cander, H. S., 1988. Dolomitization of shallow-water platform carbonates by sea water and seawater-derived brines: San Andres Formation (Guadalupian), west Texas. *Sedimentology and geochemistry of dolostones: SEPM Special Publication*, 43, 245-262.
- Sageman, B. B., Murphy, A. E., Werne, J. P., Ver Straeten, C. A., Hollander, D. J., & Lyons, T. W., 2003. A tale of shales: the relative roles of production, decomposition, and dilution in the accumulation of organic-rich strata, Middle– Upper Devonian, Appalachian basin. *Chemical Geology*, 195(1), 229-273.
- Samson, S. D., Patchett, P. J., Roddick, J. C., & Parrish, R. R., 1989. Origin and tectonic setting of Ordovician bentonites in North America: Isotopic and age constraints. *Geological Society of America Bulletin*, 101, 1175-1181.

- Scanlon, B. R., Nicot, J. P., Reedy, R. C., Kurtzman, D., Mukherjee, A., & Nordstrom, D. K., 2009. Elevated naturally occurring arsenic in a semiarid oxidizing system, Southern High Plains aquifer, Texas, USA. *Applied Geochemistry*, 24(11), 2061-2071.
- Sophocleous, M., 2010. Review: groundwater management practices, challenges, and innovations in the High Plains aquifer, USA—lessons and recommended actions. *Hydrogeology Journal*, 18(3), 559-575.
- Stueber, A. M., Saller, A. H., & Ishida, H., 1998. Origin, migration, and mixing of brines in the Permian Basin; geochemical evidence from the eastern Central Basin Platform, Texas. *AAPG Bulletin*, 82(9), 1652-1672.
- Tourtelot, H. A., 1979. Black shale-its deposition and diagenesis. *Clays and Clay Minerals*, 27(5), 313-321.
- USGS, 2002. PHREEQC Version 2.15.0; A Computer Program for Speciation, Batch-Reaction, One-Dimensional Transport, and Inverse Geochemical Calculations.
- USGS, [computer file] 2006. FGDC Digital Cartographic Standard for Geologic Map Symbolization (PostScript Implementation): U.S. Geological Survey Techniques and Methods 11-A2. Available FTP: <http://pubs.usgs.gov/tm/2006/11A02/> [July 13, 2013].
- USGS, [computer file], 2009. Digital map of aquifer boundary for the High Plains aquifer in parts of Colorado, Kansas, Nebraska, New Mexico, Oklahoma, South Dakota, Texas, and Wyoming. Available FTP: http://water.usgs.gov/GIS/metadata/usgswrd/XML/ds543.xml#Metadata_Reference_Information [July 3, 2013].
- Veizer, J., & Mackenzie, F. T., 2003. Evolution of sedimentary rocks. Mackenzie, F. T., Editor. *Sediments, diagenesis, and sedimentary rocks: Treatise on Geochemistry, Volume 7*. Elsevier.
- Veizer, J., Ala, D., Azmy, K., Bruckschen, P., Buhl, D., Bruhn, F., Carden, G.A.F., Diener, A., Ebner, S., Godderis, Y., Jasper, T., Korte, C., Pawellek, F., Podlaha, O., and Strauss, H., 1999. $^{87}\text{Sr}/^{86}\text{Sr}$, $\delta^{13}\text{C}$ and $\delta^{18}\text{O}$ evolution of Phanerozoic seawater. *Chemical Geology*, 161(1), 59-88.
- Ver Straeten, C. A., and Brett, C. E., 2000. Bulge migration and pinnacle reef development, Devonian Appalachian foreland basin. *The Journal of Geology*, 108(3), 339-352.
- Ver Straeten, C. A., 2008. Volcanic Tephra Bed Formation and Condensation Processes: A Review and Examination from Devonian Stratigraphic Sequences. *The Journal of Geology*, 116(6), 545-557.
- Ver Straeten, C.A., 2009. The classic Devonian of the Catskill Front: A foreland basin record of the Acadian orogenesis. *New York State Geological Association, Trip 7*, 1-35.

- Ver Straeten, C. A., Brett, C. E., & Sageman, B. B., 2011. Mudrock sequence stratigraphy: A multi-proxy (sedimentological, paleobiological and geochemical) approach, Devonian Appalachian Basin. *Palaeogeography, Palaeoclimatology, Palaeoecology*, 304(1), 54-73.
- Vernon, J. H., and Riecker, R. E., 1989. Significant Cenozoic faulting, east margin of the Española Basin, Rio Grande rift, New Mexico. *Geology* 17, 230-233.
- Wall, A. J., Capo, R., Stewart, B., Phan, T. T., Jain, J. C., Hakala, J. A., & Guthrie, G. D., 2013. High throughput method for Sr extraction from variable matrix waters and $^{87}\text{Sr}/^{86}\text{Sr}$ isotope analysis by MC-ICP-MS. *Journal of Analytical Atomic Spectrometry*.
- Ward, R. F., Kendall, C. G. S. C., & Harris, P. M., 1986. Upper Permian (Guadalupian) facies and their association with hydrocarbons-Permian basin, west Texas and New Mexico. *American Association of Petroleum Geologists Bulletin*, 70(3), 239-262.
- Werne, J. P., Sageman, B. B., Lyons, T. W., & Hollander, D. J., 2002. An integrated assessment of a "type euxinic" deposit: evidence for multiple controls on black shale deposition in the Middle Devonian Oatka Creek Formation. *American Journal of Science*, 302(2), 110-143.
- Wheeler, E. A., Segarra, E., Johnson, P. N., Johnson, J. W., & Willis, D. B., 2006, February. Policy alternatives for the southern Ogallala aquifer. Selected paper prepared for presentation at the Southern Agricultural Economics Association Annual Meeting.
- Wilkinson, M., Haszeldine, R. S., Fallick, A. E., Odling, N., Stoker, S. J., & Gatliff, R. W., 2009. CO_2 -Mineral Reaction in a Natural Analogue for CO_2 Storage—Implications for Modeling. *Journal of Sedimentary Research*, 79, 486-494.
- Wood, W. W., & Sanford, W. E., 1995. Chemical and isotopic methods for quantifying ground-water recharge in a regional, semiarid environment. *Ground Water*, 33(3), 458-468.
- Zheng, L., Apps, J. A., Zhang, Y., Xu, T., and Birkholzer, J.T., 2009. On mobilization of lead and arsenic in groundwater in response to CO_2 leakage from deep geological storage. *Chemical Geology* 268, 281-297.